

Frequency Performance Assessment of Future Grids

Ahmad Shabir AHMADYAR

Centre for Future Energy Networks
School of Electrical and Information Engineering
Faculty of Engineering and Information Technology
The University of Sydney

A thesis submitted in fulfilment of the requirements for the degree of
Doctor of Philosophy

May 2018

I would like to dedicate this thesis to my parents for making me be who I am, and my loving wife, Sahar, for supporting me through this journey.

Declaration

I hereby declare that except where specific reference is made to the work of others, the contents of this dissertation are original and have not been submitted in whole or in part for consideration for any other degree or qualification in this, or any other university. This dissertation is my own work and contains nothing which is the outcome of work done in collaboration with others, except as specified in the text and Acknowledgements. This dissertation contains fewer than 50,000 words including appendices, bibliography, footnotes, tables and equations and has fewer than 150 figures.

Ahmad Shabir AHMADYAR

May 2018

Acknowledgements

I would like to express my deepest gratitude to my supervisor Dr. Gregor Verbič. He has been an exceptional mentor for me during the period of my candidature. His advice and encouragement in this thesis, as well as my professional career, have been crucial. I would not have been able to finish my dissertation without his guidance.

I would also like to sincerely thank Professor David J. Hill and Dr. Hisamoddin Marzoghi who collaborated with me on Chapter 2 of this thesis. I would like to greatly thank Mr. Shariq Riaz, PhD candidate at The University of Sydney with whom I completed a joint project which is included in Chapter 3 of this thesis. Furthermore, I would like to acknowledge the support of my colleagues, namely Dr. Mehdi Gramroodi and Mr. Mohammad Seidaliseifabad.

I would especially like to appropriate DigSILENT® for providing me a license for DIgSILENT Power Factory software package, and other technical manuals during the life-cycle of my project. An special thanks to Artelys® for providing me license for the Knitro Optimisation toolbox during my candidature.

I am particularly thankful to those who provided me financial support during my PhD program in the form of scholarship and prizes:

- The Australian Commonwealth Government for the Research Training Program (formerly Australian Postgraduate Awards) scholarship at The University of Sydney,
- The University of Sydney for the Postgraduate Research Scholarship Scheme, and
- The School of Electrical and Information Engineering at The University of Sydney for the Norman I Price scholarship.

Last but not least, I would like to express my deepest appreciation to my family, especially my wife Sahar, who has provided a tremendous amount of support throughout these years.

Abstract

Future grids security will be challenged by the increasing penetration of non-synchronous renewable energy sources (NS-RES). With the increasing integration of NS-RES, power systems' dynamic complexity increases. This makes the stability assessment of future grids very difficult. Studies of future grids with high penetration of NS-RES suggest that along with other issues, system frequency control will become a challenging task. Nonetheless, it is very difficult to quantify the findings of those studies and make general conclusions, because most of those studies are based on specific networks under specific operating conditions. Furthermore, the impact of market dynamics and emerging technologies, such as distributed generation with battery storage, on system frequency performance have been overlooked. Hence, in this thesis, we propose a suitable frequency performance assessment framework, as well as utilise some of the conventional and non-conventional resources to enhance system frequency performance with high penetration of NS-RES.

First, we study the impact of high penetration of NS-RES and different penetration levels of prosumers on the performance and frequency stability of the Australian national electricity market (NEM). By doing this, we quantify the connection between the NS-RES and the system frequency performance, as well as different penetration levels of prosumers and the system frequency performance.

Second, we propose a frequency performance assessment framework based on a time-series approach that facilitates the analysis of a large number of future grid scenarios. We use this framework to assess the frequency performance of the Australian future grid by considering a large number of future scenarios and sensitivity of different parameters. By doing this, we identify a maximum non-synchronous instantaneous penetration range for the system from the frequency performance point of view.

Then, to improve the frequency performance of the system with high penetration levels of NS-RES, we evaluate the contribution of different resources, such as synchronous condensers, wind farm's synthetic inertia and a governor-like response from the de-loaded wind farms, on frequency control. The results show that the de-loaded wind farms add more flexibility to the system for frequency control. Considering this, we propose optimal operation and control strategies for the participation of wind farms in frequency control. We do this by explicitly

modelling a wind farm and considering the aero-dynamical coupling (i.e. wake effect) among the wind turbines within a wind farm. The results show that with the proposed strategies, it is possible to enhance frequency performance of the system without compromising the efficiency of the wind farms.

Finally, we further develop the concept of wind farm participation in frequency control and propose a coordinated operation strategy for wind farms. In contrast to the conventional wind farm operation strategy, where each wind turbine is optimised individually, we propose different operation strategies to maximise the total output power and rotational kinetic energy of a wind farm for frequency control. The results show that by operating the wind farm in a coordinated way, we can increase both the output power and the rotational kinetic energy of the wind farm. Time-domain simulations show that the proposed operation strategies noticeably improve the wind farm's performance in frequency control.

Publications Included in this Thesis

Journal Articles

- [JA1] A.S. Ahmadyar, G. Verbič, "Coordinated Operation Strategy of Wind Farms for Frequency Control by Exploring Wake Interaction," *IEEE Transactions on Sustainable Energy*, vol. 8 no. 1, pp. 230-238, Jan. 2017.

This paper is included in Chapter 5.

Contributors	Modelling	Analysing the results	Writing the paper
A.S. Ahmadyar	90 %	85 %	80 %
G. Verbič	10 %	15 %	20 %

- [JA2] A.S. Ahmadyar, S. Riaz, G. Verbič, A. Chapman, D. J. Hill "A Framework for Assessing Renewable Integration Limits with Respect to Frequency Performance," *IEEE Transactions on Power Systems*, vol. PP. no. 99 pp 1-1, Nov. 2017.

My Contribution on this paper is incorporated in Chapter 3.

Contributors	Modelling	Analysing the results	Writing the paper
A.S. Ahmadyar	70 %	80 %	80 %
Others	30 %	20 %	20 %

- [JA3] H. Marzooghi, M. Gramroodi, A.S. Ahmadyar, R. Liu, G. Verbič, D. J. Hill "Scenario and Sensitivity Based Stability Analysis of the Australian Future Grid," to be Submitted to *IEEE Transactions on Power Systems*, Mar 2018.

My contribution on this paper is included in Chapter 2.

Contributors	Modelling	Analysing the results	Writing the paper
A.S. Ahmadyar	15 %	15 %	15 %
Others	85 %	85 %	85 %

Conference Papers

- [CP1] A.S. Ahmadyar; G. Verbič, "Exploring Wake Interaction for Frequency Control in Wind Farms," in *the 13th Wind Integration Workshop Berlin*, 11 - 13 Nov. 2014.

This paper is included in Chapter 4.

Contributors	Modelling	Analysing the results	Writing the paper
A.S. Ahmadyar	70 %	75 %	75 %
G. Verbič	30 %	25 %	25 %

- [CP2] A.S. Ahmadyar; G. Verbič, "Control Strategy for Optimal Participation of Wind Farms in Primary Frequency Control," in *PowerTech, 2015 IEEE Eindhoven*, 29 June. - 2 July. 2015.

This paper is incorporated in Chapter 4.

Contributors	Modelling	Analysing the results	Writing the paper
A.S. Ahmadyar	90 %	85 %	85 %
G. Verbič	10 %	15 %	15 %

- [CP3] A.S. Ahmadyar, S. Riaz, G. Verbič, J. Riesz, A. Chapman "Assessment of Minimum Inertia Requirement for System Frequency Stability," in *Power System Technology (POWERCON), 2016 IEEE International Conference*, 28 Sept. - 1 Oct. 2016.
(Winner of the IEEE-PES PowerCON2016 Poster Award)

My contribution on this paper is presented in Chapter 2.

Contributors	Modelling	Analysing the results	Writing the paper
A.S. Ahmadyar	70 %	80 %	75 %
Others	30 %	20 %	25 %

- [CP4] A.S. Ahmadyar, H. Marzooghi, G. Verbič, D. J. Hill "Impact of Prosumers on Frequency Stability of the Australian Future Grid," in *2017 IEEE Power and Energy Society General Meeting Chicago*, 16 - 20 July. 2017.

My contribution on this paper is presented in Chapter 2.

Contributors	Modelling	Analysing the results	Writing the paper
A.S. Ahmadyar	80 %	80 %	80 %
Others	20 %	20 %	20 %

Table of contents

List of figures	xvii
List of tables	xxi
Symbols and Abbreviations	xxiii
1 Introduction	1
1.1 Motivation	1
1.2 Literature Review	3
1.2.1 Frequency Stability of Future Grids	4
1.2.2 Participation of Wind Generation in Frequency Control	7
1.3 Research Questions	11
1.4 Research Contribution	12
2 Impact of Prosumers and Security Constraints on Frequency Performance of FGs	15
2.1 Introduction	15
2.2 Impact of Prosumers on Frequency Performance	16
2.2.1 Modelling Framework	16
2.2.2 Test Model and Scenarios	19
2.2.3 Simulation Results	19
2.3 Impact of Security Constraints on Frequency Performance	24
2.3.1 Market Model and Inputs	25
2.3.2 Test Model	28
2.3.3 Simulation Results	28
2.3.4 Discussion	32
2.4 Summary	35

3	A Frequency Performance Assessment Framework for Future Grids	37
3.1	Introduction	37
3.2	Background	38
3.3	Frequency Performance Assessment Framework and Case Studies	40
3.3.1	Inputs and Scenarios	40
3.3.2	Market Simulation (Line 1-6, Algorithm 1)	42
3.3.3	Sensitivity Cases and Frequency Performance Assessment (Line 7-12, Algorithm 1)	43
3.3.4	Outputs	45
3.4	Frequency Performance Assessment Results	45
3.4.1	Market Dispatch Results	45
3.4.2	Frequency Performance Results	47
3.5	Improving Frequency Response of the System with High Penetration of NS-RES	55
3.5.1	Dynamic Inertia Based Frequency Control Security Constraint	55
3.5.2	Utilisation of Other Sources for Frequency Control	57
3.6	Summary	59
4	Participation of Wind Generation in Frequency Control	61
4.1	Introduction	61
4.2	Exploring Wake Interaction for Frequency Control	62
4.2.1	Participation of Wind Power in Frequency Control	62
4.2.2	Stationary Wake Model	64
4.2.3	Wind Farms Optimal Operation Strategy for Frequency Control	66
4.2.4	Case Study	68
4.3	An Optimal Control Strategy for Participation of Wind Farms in Frequency Control	73
4.3.1	Proposed Control Strategy	74
4.3.2	Time-Domain Simulation Results	77
4.4	Summary	80
5	Coordinated Operation of Wind Farms for Frequency Control	81
5.1	Introduction	81
5.2	Wind Farm Controllers	82
5.3	Coordinated Operation of Wind Farms	83
5.3.1	The Optimisation Problem	85
5.3.2	The Central Wind Farm Controller	88

5.4	Case Study	89
5.4.1	Optimisation Results	90
5.4.2	Contribution of Wind Farm in Frequency Control	95
5.4.3	The Performance of the Central Wind Farm Controller	96
5.5	Summary	98
6	Conclusion	99
	References	103

List of figures

2.1	Demand profile of the NEM for a typical summer week.	20
2.2	Balancing results for a typical summer week for Scenario PBS-Z	20
2.3	Balancing results for a typical summer week for Scenario PBS-L	21
2.4	Balancing results for a typical summer week for Scenario PBS-H	21
2.5	Inertia of the system for a typical summer week.	22
2.6	Inertia duration curve of the system for a whole year.	22
2.7	Histogram of the minimum RoCoF and frequency nadir for the studied year.	23
2.8	System frequency behaviour after a contingency for a typical hour ($t = 132$ h).	24
2.9	Dispatch results for the first week of July 2020 considering Case NoIC	29
2.10	Dispatch results for the first week of July 2020 considering Case SgN30	29
2.11	Dispatch results for the first week of July 2020 considering Case Ek30	29
2.12	Dispatch results for the first week of July 2020 considering Case SgP30	30
2.13	System inertia during the first week of July 2020, for all cases.	31
2.14	Inertia duration curve of the system for four representative weeks of the year 2020 i.e. first weeks of January, April, July, and October.	31
2.15	Minimum RoCoF after the loss of the largest in-feed for the first week of July 2020.	33
2.16	Frequency nadir after the loss of the largest in-feed for the first week of July 2020.	33
2.17	System frequency behaviour after the loss of the largest in-feed for a typical hour in July 2020.	34
3.1	Simplified network diagram of the Australian NEM.	41
3.2	A summary of scenarios and sensitivity cases, NSXX is the NSAP and varies from 10 % to 90 %.	44
3.3	Histograms of system synchronous inertia for all scenarios; for consistency all histograms are plotted on the same scale.	46
3.4	System primary reserve for all scenarios; $\bar{P}_g(t) - P_g(t)$, $g \in \mathcal{G}_{\text{sych}}$	46

3.5	Size of credible contingency (i.e. C_v) based on Algorithm 1.	47
3.6	Minimum RoCoF following the loss of CC for the simulated year; the red line shows the critical RoCoF.	48
3.7	Frequency nadir following the loss of CC for cases <i>NSxx-LsCvQLD-QLD</i>	49
3.8	RoCoF for two typical days considering the sensitivity of load model, for a low NSAP scenario (i.e. NS20) and a high NSAP scenario (i.e. NS80).	50
3.9	RoCoF for two typical days considering the sensitivity of contingency size, for a low NSAP scenario (i.e. NS20) and a high NSAP scenario (i.e. NS80).	51
3.10	RoCoF for two typical days considering the sensitivity of contingency location, for a low NSAP scenario (i.e. NS20) and a high NSAP scenario (i.e. NS80).	52
3.11	The impact of prosumers with different battery storage capacity on (a) the net demand level (P_{net}^{dm}), (b) level of system inertia (I_s), (c) size of CC (p^{cc}), and (d) RoCoF for two typical days for case <i>NS80-LsCvVIC-VIC</i>	53
3.12	Minimum RoCoF following a credible contingency based on NSIP.	54
3.13	Impact of dynamic inertia constraint on (a) synchronous inertia of the system and (b) RoCoF for QLD.	56
3.14	Distribution of (a) RoCoF, and (b) frequency nadir for Case <i>NS80-LdCvQLDQLD</i> ; considering cases Normal , SC , IE , and DL	58
3.15	System frequency behaviour for a typical hour considering cases Normal , SC , IE , and DL	58
4.1	Power coefficient characteristic and de-loading strategy of a Type III WT.	64
4.2	A row of wind turbines in a wind farm for wake modelling.	65
4.3	Power, rotor speed and pitch angle characteristics of a Type III WT.	66
4.4	One-line diagram of the power system for simulation.	68
4.5	The pitch angle and the rotor speed of the wind turbines in the wind farm: a) Case I, $\delta = 0\%$, b) Case II, $\delta = 5\%$, c) Case III, $\delta = 10\%$	69
4.6	The optimised kinetic energy in p.u, based on the ratings of the wind turbine, and the power of the wind farm with different de-loading margins.	70
4.7	System frequency behaviour during the generation loss.	72
4.8	The rotor speed of wind turbines during the generation loss: a) Case I, $\delta = 0\%$, b) Case II, $\delta = 5\%$, c) Case III, $\delta = 10\%$	73
4.9	The proposed rotor speed controller diagram.	75
4.10	The rotor speed transition representation from the sub-optimal to the optimal operation mode during the system frequency excursion.	75
4.11	The proposed pitch angle blade controller diagram.	77

4.12	Rotor speed of $WT_{1,1}$ in the WF under different operation scenarios.	78
4.13	System frequency under different operation scenarios.	79
4.14	Total output power of the WF under different operation scenarios.	79
5.1	Thrust and power coefficient of the NREL's 5 MW Type III wind turbine. . .	84
5.2	The proposed CWFC for coordinated operation of wind farms with frequency control capability. Double lines show vector signals.	88
5.3	One-line diagram of test power system for simulation.	89
5.4	The rotor speed and the pitch angle of $WT_{1,1}$ in different operation cases. .	92
5.5	The relative changes in the output power of wind turbines in Case MaxEk compared to Case MaxPwt.	92
5.6	Wind speed profile of the wind farm for an initial wind speed of $v_{1,1} = 10 \frac{m}{s}$. .	93
5.7	The relative changes in the available wind speed " Δv_i " in Case MaxEk compared to Case MaxPwt.	94
5.8	Power and kinetic energy of the wind farm in all four cases.	94
5.9	System frequency behaviour after a 12 % step increase in the load.	96
5.10	Power and kinetic energy of the wind farm in Case MaxEk5.	96
5.11	Power and kinetic energy of the wind farm with variable wind speed.	97
5.12	The effect of wake on the wind speed and the output power of individual wind turbines within the wind farm for Case MaxEK5.	97

List of tables

2.1	Parameters of synchronous generators.	28
3.1	The assumed large-scale generation portfolio of NEM; base scenario with 10 % annual energy from NS-RES.	42
4.1	Settings and characteristics of synchronous generators	71
5.1	Settings and characteristics of synchronous generators.	90
5.2	The parameters and settings of the reference wind turbine.	90
5.3	The wind farm characteristics and the central wind farm controller parameters.	91
5.4	Simulation cases for wind farm contribution in frequency control.	95

Symbols and Abbreviations

Parameters and Constraints

$\mathcal{G}_{\text{synch}}$ Set of synchronous generators

τ_g^+ Minimum up time of generator g

τ_g^- Minimum down time of generator g

$B_{i,j}$ Susceptance of a transmission line between nodes i and j

$g \in \mathcal{G}$ Generator g in set of \mathcal{G} generators

$h \in \mathcal{H}$ Time slot h in set of \mathcal{H} time slots in horizon

$m \in \mathcal{M}$ Load aggregator m in set of \mathcal{M} load aggregators

$n \in \mathcal{N}$ Node n in the system and set of \mathcal{N} nodes

$r \in \mathcal{R}$ Region r in the system and set of \mathcal{R} regions

r_g^+ Ramp-up rate of generator g

r_g^- Ramp-down rate of generator g

ρ Air density ($\frac{kg}{m^3}$)

C_p Power coefficient of a wind turbine

C_t Thrust coefficient of a wind turbine

E_k Rotational kinetic energy of a wind turbine or a wind farm (MWs, pu)

f System frequency (Hz)

G Gearbox ratio of a wind turbine

H	Normalised inertia constant of a generator (s)
K	Gain parameter
L	Distance between each wind turbine in a row, in the wind speed direction (m)
N	Number of wind turbines or generators
P	Electrical power (MW, GW, pu)
R	Blade radius of a wind turbine (m)
t	Time (s)
v	Wind speed ($\frac{m}{s}$)
pu	Per unit value

Variables

$\Delta p_{l,h}^{i,j}$	Power loss of transmission line between nodes i and j
$\delta_{n,h}$	Voltage angle at node n in hour h
\bar{p}_g	Maximum stable limit of a generator g (MW)
\bar{S}_g	Maximum stable limit of a generator g (MVA)
\underline{p}_g	Minimum stable limit of a generator g (MW)
D	Frequency damping of the system load
$d_{g,h}$	Binary variable to indicate shut-down status of generator g in hour h
$e_{b,h}^m$	Aggregated battery storage state of charge (SoC) of prosumers in hour h
H_g	Inertia constant of generator g (s)
I	Inertia of a generator or a system (GWs)
$p_{b,h}^m$	Charging/discharging power of prosumers' battery storage
$p_{b,h}^m$	Aggregated residential battery power of prosumers in hour h
$p_{d,h}^{\text{fx},m}$	Flexible demand power of aggregator m in hour h

$p_{d,h}^{\text{inf},m}$	Inflexible demand power of aggregator m in hour h
$p_{d,h}^{\text{u},m}$	Conventional demand of prosumers in hour h
$p_{\text{pv},h}^m$	Aggregated rooftop-photovoltaic generation of prosumers in hour h
$p_{g,h}$	Power dispatch from generator g in hour h
p_h^{load}	System net load active power requirement (MW)
$p_{l,h}^{i,j}$	Transferred power by transmission line between nodes i and j
$p_{r,h}^{\text{res}}$	System reserve requirement in region r (MW)
$s_{g,h}$	Binary variable to represent on/off status of generator g in hour h
S_h^{load}	System net load apparent power requirement (MVA)
$u_{g,h}$	Binary variable to indicate start-up of generator g in hour h
β	Rotor blade pitch angle of a wind turbine
Δ	De-loading margin of a wind farm
δ	De-loading margin of an individual wind turbine
λ	Tip speed ratio of a wind turbine
ω	Rotor speed of a wind turbine

Indices

\bar{x}	Maximum value of x
\underline{x}	Minimum value of x
\hat{x}	Measured value of x
x^*	Reference value of x
des	Desired value
load	Values referred to load
mec	Mechanical value
nom	Nominal value

opt	Optimal value
sub	Sub-optimal value
synch	Values referred to synchronous generators
wf	Values referred to a wind farm
wt	Values referred to a wind turbine

Other Symbols

c_g^{fix} (.)	Fix operation and maintenance cost of a generator g
c_g^{sd} (.)	Shut-down cost of a generator g
c_g^{su} (.)	Start-up cost of a generator g
c_g^{var} (.)	Variable operation and maintenance cost of a generator g
\mathbf{x}	Vector $\in \mathbb{R}^N$

Acronyms / Abbreviations

AEMO	Australian Energy Market Operator
AEN	Australia Energy Network
AGC	Automatic Generation Control
BESS	Battery Energy Storage Systems
BS	Battery Storage
CC	Credible Contingency
CCGT	Combined Cycle Gas Turbine
CSIRO	Commonwealth Scientific and Industrial Research Organisation
CST	Concentrated Solar Thermal
CWFC	Central Wind Farm Controller
DFAG	Doubly Fed Asynchronous Generator
DG	Distributed Generation

DR	Demand Response
FACTS	Flexible Alternating current Transmission System
FCAS	Frequency Control Ancillary Service
FFR	Fast Frequency Response
FG	Future Grid
FRC	Fully Rated Converter
FS	Frequency Support
FSIG	Fixed Speed Induction Generator
GT	Gas Turbine
HEM	Home Energy Management
HVDC	High Voltage Direct Current
IE	Inertia Emulation
IEA	International Energy Agency
IM	Induction Motor
KKT	Karush Kuhn Tucker
MC	Main Controller of a Wind Farm
MILP	Mixed-Integer Linear Programming
MPT	Maximum Power Tracker
NEM	National Electricity Market (Australia)
NREL	National Renewable Energy Laboratory
NS-RES	Non-Synchronous Renewable Energy Sources
NSAP	Non-Synchronous Annual Penetration
NSIP	Non-Synchronous Instantaneous Penetration
NSW	New South Wales

NTNDP	National Transmission Network Development Plan (Australia)
OCGT	Open Cycle Gas Turbine
PEV	Plug-in Electric Vehicle
PV	Photovoltaic
QLD	Queensland
RES	Renewable Energy Sources
RET	Renewable Energy Target
RoCoF	Rate of Change of Frequency
SA	South Australia
SC	Synchronous Condenser
SG	Synchronous Generator
SoC	Battery State of Charge
SRMC	Short-Run Marginal Costs
TAS	Tasmania
TL	Transmission Line
UC	Unit Commitment
UFLS	Under-Frequency Load Shedding
VCM	Voltage Control Mode
VG	Variable Generation
VIC	Victoria
VSWT	Variable Speed Wind Turbine
WECC	Western Electrical Coordinating Council
WF	Wind Farm
WT	Wind Turbine

WTG Wind Turbine Generator

ZCA Zero Carbon Australia

ZIP Constant Impedance, Current and Power Load

Chapter 1

Introduction

1.1 Motivation

Conventionally, power systems operation has been based on large-scale synchronous generators (SGs). Those SGs utilise relatively reliable resources, such as natural gas and coal, and, therefore, can be considered fully dispatchable¹. On the other hand, electricity demand is variable in nature, and, thus, can be considered non-controllable². Therefore, fully dispatchable SGs have to follow the non-controllable electricity demand using an optimal combination of dispatch and regulation processes. Power system behaviour with SGs have been widely studied and is well understood [1]. Controllers have evolved to assure secure and reliable operation of a power system under normal and abnormal conditions. The operation and stability of future grids (FGs), however, will be challenged with the increasing deployment of emerging technologies, e.g. non-synchronous renewable energy sources (NS-RES), such as wind farms (WFs); distributed generation (DG), such as rooftop-photovoltaic (PV); energy storage systems, such as residential battery storage; and new loads, such as plug-in electric vehicles (PEVs).

The aforementioned changes add more complexity to planning, operation and stability of FGs, which can be seen on different time-scales from years (i.e. transmission network planning) to hours (i.e. unit commitment (UC) and spot market due to intermittent nature of renewable generations) to seconds (i.e. frequency stability issues due to insufficient governor response) and finally to milliseconds (i.e. high rate of change of frequency (RoCoF) due to low system inertia). Considering these, optimal network planning that considers

¹The flexibility of conventional generation for dispatch process varies according to their technical constraints, e.g. minimum up and down times, ramp rate limits, etc.

²Note that this might not be valid any more in power systems with the increasing penetration of emerging demand-side technologies like distributed generation (DG), energy storage and demand response (DR). It is expected that the electrical loads become more controllable in a foreseen future using such technologies.

both generation and grid becomes more complicated because of renewable generations diversity (e.g. their technology, location and size) and grid technologies uncertainty (e.g. utilising high voltage direct current (HVDC) or continuing with current technologies). Indeed, this is an important issue that has to be considered while planning the FGs structure. In countries like Australia, where most of the high potential renewable sites are located far from the load centres, HVDC transmission lines might be the only viable option. Furthermore, due to intermittent nature of renewable energy sources (RES), balance between generation and demand also becomes a challenging task. Nonetheless, the emergence of cheaper battery energy storage systems (BESS) facilitates large-scale deployment of BESS at all levels in power systems. This can be seen as a potential solution to cope with the intermittency of variable generations (VGs). Utilisation of emerging technologies with different characteristics compared to conventional SGs, such as NS-RES, would increase the dynamic complexity of power systems. Thus, maintaining power system security and operating the system within its permissible stable bounds under normal and abnormal conditions becomes an even more challenging task.

The above-mentioned changes necessitate a reassessment of power system planning, operation and stability based on new conditions and requirements. For instance, with high penetration levels of NS-RES, power system's dynamics changes in new ways, which makes it very difficult to define the worst case scenarios used for system stability assessment. Furthermore, with a high level of uncertainty related to NS-RES, even the process of defining the worst case scenarios becomes a challenging task. Therefore, the traditional way of assessing system stability, where the worst case scenarios are usually well defined, may no longer be valid. As a result, using the current widely accepted criteria for defining critical operation points and contingencies may fail to identify all critical conditions that might threaten power system stability. This, particularly, has a profound impact on system frequency stability where the increased penetration of NS-RES reduces the total inertia, as well as the governor response of the system. Note that the reduced amount of inertia and governor response have adverse effects on the system frequency response, and can significantly change the system frequency behaviour, as characterised by the RoCoF and the frequency nadir [2–5]. Therefore, with a high penetration level of NS-RES, system frequency control becomes a challenging task and needs to be dealt with in a systematic way.

In the following, we will review literature related to performance and stability assessment of FGs focusing on frequency stability. Furthermore, we will review studies related to the existing methods for the participation of wind generation in frequency control, as well as modelling and operation of WFs.

1.2 Literature Review

FG studies have shown that even with high penetrations of RESs, balance between generation and demand is feasible [4, 6–9]. Nonetheless, those studies have made a range of assumptions that limit their application for FG studies. First, most of those studies are based on simple balancing using a copperplate transmission model [7–9], which does not take into account network related issues (e.g. transmission lines' (TLs') limits and stability issues). Second, they have used conventional demand models, which neglect the impact of emerging demand-side technologies (i.e. DG, small scale battery storage (BS)) when modelling net future demand [4, 7–9]. Third, the grid integration of RESs is based on specific market structures [4, 6–9]. These market structures will not allow the changes that might result in a more cost-effective delivery of electrical power.

To address the above issues, a simulation platform for the performance and stability assessment of the FG scenarios was proposed in [10], which considers market simulation, power flow calculation, and stability assessment altogether. For accurate system stability assessment, it is also crucial to model the net demand of the system at the high voltage buses as an aggregated function of powers and voltages [1]. But, the increasing penetration of DG, such as rooftop-photovoltaic (PV)³ and residential BS invalidated the conventional demand models for system studies. So, it is necessary to develop demand models considering the aggregated effect of price-responsive users equipped with the emerging demand-side technologies, such as rooftop-PV and BS⁴ for FG scenario studies [12]. We will employ this model in our study and will return to these in Section 2.2 when discussing the impact of prosumers on the frequency performance of the Australian FG.

Among different RES, wind generation is considered as one of the most economically viable options [13], so it has been one of the main components on achieving the renewable energy target (RET) programs around the globe. International Energy Agency (IEA) predicts that from 2014 to 2035, under the 450 ppm scenario of CO₂ emission reduction, \$3.027 B will be invested in the wind generation technologies, which is the highest investment among different renewable and conventional generation technologies [14]. It appears that the penetration of wind energy in the power system of most countries will keep increasing in the foreseeable future. For instance, in 2015, the global wind generation market grew by 22 % - the highest annual growth among all RESs [13]. In Australia, over the past decade, the installed capacity of wind generation has been growing at an average rate of 30 % [15], and it is anticipated that wind generation will play a major role in reaching the 20 % RET by 2020.

³Globally, the installed capacity of rooftop-PV increased from nearly 4 GW in 2003 to approximately 227 GW in 2015 [11].

⁴Consumers equipped with DG (e.g. rooftop-PV and BS) are referred to **prosumers (producer - consumer)**.

The USA (the largest electricity consumer in the world) is planning to produce 20 % of its electricity from wind by 2030 [16]. Denmark - one of the pioneers of wind technology and the country with the highest penetration of wind generation in its power system - has set the target of supplying 50 % of its electricity from wind energy by 2020, and 100 % from RES by 2035 [13]. Although financially wind generation is one of the most viable RES, and can compete even with some of the conventional generations [17]; technically, it is considered as a less reliable resource because of the intermittent nature of wind, as well as the inherent inertia-less characteristic of variable speed wind turbines (VSWTs). Nonetheless, studies have shown that wind energy can provide ancillary services, such as primary frequency control [18–21]. We will further discuss this in Section 1.2.2.

1.2.1 Frequency Stability of Future Grids

Frequency stability is defined as the ability of a power system to maintain steady frequency after a severe contingency, resulting in a considerable imbalance between generation and demand [22]. Thus, from a stability perspective, it is crucial to maintain the frequency of a power system within acceptable bounds in all situations. Severe frequency excursions might cause generator tripping, which can jeopardise power system security and even lead to cascading failures and a blackout. Further, it can affect the performance of the system by damaging equipment, overloading transmission lines, and degrading the performance of sensitive electronic loads.

Conventional power systems operation has been based on large-scale dispatchable SGs (e.g. thermal and hydro). Those generators are controllable and have inherent rotational kinetic energy, which is an important feature for system frequency stability and control. During a frequency event, SGs can provide kinetic energy or absorb it from the grid that is proportional to the RoCoF [1]. Stable operation of a system requires that the difference between the generation and consumption should be nearly zero, however, in normal operation, due to the variable nature of the electrical demand, there is a spontaneous imbalance between those two. Thus, the system frequency deviates from its nominal value. This variation should be kept small because larger frequency variations might result in unnecessary load shedding and even generator tripping.

The operation and stability of FGs, however, will be further challenged with the increasing penetration of NS-RES, such as WFs, distributed generations (DG), battery energy storage systems (BESS), and new loads such as PEVs. Indeed, studies have shown that with high penetration levels of NS-RES, it might be very difficult to maintain system frequency within the stable limits [2–5, 23–25]. In [4], the frequency stability of the US Western Interconnection was assessed. The results show that a 50 % non-synchronous instantaneous

penetration (NSIP) deteriorates the frequency response of the system compared to the current situation, where the NSIP is approximately 4 %. However, it is not considered as an immediate issue provided that adequate fast frequency responsive resources are available. In contrast, EirGrid in Ireland has introduced a maximum of 50 % NSIP to maintain the system frequency response within the permissible bounds [25].

The above studies used either a typical operation scenario (i.e. assessed only one typical operation point) [4], or a simplified transmission model (i.e. copperplate model of the network) [5]. Further, they have used conventional demand models and ignored the impact of prosumers for modelling net future demand. Although the above studies give some insight into the effect of high penetration levels of NS-RES on system frequency performance, it is difficult to make general conclusions from their findings because of the above-mentioned limitation. Nonetheless, studies have shown that system frequency stability is an especially serious issue for small and weakly interconnected systems, such as Ireland grid [2] and the Australian National Electricity Market (NEM). Hence, the Australian Energy Market Operator (AEMO) has identified system frequency control as an immediate challenge for FG security [24], mainly because the transmission network is very long (i.e. more than 5000 km long), and areas can be disconnected.

Currently, in the NEM, eight frequency control ancillary service (FCAS) markets conjointly operate with other spot markets in real time [26]. From the above eight markets, three are associated with short-term frequency support. These FCAS markets provide primary frequency support with three different speeds of response - 6 s, 1 min, and 5 min. Hence, the primary frequency control might not be considered as an immediate issue for the FGs provided that a similar model is implemented. On the other hand, a higher RoCoF, which is a consequence of low system inertia, is considered as an immediate challenge [23, 24]. Indeed, low system inertia was identified as one of the main reasons for the blackout in South Australia (SA) on 28 September 2016 [27]. After separation of the SA system from rest of the NEM, inertia was very low in the SA system, which resulted in a considerably fast RoCoF; consequently, the system frequency dropped below 47 Hz before the activation of the under frequency load shedding (UFLS) scheme. As a result, the SGs' under-frequency protection scheme disconnected them from the system causing a larger imbalance. This eventually accelerated the occurrence of the system going black. Note that a higher RoCoF leaves insufficient time for activation and deployment of primary frequency response, and it might trigger generators RoCoF protection, which would result in tripping of additional SGs. Further, with the increased RoCoF, the maximum torque and mechanical stress increase in the machines. In some situations, with a $\text{RoCoF} = -1 \frac{\text{Hz}}{\text{s}}$, an under-excited machine's rotor cannot follow the fast speed reduction of the grid, so it loses its opposing force and speeds up,

which would eventually result in a pole slip [28]. It has also been reported that fast frequency events can have detrimental effects on combustion turbines because of a potential turbine combustor lean-blowout [29].

Therefore, with high penetration levels of NS-RES, it is more challenging to maintain system frequency within its stable limits. To deal with this issue, some studies have proposed a maximum NSIP limit, which requires a certain portion of power to be produced by the SGs at all times [2, 30]. Similar approaches have been proposed in [5] and [31], where a frequency control security constraint was integrated into the market dispatch model. However, before integrating any frequency control security constraint into the market dispatch model, it has to be defined precisely, and the limits for this constraint have to be identified accurately. To do this in a systematic way, it is vital to have a suitable framework to precisely assess the frequency performance of FGs, and determine the maximum NSIP (or minimum inertia level) that a system can operate without violating its frequency stability limits at all time, (This is explained in more detail in Chapters 2 and 3).

To ensure system frequency stability of the system is maintained, frequency operating standards have been introduced, which might vary in different jurisdictions. For instance, in the Nordic system, the RoCoF relays are set to $-0.5 \frac{\text{Hz}}{\text{s}}$, and the UFLS relays are set to 49.4 Hz@0.15 s [32], whereas, in the UK National Grid and the Ireland Grid, the RoCoF relays are set to $-0.125 \frac{\text{Hz}}{\text{s}}$ [33] and $-0.5 \frac{\text{Hz}}{\text{s}}$ [2], respectively. In the NEM, the frequency operating standard for the mainland NEM (excluding Tasmania) in a generation or load event is between 49.5 Hz-50.5 Hz [34], and the allowable RoCoF limits are determined indirectly [35]. The same standard for Tasmania (TAS) for such events is between 48 Hz - 52 Hz. The connection standards for new connections specify minimum access ($-1 \frac{\text{Hz}}{\text{s}}$ for 1 s) and automatic access ($-4 \frac{\text{Hz}}{\text{s}}$ for 0.25 s) standards for RoCoF where the plant must be capable of continuous, uninterrupted operation. Violation of these limits activates their respective relays and can disconnect even more generations. Thus, a power system should be robust enough not to violate those limits after an incident (e.g. loss of generation, increase in load).

In the past decade, the efficiency of PV and BS have improved, while their price has dropped significantly. As a result, it is anticipated that in the future a high portion of electricity will be generated locally by the customers. For instance, a recent transformational roadmap for the Australian FG published by the Australian Commonwealth Scientific and Industrial Research Organisation (CSIRO) and Australia Energy Network (AEN) suggests that by 2050 up to 50 % of electricity demand would be generated by the customers using DG technologies (i.e. predominantly PV and BS) [36]. The increasing penetration of DGs and price responsive users (i.e. users with PV and BS also referred to as prosumers) might

invalidate the conventional demand models [37]. This can have a significant impact on the stability of FG. Thus, in the following, we discuss the impact of prosumers for modelling net future demand.

Aggregated Demand Model Considering the Impact of Prosumers

Due to the important impact of loads on the stability of power systems, recent studies have attempted to integrate the aggregated impact of prosumers directly into the conventional demand models [38–41]. Although these models have shown their advantages for existing market structures, they are dependent on specific practical details, such as the electricity price signal or implementation of a mechanism for demand response (DR) aggregation. Consequently, they are computationally very expensive for applications, such as FG scenario studies. Furthermore, most of the existing models have focused on the interaction between the load aggregators/retailers and the prosumers in lower voltage levels [38, 39], so they are not useful for stability analysis. Few frameworks have attempted to represent the interaction between the wholesale electricity market and the load aggregators in higher voltage levels assuming an existing market structure [40, 41], however, they are intended for today's market modelling and/or operation studies. The studies in [12, 37] proposed *generic* frameworks in order to model net future demand by including the impact of prosumers in FG scenario studies. A key feature of such generic models is that they do not depend on specific practical details that will vary in the long-run. Note that the main purpose of developing such generic models is to provide accurate initial conditions/equilibria (i.e. dispatch decisions and net demand) for balancing and stability analysis of large numbers of FG scenarios. In our study, we will use the framework proposed in [37], (see Section 2.2).

1.2.2 Participation of Wind Generation in Frequency Control

Approximately 95 % of the wind turbines (WTs) installed capacity are VSWTs [42], either using Type III doubly fed asynchronous generators (DFAG), or Type IV, with a generator connected through a fully rated converter (FRC). The main reasons for the widespread adoption of VSWTs are their ability to optimise the power extraction over a wide range of wind speeds, as well as being able to comply with the grid codes' connection requirements. These capabilities are achieved by the use of power electronic converters, however, these converters de-couple WT's inertia from the system. Thus, high penetration levels of VSWTs can change the system frequency behaviour and can have wider implications on the system stability [5]. Thus, system operators around the globe have conducted series of studies to assess the dynamic behaviour of the system with high penetration levels of wind generation [2,

4, 43, 44]. For instance, the Australian Energy Market Operator (AEMO) conducted a series of studies to identify the issues related to high penetration levels of wind generation in the Australian NEM, and efficiently deal with those issues [43, 44]. Some of the critical issues highlighted in those studies were related to the system frequency control and inertial response. It was revealed in [44] that shifting from SGs to wind technologies can result in a significantly lower inertia level in the power system. This can result in a higher RoCoF, which consequently necessitates the need for other ancillary services, such as fast frequency response (FFR) [24], as well as increase the need for the current FCAS. Indeed, the FCAS market value has increased from \$25 M in 2012 to \$70 M in 2015 [26]. To overcome these issues, specifically during low demand and high penetration of NS-RES, it was suggested that a minimum inertia requirement for the system should be provided by SGs. This will result in curtailment of wind generation or other forms of inertia-less generations [43, 44]. Nonetheless, this can negatively impact the financial viability of wind generation. Another approach that can partially address this issue is that WFs should participate in frequency control and provide ancillary services, such as FFR, which is already a requirement in some jurisdictions [19]. This will, in turn, reduce the pressure on conventional generators and facilitate higher integration of wind generation in power systems [5, 45, 46]. According to [47], kinetic energy released by a WT exceeds that released by an SG, which makes wind generation very attractive to be used for inertial contribution and primary frequency control. The wind speed namely does not change significantly in short durations while the primary control is active, so the kinetic energy stored in rotors of WTs can be used in frequency control. Due to the effective decoupling between the mechanical and the electrical systems of VSWTs, this capability needs to be emulated through appropriate controllers.

Frequency Control by Wind Generation

Several techniques have been proposed for the participation of VSWTs in frequency control [18, 19, 48–51]. These techniques can be classified into *WTs' inertial response* and *de-loaded operation*. In WTs' inertial response, an additional control loop is required to link the inertia of a VSWT to the system [48]. This strategy exploits the rotational kinetic energy of a VSWT to deliver additional power to the system that is proportional to RoCoF. Thus, in such strategy, the VSWT initially operates in an optimal operation mode, and during a frequency event in a temporary overproduction mode, which is followed by an energy recovery period. In some references, this inertia is referred to as synthetic or virtual inertia [52]. In addition to the inertia control loop, authors in [49] proposed a primary frequency control loop. In this strategy, during a frequency event, the output power of the WT is proportional to the system frequency deviation. Nonetheless, during a frequency excursion, the inertial

response decreases the rotor speed of the WT, which consequently reduces the coefficient of performance. Recovery of the coefficient of performance requires kinetic energy, which should be provided by the grid. Extraction of kinetic energy from the grid can result in another frequency event [49, 53] (i.e. recovery period), which in some situations can be worse than the first one [54].

In contrast to the inertial response, where no energy is curtailed, in the de-loaded operation strategy, a VSWT should permanently operate in a sub-optimal mode with a lower coefficient of performance. The de-loading can be achieved by adjusting the pitch angle of the rotor blade in all wind speeds [18], or by increasing the rotor speed for lower wind speeds where the rotor speed is not maximum and adjusting the pitch angle for higher wind speeds where the rotor speed is maximum [19, 50]. A combination of these two methods was suggested in [51], where de-loading is achieved by a combined optimisation of rotor speed and blade pitch angle for the wind speeds where the rotor speed is not maximum. An advantage of the last two methods is that during a frequency excursion not only the WT increases its active power (i.e. due to an increase in the value of the coefficient of performance), but it also injects additional power from its kinetic energy into the system because of the rotor speed deceleration. There are different strategies for injection of the WT's kinetic energy into the system during a frequency excursion [20, 55]. In [20], an algorithm regulates the amount of kinetic energy as well as the power to be released into the system within a pre-defined time frame. While, in [55], an algorithm determines the amount of kinetic energy to be extracted from the WT based on the system frequency deviation.

Most of the studies on the participation of wind generation in frequency control have been conducted on either an individual WT model or an aggregated WF model, in which a WF is considered as a single WT [18, 19, 48–51]. Therefore, because of the aerodynamic coupling due to the wake effect, it is very difficult to quantify the actual contribution of WFs to frequency control. There are only a few studies that consider a more detailed WF model to assess its contribution in frequency control [56, 57]. In [56], it was shown that the inertial response, as well as frequency response of a WF, is significantly influenced by the wake effect. The authors in [57] propose an adaptive de-loading strategy for WFs using fuzzy control and optimise kinetic energy of a WF for frequency control. None of the above studies explicitly integrate the wake equations in the optimisation formulation of kinetic energy for frequency control. To quantify the contribution of WFs in the primary frequency control, and assess the operational flexibility that the WFs can provide to the system more accurately, it is crucial to consider a more realistic WF model, and investigate the aero-dynamical interaction among WTs within a WF. In the next section, we review and analyse the existing wake models to identify the most suitable wake interaction model for the purpose of this thesis.

Wind Farms Wake Models

WTs in a WF extract energy from the air mass which leaves the air mass with less energy and by implication lower speed than it had before passing the WT. This phenomenon which affects the active output power of the WF, and has mechanical impacts on the operation of WTs is called wake effect. Accurate wake modelling is a challenging task in a WF. Some of the factors which are considered for wake modelling are the distance between the WTs, the radius of the WTs, the geography of the site and the operating points of WTs. Study of wake interaction in a WF has several dimensions, e.g. turbulence intensity, wake loading, and wind speed deficit. However, our focus is on the wind speed deficit which is directly linked to the active power production of the WF.

Although both the electrical interconnection of WTs in a WF as well as the wake interaction among the WTs in a WF have been studied extensively [58–61], the coordinated control of WTs in a WF is less understood [62]. In [63], the coordinated control of WFs has been studied. However, the wake interaction among the WTs in the WF was not considered. In [64], the coordinated control of WFs, by considering the wake interaction, was studied. It was demonstrated that by selecting the operational set point of up-WTs intelligently, it is possible to improve the row efficiency of a WF. The concept of controlling the operational set point of up-WTs to optimise the total output power of the WF was further developed in [65]. It was shown that by coordinating the power production of individual WTs, it is possible to increase the total output power of the WF. This was done by operating the up-WTs in a sub-optimal operation mode to curtail some power, and operating the down-WTs in the optimal operation mode to capture the curtailed power of up-WTs. Further investigation on the concept of coordinated control of WTs in a WF requires a deep understanding of wake interaction among WTs in a WF.

Wake models fall into two broad categories: (i) experimental and (ii) analytical. *Experimental wake models* are based on measurements from the WFs [66] and are specific to those WFs. Therefore, with the experimental wake models, it is very difficult to make general conclusions regarding the operation of WFs under different operational strategies. *Analytical wake models* are based on the laws of fluid dynamics, i.e. global momentum conservation [58] and can be classified into subclasses, e.g. kinematic models, field models, and roughness element models. *Kinematic models* are based on conservation of momentum and start by modelling a single wake for a WF. Although these models are very simple and suitable for large WFs, it is very difficult to justify their accuracy because of some of the assumptions which are made in formulating these models [58]. Some well-known kinematic models are Jensen's model [67] and Frandsen's model [68]. *Field models* give wind speed at every point behind a WT [58], so computationally they are more complicated to implement.

Roughness element models are subdivided into infinite cluster models and finite cluster models. In the infinite cluster models, a WF is considered as a single element and the effect of individual WTs are lost. Whereas, the finite cluster models give the wind speed in each row of the WTs. Most of these wake models are not suitable for control purpose because either they are too complicated or unreliable.

A *Stationary wake model* which was recently developed in [65] is a suitable wake model for the control purposes because it requires minimum data, and its parameters have clear representation. Furthermore, this wake model is very accurate for a single row of WTs, but in a WF with multiple rows of WTs, the wake of up-WTs which are not right in front of the down-WT or partial shadow of neighbouring rows should also be considered. The stationary wake model maps the thrust coefficient of up-WTs, which is directly linked to the wind speed deficit and the operational set point of up-WTs, to identify and calculate their effects on the down-WTs. Using this model, in a WF with ten WTs in a row, it was shown that by operating the up-WT in a sub-optimal mode, it is possible to increase the total output power of the WF by up to 5 % [65]. The operation of up-WTs in the sub-optimal mode results in extraction of less energy and by implication lower coefficient of thrust leaving the wind speed with higher energy which can be captured by down-WTs. It was shown that the coefficient of thrust is a function of the power extracted by the WT's rotor blade. Therefore, an increase in the rotor speed results in a higher coefficient of thrust which in turn increases the wind speed deficit. On the other hand, an increase in the pitch angle results in a lower coefficient of thrust which in turn decreases the wind speed deficit. An experimental investigation in a WF with two WTs in a row shows that the operation condition of the up-WT, namely the blade pitch angle position, and the distance between the up-WT and the down-WT affect the power production of the down-WT [66]. It was demonstrated that by de-loading the up-WT using pitch angle, it is possible to increase the output power of the WF by 12 %. Thus, to optimise the total output power of the WF by curtailment of up-WTs, it is very important to assess the sub-optimal operation strategies (discussed in Section 1.2.2) and implement the most suitable strategy. Despite the fact that the aims of developing a coordinated control strategy for a WF in [64–66] were to improve the row efficiency of a WF, the results of their studies create a potential opportunity for providing frequency control service by de-loading of up-WTs in a WF, as discussed in Section 1.2.2.

1.3 Research Questions

Studies of FGs with high penetration levels of NS-RES suggest that the system frequency control will become a challenging task, however, it is very difficult to quantify their findings

and make general conclusions, because most of those studies are based on specific networks (sometimes a simplified copperplate model of the network) under a specific operation condition. Furthermore, the impact of market dynamics, as well as emerging technologies, such as prosumers on system frequency performance, have been overlooked. Considering these, some of the fundamental issues that need to be addressed are as follows:

- How does the reduced amount of inertia affect the frequency performance of FGs, and which metrics should be used for assessing the frequency stability of the system? In conventional power systems, a normalised inertia constant is used for measuring the level of inertia and assessing frequency performance of a system; whereas, with a high penetration level of non-synchronously connected resources this might not be valid.
- What are the impacts of prosumers and market dynamics on the performance and frequency stability of a power system?
- Considering the intermittent nature of RES, prosumers and market dynamics, how can we assess the frequency performance of the FGs in a systematic way? Furthermore, how much NS-RES can be integrated into a system without violating system frequency stability limits?
- How can we enhance the flexibility of the system and improve the frequency performance of FGs by utilising different resources, and how can we quantify the contribution of those resources on the frequency control?
- Can wind generation provide frequency support, and to what extent? So far, the technical ability of VSWT to provide frequency support has been examined; whereas, to accurately quantify the amount of support that wind generation can provide, the level of support needs to be quantified in WF as well as system level. Furthermore, what would be the optimal way for a WF to participate in frequency control?

1.4 Research Contribution

The answers to the above questions lead us to the aims of this research thesis, as summarised in the following.

In Chapter 2, we study the impact of high penetration levels of NS-RES and different penetration levels of prosumers on the performance and frequency stability of the Australian FG. By doing this, we quantify the connection between the NS-RES and the system frequency response, as well as different penetration levels of prosumers on the system frequency

response. Also, we show that the frequency response of the system can be sensitive to different BS capacities of prosumers. We have also shown that to maintain system frequency stability within its allowable bounds, it is very important to incorporate security constraints in the market dispatch model. Therefore, to identify the most relevant and accurate metric that has to be considered as a frequency control security constraint in the market dispatch model, we consider three different metrics, namely i) minimum power penetration from synchronous generators, ii) minimum rated power of synchronous generators, and iii) minimum synchronous kinetic energy, as frequency control security constraints in the market dispatch model. We assess the impact of the above constraints on the performance and frequency stability of the system and show that the former one is the most relevant one.

Chapter 3 proposes a frequency performance assessment framework based on a time-series approach that facilitates the analysis of a large number of FG scenarios. We use this framework to assess the frequency performance of the Australian FG by considering a large number of future scenarios and sensitivity of different parameters. By doing this, we identify a maximum non-synchronous instantaneous penetration range from the frequency performance point of view. Further, to reduce the detrimental impacts of high NS-RES penetration on system frequency performance, a dynamic inertia constraint is derived and incorporated into the market dispatch model. The results show that such a constraint guarantees frequency stability of the system for all credible contingencies. Also, we assess and quantify the contribution of synchronous condensers, the synthetic inertia of wind farms and a governor-like response from the de-loaded wind farms on system frequency performance. The results show that the governor-like response from WTs is the most effective one. Note that enforcement of the inertia constraint results in curtailment of wind energy. We show that by curtailing wind energy in a coordinated way, we can add more flexibility to the system. This is done by de-loading the WTs and engaging them in frequency control using a governor-like response, which not only improves the RoCoF and the frequency nadir but it also improves the settling frequency following a contingency.

In Chapter 4, we propose an optimal operation strategy for the participation of WFs in frequency control. In this strategy, we maximise the rotational kinetic energy of the WTs within a WF by an optimal combination of their rotor speeds and pitch angles. We do this by exploiting the wake interaction in a WF, and de-loading some of the up-WTs. The results show that the kinetic energy accumulated in the rotating masses of WTs can be increased compared to the base case without compromising the row efficiency of a WF. Furthermore, we propose a control strategy for the participation of WFs in primary frequency control. In this strategy, we control the injection of WTs' rotational kinetic energy into the system during a frequency excursion. This is done by controlling the rate of change of the WTs' rotor

speed based on the RoCoF and the frequency deviation after a contingency. By implementing the proposed operation and control strategies in a test system, we show that the frequency response of the system can significantly improve after an incident.

In Chapter 5, we further develop the concept of WF participation in frequency control discussed in Chapter 4 and propose a coordinated operation strategy for WFs. In contrast to the conventional WF operation strategy, where each wind turbine (WT) is optimised individually, three operation strategies are suggested: 1) maximisation of the WF's power while maintaining WF's rotational kinetic energy; 2) maximisation of the WF's rotational kinetic energy while maintaining WF's output power; and 3) a de-loaded strategy whereby the WF's rotational kinetic energy is maximised for a fixed de-loading margin. The three operation strategies are formulated as nonlinear optimisation problems and solved in a central wind farm controller. The optimal rotor speeds and pitch angles are used as reference values in the individual WTs. The optimisation results for the three respective operation strategies show that: 1) up to 3 % increase in the WF's output power; 2) up to 23 % increase in the WF's rotational kinetic energy; and 3) up to 28 % increase in the WF's rotational kinetic energy and 8 % reserve power while operating the WF in a 5 % de-loaded mode with respect to the conventional operation strategy. Time-domain simulations show that the proposed operation strategy noticeably improves the WF's performance in frequency control.

Finally, Chapter 6 concludes this research thesis and provides some directions for potential future works related to this thesis.

Chapter 2

Impact of Prosumers and Security Constraints on Frequency Performance of FGs

2.1 Introduction

As described in Chapter 1, a high uptake of prosumers¹ and NS-RES will influence the performance and stability of FGs. The conventional power system operation and stability have been extensively studied and are well understood [1]; however, the inclusion of emerging technologies, e.g. distributed generation (DG), battery storage (BS) and non-synchronous renewable energy sources (NS-RES) with different dynamic behaviour changes the performance and stability of future grids (FGs) in new ways that have not been experienced previously. Thus, it is important to assess and quantify the impact of the aforementioned changes on the performance and stability of FGs. Therefore, in the first part of this chapter, we assess the impact of high penetration levels of prosumers as well as NS-RES on the performance and frequency stability of the Australian FG to quantify their impacts. The outcome of this part is published as a conference paper in [CP4]. In the second part of this chapter, to improve the frequency performance of FGs, we incorporate frequency control security constraints into the market dispatch model and assess their impacts on the performance and frequency stability of the Australian FG. By doing this, we identify the most relevant constraint that has to be integrated into the market dispatch model as a frequency control security constraint. The outcome of this part is also published as a conference paper in [CP3].

¹Consumers equipped with DG (e.g. rooftop-PV and BS) are referred to **prosumers** (producer - consumer).

The remainder of this chapter is organised as follows: in Section 2.2, we study the impact of prosumers on the performance and frequency stability of the Australian FG. In Section 2.3, we assess the minimum inertia requirement of FGs by considering different security constraints, and finally, Section 2.4 summarises the chapter.

2.2 Impact of Prosumers on Frequency Performance

This section aims to explore the impact of high penetration levels of NS-RESs as well as different penetration levels of prosumers on the operation and frequency stability of the Australian FG. Given that the increasing renewable penetration will likely require different market structures, we have adopted a generic modelling framework initially proposed in [12, 37]. Our framework, therefore, is market structure agnostic, is based on a bi-level optimisation problem [12] in which a modified unit-commitment (UC) problem is taken as the upper-level optimisation (leader problem) aiming to minimise the total electricity costs. In the lower-level (follower problem) the aggregation of prosumers is formulated so that they maximise self-consumption of rooftop-PV generation by employing BS system. To capture the inter-seasonal variation of RESs, we use a time-series approach to assess the frequency performance of the system for a whole year.

2.2.1 Modelling Framework

In this section, we use the simulation platform presented in [10], which considers the market simulation, power flow calculation, and stability assessment altogether. Our market model is the generic framework in [12], which is based on a bi-level optimisation problem. The upper-level optimisation is a modified UC problem aiming to minimise the total electricity cost, and the lower-level optimisation represents the aggregation of prosumers aiming to maximise their self-consumption. The detailed formulation is explained in the following.

Leader Problem

The aim of the objective function (UC problem) is to minimise the total electricity cost as follows:

$$\underset{s_{g,h}, u_{g,h}, d_{g,h}, p_{g,h}, \delta_{i,h}}{\text{minimise}} \sum_{h \in \mathcal{H}} \sum_{g \in \mathcal{G}} \left(c_g^{\text{fix}} s_{g,h} + c_g^{\text{su}} u_{g,h} + c_g^{\text{sd}} d_{g,h} + c_g^{\text{var}} p_{g,h} \right), \quad (2.1)$$

where $s_{g,h}, u_{g,h}, d_{g,h} \in \{0, 1\}$, $p_{g,h} \in \mathbb{R}^+$, $\delta_{i,h} \in \mathbb{R}$ are the decision variables of this problem. The objective function is subject to the following constraints:

$$\sum_{g \in i} p_{g,h} = \sum_{m \in i} (p_{d,h}^{\text{inf},m} + p_{d,h}^{\text{flx},m}) + \sum_{\forall j} (p_{l,h}^{i,j} + \Delta p_{l,h}^{i,j}), \quad (2.2)$$

$$p_{l,h}^{i,j} = B_{i,j}(\delta_{i,h} - \delta_{j,h}), \quad (2.3)$$

$$\underline{p}_l^{i,j} \leq p_{l,h}^{i,j} \leq \bar{p}_l^{i,j}, \quad (2.4)$$

$$\underline{p}_g s_{g,h} \leq p_{g,h} \leq \bar{p}_g s_{g,h}, \quad (2.5)$$

$$u_{g,h} - d_{g,h} = s_{g,h} - s_{g,h-1}, \quad (2.6)$$

$$\sum_{g \in \mathcal{G}_{\text{synch}}} \bar{p}_g s_{g,h} \geq \sum_{m \in r} (p_{d,h}^{\text{inf},m} + p_{d,h}^{\text{flx},m}) + p_{r,h}^{\text{res}}, \quad (2.7)$$

$$u_{g,h} + \sum_{\tilde{h}=0}^{\tau_g^u-1} d_{g,h+\tilde{h}} \leq 1, \quad (2.8)$$

$$d_{g,h} + \sum_{\tilde{h}=0}^{\tau_g^d-1} u_{g,h+\tilde{h}} \leq 1, \quad (2.9)$$

$$-r_g^- \leq p_{g,h} - p_{g,h-1} \leq r_g^+. \quad (2.10)$$

Constraint (2.2) is the power balance equation for the demand and supply at each node of the system. $p_{d,h}^{\text{inf},m}$, $p_{d,h}^{\text{flx},m}$, $p_{l,h}^{i,j}$ and $\Delta p_{l,h}^{i,j}$ represent the inflexible and flexible power demand of aggregator m , transmission line (TL) power and losses between nodes i and j in the system in slot h , respectively. Flexible demand power of each load aggregator, $p_{d,h}^{\text{flx},m}$, reflects the aggregated impact of prosumers and is determined in the follower problem. Note that the interaction between the leader and the follower problems is through the flexible demand of each prosumer aggregator $p_{d,h}^{\text{flx},m}$. Constraint (2.3) represents the transferred power between different nodes in the system, and it is constrained by the TLs' limits in (2.4). The dispatch level of each generator is constrained between its minimum and maximum stable limits in (2.5). Constraint (2.6) represents the on/off status of thermal units. To deal with the unpredictability of loads and generations, a minimum of 10 % spinning reserve is considered in (2.7). Constraints (2.8) and (2.9) assure that the minimum up and minimum down time restriction of generators are considered. Finally, constraint (2.10) restricts the changes in dispatch level of generators within their permissible ramp rates.

Follower Problem

The follower problem aims to integrate the aggregated effect of prosumers into the UC problem using the bi-level optimisation framework. In each node, consumers are divided into

flexible (i.e. prosumers) and *inflexible* users. Note that prosumers aim to minimise their feed-in power from the grid by exploiting the flexibility of their BS as follows:

$$\underset{p_{b,h}^m}{\text{minimise}} \sum_{h \in \mathcal{H}} p_{d,h}^{\text{flx},m}, \quad (2.11)$$

the decision variable of the follower problem is, $p_{b,h}^m \in \mathbb{R}$, and is subjected to the following constraints:

$$p_{d,h}^{\text{flx},m} = p_{d,h}^{u,m} - p_{pv,h}^m + p_{b,h}^m, \quad (2.12)$$

$$\underline{p}_{d,h}^{\text{flx},m} \leq p_{d,h}^{\text{flx},m} \leq p_{d,h}^{u,m} + \bar{p}_b^m, \quad (2.13)$$

$$\underline{p}_b^m \leq p_{b,h}^m \leq \bar{p}_b^m, \quad (2.14)$$

$$\underline{e}_b^m \leq e_{b,h}^m \leq \bar{e}_b^m, \quad (2.15)$$

$$e_{b,h}^m = \eta_b^m e_{b,h-1}^m + p_{b,h}^m. \quad (2.16)$$

Constraints (2.12) represent the power balance of prosumers in which part of the required power is supplied by rooftop-PV and the remainder from the grid and/or BS. Notice that the BS can either supply or consume power depending on its state of charge (SoC) as well as the optimisation results. The flexible demand of each load aggregator, $p_{d,h}^{\text{flx},m}$, reflects the aggregated effect of prosumers, and it is bounded between the minimum and the maximum limits in (2.13). Notice that, $\underline{p}_{d,h}^{\text{flx},m}$, can be either positive (i.e. where the prosumers do not send power back to the grid), or negative (i.e. where the prosumers send their excess power back to the grid). Finally, to ensure that the prosumers' BS power and SoC remain within the limits at all time, constraints (2.14) - (2.16) are introduced.

Although the follower problem individually is similar to a home energy management (HEM) problem, its aim is to minimise feed-in power from the grid, whereas, the traditional HEM problems' objective is to minimise the total energy cost. As discussed in [12] in detail, due to the inclusion of the Karush Kuhn Tucker (KKT) optimality conditions along with complementarity slackness variables of the follower problem in the constraints of the leader problem, the price signal is not needed in the objective of the follower problem. The proposed model is formulated as a mixed-integer linear programming (MILP), which can be solved using an off-the-shelf solver.

2.2.2 Test Model and Scenarios

We use the simplified 14-generator model of the Australian NEM as the test system² [69, 70]. The hourly demand, wind and solar traces are extracted from the Australian National Transmission Network Development Plan (NTNDP) in 2040 [71]. The generation portfolio is inspired by the 100 % renewable studies in Australia [8, 72] including WFs, utility-PVs, concentrated solar thermal (CSTs), hydro turbines, and biogas turbines (GT) with installed capacities of 55 GW, 6.4 GW, 3.6 GW, 9 GW, and 33 GW, respectively. All WFs are modelled as Type IV wind turbine generators, and all utility-PV plants are modelled as full converter interface generators. The CST, hydro and GT plants are modelled as SGs, and their governor, excitation system and power system stabilisers are adopted from [69]. Since the inertia contribution of a synchronous power plant is directly related to the number of online units within a power plant, each SG is modelled explicitly. We simulate the system and compare the results for the three scenarios described below:

- **PBS-Z:** As the base scenario, a conventional demand model is considered with no prosumers.
- **PBS-L:** The percentage of prosumers with BS for NSW, VIC, QLD, and SA are 26 %, 29 %, 17 %, and 10 %, respectively inspired by the Australian Energy Market Operator (AEMO) [73]. Further, BS capacity of 1.8 kWh per 1 kW of rooftop-PV is considered [73].
- **PBS-H:** It is assumed that all the prosumers have installed BS system, with a capacity of 3 kWh per 1 kW of rooftop-PV.

Note that in Scenarios **PBS-L** and **PBS-H**, the rooftop-PV capacity of prosumers in NSW, VIC, QLD, and SA are 5.5 GW, 5.4 GW, 6.9 GW, and 2.8 GW, respectively [73]. The prosumers correspond to 33 %, 35 %, 40 %, and 45 % of the total load in those states.

2.2.3 Simulation Results

We used the generic framework (Section 2.2.1) to provide the initial condition/equilibrium (i.e. net demand and dispatch results) for power flow studies. The power flow results are used as the initial conditions for the frequency stability assessment of the system.

²We have only considered the inter-state TLs' limits between the states, i.e. Queensland (QLD), New South Wales (NSW), Victoria (VIC), and South Australia (SA).

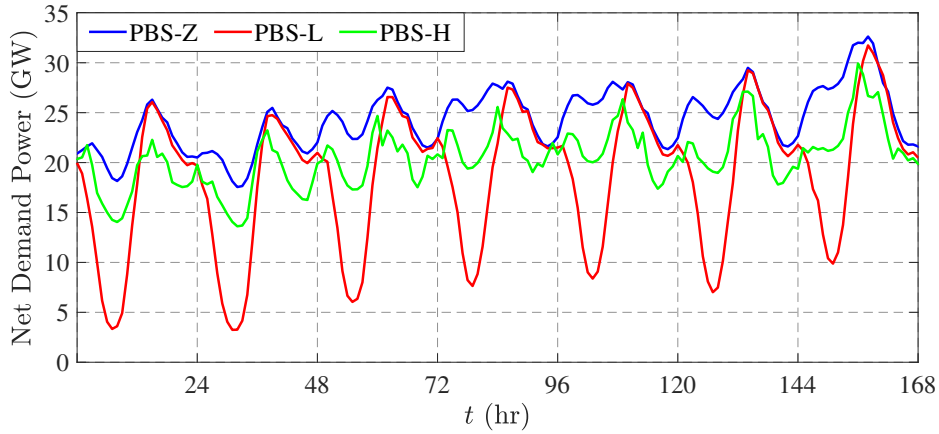


Fig. 2.1 Demand profile of the NEM for a typical summer week.

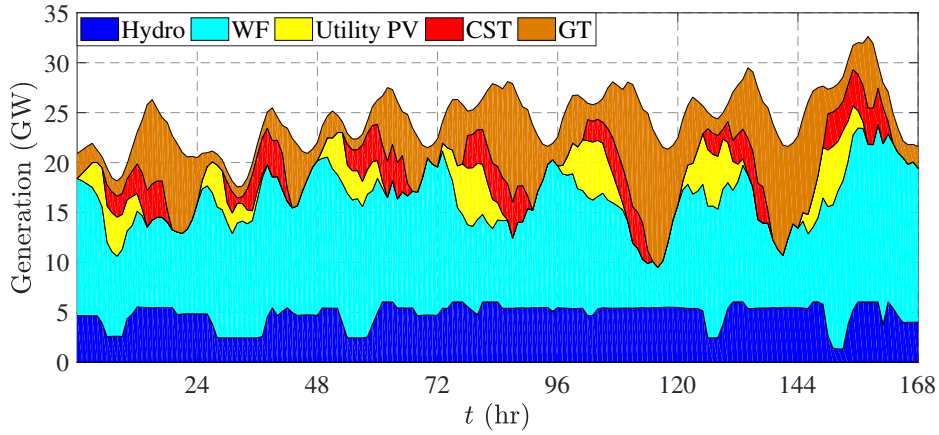
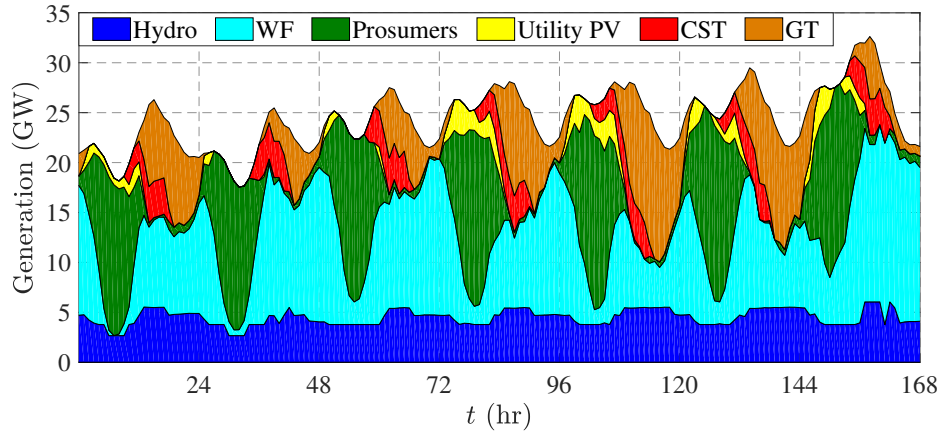
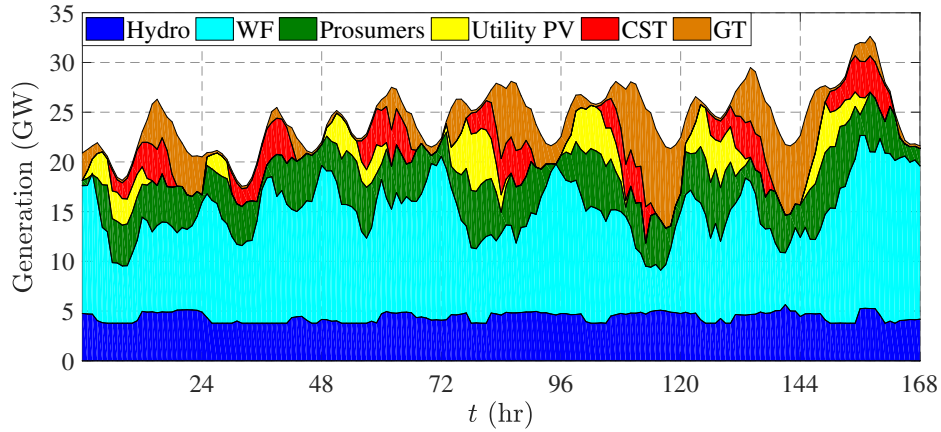


Fig. 2.2 Balancing results for a typical summer week for Scenario **PBS-Z**.

Market Dispatch Results

We performed simulations for the three scenarios introduced in Section 2.2.2 for the year 2040. Fig. 2.1 compares the net demand profile for the three scenarios for a typical summer week in the NEM. Notice that with a lower BS capacity (i.e. Scenario **PBS-L**) during the sunlight hours, the prosumers send their excess rooftop-PV generation back to the grid when it exceeds their power requirement and BS capacity. So, during the sunlight hours in Scenario **PBS-L**, the prosumers' net demand is negative. As a result on average, there is a 75 % reduction in the minimum net demand of the system, whereas the net peak demand slightly reduces compared to the conventional Scenario **PBS-Z**. This not only increases the ramp rate requirement of the system, but it also has negative impacts on the system frequency performance as discussed in the next subsection. On the other hand, with a higher BS capacity (i.e. Scenario **PBS-H**) of prosumers, the system net peak demand reduces

Fig. 2.3 Balancing results for a typical summer week for Scenario **PBS-L**.Fig. 2.4 Balancing results for a typical summer week for Scenario **PBS-H**.

significantly, and the net demand becomes smoother. In this scenario, the prosumers exploit the flexibility of their high BS capacity, and store most of their excess energy during the day, and utilise it during the peak hours (i.e. usually expensive hours) in order to maximise their self-consumption. This not only reduces the total electricity cost of the prosumers, but it also decreases the ramping stress (due to a flatter net demand profile) which has positive effects on the system frequency performance as discussed in the next subsection.

For a typical week, Figs. 2.2, 2.3 and 2.4 show the system's balancing results including the prosumers' contribution for Scenarios **PBS-Z**, **PBS-L** and **PBS-H**, respectively. Observe that in Scenario **PBS-Z**, wind dominates the generation portfolio, and there is not much ramping requirement from the SGs. Whereas, in Scenario **PBS-L**, because of the prosumers contribution during the day, the system's ramp-up/down requirement is very high. Nonetheless, in Scenario **PBS-H**, due to a higher BS capacity of prosumers and flatter demand

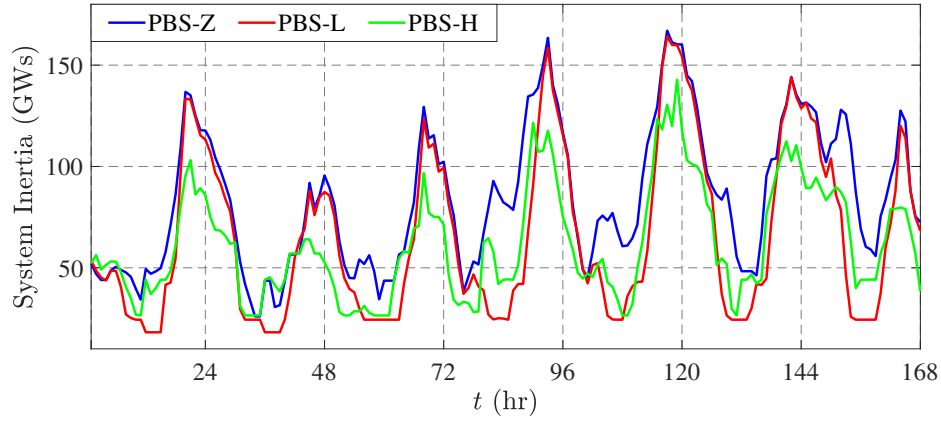


Fig. 2.5 Inertia of the system for a typical summer week.

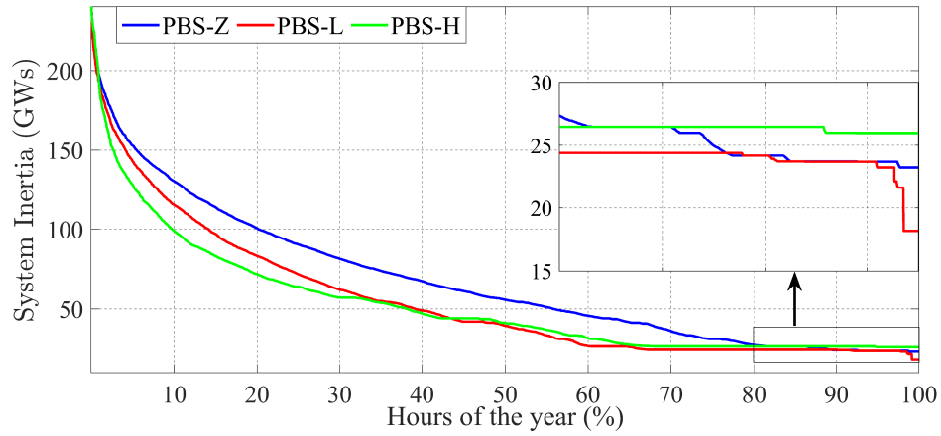


Fig. 2.6 Inertia duration curve of the system for a whole year.

profile, both the ramp rate requirement of the system, as well as the wind generation and GT generation are reduced. Fig. 2.5 illustrates the inertia of the system for the same horizon. Observe that in Scenario **PBS-L** the system inertia is more variant and it is the lowest during the hours that the prosumers send their excess rooftop-PV power back to the grid. This is due to the fact that on those hours the number of online SGs is minimum in the system. Fig. 2.6 evaluates the inertia of the system for the whole year. Observe that for all scenarios in approximately 80 % of the year, the inertia of the system is above 25 GWs, whereas, in the remaining 20 % of the time, which is very critical for the system frequency performance because the system inertia is very low, Scenarios **PBS-H** and **PBS-L** have the highest and the least amount of inertia, respectively.

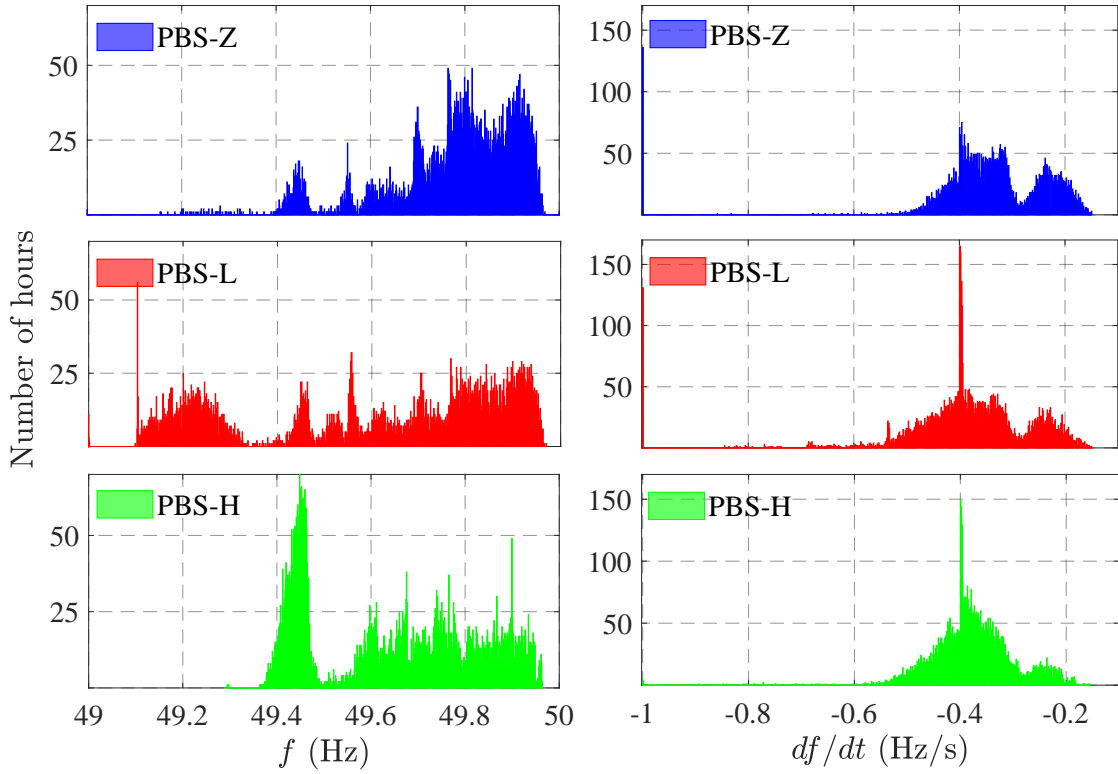


Fig. 2.7 Histogram of the minimum RoCoF and frequency nadir for the studied year.

System Frequency Performance

We assess the frequency performance of the system in every hour for the whole year by considering the loss of the largest in-feed unit (i.e. 444.4 MW) as a contingency. The minimum RoCoF and the frequency nadir of the system are summarised in Fig. 2.7. Observe that with the increased penetration of prosumers and low BS capacity (i.e. Scenario **PBS-L**), the number of hours that violates the minimum RoCoF limit (i.e. $-0.5 \frac{\text{Hz}}{\text{s}}$ [2, 35]) and the minimum system frequency limit (i.e. 49.5 Hz [74]) are the highest. This is mainly due to the fact that during the day prosumers do not have sufficient BS capacity, and send their excess rooftop-PV generation back to the grid, which results in a minimum level of synchronous capacity in the system as shown in Fig. 2.3. Whereas, in Scenario **PBS-H**, the total number of hours that both the RoCoF and the frequency nadir are violated has reduced significantly compared to Scenario **PBS-L**. This is because of a higher BS capacity in Scenario **PBS-H** that allows the prosumers to store most of their excess rooftop-PV generation rather than sending it back to the grid. This, in turn, results in a flatter net demand profile in the system and a more uniform operation of SGs as shown in Fig. 2.1. Note that the system frequency performance is directly related to the synchronous capacity of the system. Hence,

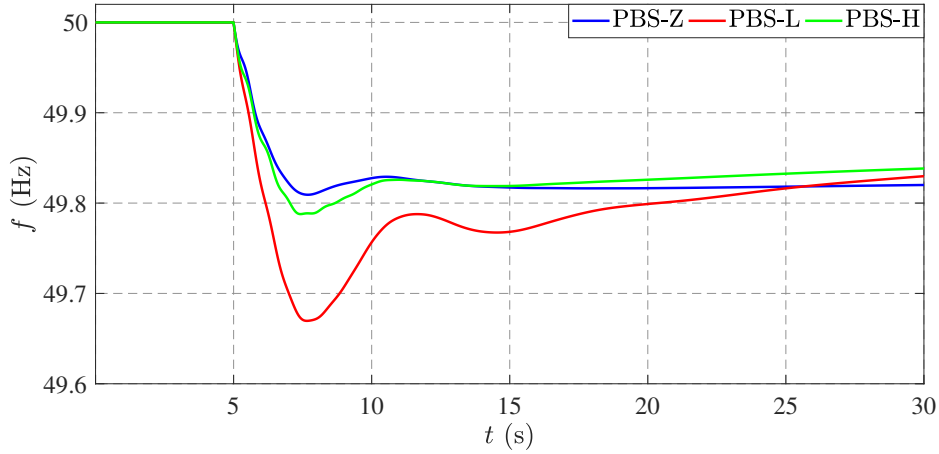


Fig. 2.8 System frequency behaviour after a contingency for a typical hour ($t = 132$ h).

in Scenario **PBS-Z**, the synchronous capacity is more than Scenarios **PBS-L** and **PBS-H** most of the hours, thus the system frequency response is better. Further, Fig. 2.8 illustrates the frequency behaviour of the system for a typical hour for all three scenarios. Observe that in Scenario **PBS-L** both the RoCoF and the frequency nadir is the lowest. It has to be mentioned that the automatic generation control (AGC) is not considered in this section, so there is an error in the steady-state frequency of the system. In the next section, we assess the impact of different frequency control security constraints on the performance and frequency stability of the Australian future grid.

2.3 Impact of Security Constraints on Frequency Performance

In the previous section, it was shown that with the increasing penetration of NS-RES and prosumers, maintaining system frequency stability would be a challenging task. While prosumers with higher BS capacity can improve the system frequency response to some extent, there might be a need to include some metrics in future electricity markets, either in the form of constraint or as an ancillary service market. By doing this, we can assure that the system frequency response is within its permissible bounds. So far, several technical options have been proposed for addressing system frequency control constraints. Introducing a non-synchronous instantaneous penetration (NSIP) limit is one possible approach, which necessitates a certain proportion of synchronous generation to operate continuously at all times. For example, EirGrid in Ireland has introduced a maximum NSIP level of 50 %, with an ongoing review, and an ultimate aim to increase this limit to 75 % [25]. Also, in [2], it was

suggested that at least 20 % to 30 % of power in the grid should be supplied by SGs, or the ratio of system kinetic energy over the power of the largest in-feed generator should be larger than 20 s (i.e. $\frac{E_{k_{sys}}}{P_{Linf}} \geq 20 \frac{MW_s}{MW}$) for the Ireland's All Island system. In the 100 % Australian renewable scenario, the AEMO has considered a minimum of 15 % synchronous generation in the NEM [8].

It has to be mentioned that the RoCoF and the frequency nadir are functions of the system's kinetic energy and the SGs' response, respectively [1, 75]. In this respect, neither a single NSIP nor the minimum level of synchronous generation provides accurate information about the parameters that contribute to frequency control, such as system kinetic energy and SGs' governor responses. Indeed, it was shown in [30] that for NSIP ranging from 65 % to 80 %, it might be possible to have the same number of online SGs, i.e. the same amount of rotational kinetic energy and similar governor response. Another approach would be to consider the rated power of SGs as a constraint because the inertial response of an SG is related to its rated apparent power not to its operating point. Another more detailed approach for a minimum frequency constraint was introduced in [76], in which the constraint is a function of the system kinetic energy, UFLS relays' setting, RoCoF relays' setting, and the size of a single possible contingency. Note that those parameters are system specific and might vary in different jurisdictions as discussed in Section 1.2.1. Hence, in this section, we explore the impact of different frequency control security constraints on the operation and frequency performance of the Australian FG, and, moreover, introduce a more precise metric for the frequency control security constraint. To do this, we assess the performance and frequency stability of the NEM with a high penetration of NS-RES by considering three different approaches: i) minimum power penetration from SGs, ii) minimum rated power of SGs, and iii) minimum synchronous kinetic energy. Given that the increasing renewable penetration will likely require different market structures, we have adopted a generic modelling framework, previously used in major national FG studies in Ireland [2], the US [4], and continental Europe [6]. Similar to Section 2.2.1, the framework is based on a modified UC problem that considers the frequency control security constraints using the three mentioned approaches.

2.3.1 Market Model and Inputs

In this section, we consider a 100 % renewable scenario by using NEM's predicted data for 2020. The generation portfolio is inspired by the 100 % renewable studies in Australia [72, 8]. In [72], the least-cost mix of diverse renewable technologies is: WFs, hydro turbines, biogas turbines, utility-PV, and CST. For this section, hourly demand, wind, and solar data are obtained from AEMO's predictions for 2020 [71].

The market dispatch model is similar to the market model of Section 2.2.1; however, we use the conventional demand models in this Section, which allows us to assess the sole impact of the frequency control constraints using three different approaches: i) minimum power penetration from synchronous generators, ii) minimum rated power of synchronous generators, and iii) minimum synchronous kinetic energy. In the market simulation, we assume that the SGs (i.e. bio-GT and hydro) bid at their respective short-run marginal costs (SRMC), estimated using the predicted fuel price, thermal efficiency, and variable operation and maintenance (O&M) in 2020 [71], while CST, WFs, and utility-PVs bid with zero SRMC. The UC problem aims to minimise the total electricity cost. For the optimisation problem, the decision horizon is divided into one hour time steps. The objective function of the UC problem is given in (2.1). Note that constraints (2.5), (2.6), (2.8), (2.9) and (2.10) introduced in Section 2.2.1 (leader problem) are applicable here; whereas, constraints (2.2) and (2.7) change to constraints (2.17) and (2.18), respectively. Furthermore, frequency control security constraints are also incorporated in the market dispatch model.

$$\sum_{g \in \mathcal{G}} p_{g,h} = p_h^{\text{load}} \quad \forall h, \quad (2.17)$$

$$\sum_{g \in \mathcal{G}_{\text{synch}}} s_{g,h}(\bar{p}_g - p_{g,h}) \geq p_h^{\text{res}} \quad \forall h. \quad (2.18)$$

Inertia Based Frequency Control Security Constraint

In a system with constant power load, the initial RoCoF is directly related to the system inertia and the amount of power imbalance during an incident, as given by:

$$\frac{df}{dt} = \frac{f_0}{2HS_B}(\Delta P_g - \Delta P_l), \quad (2.19)$$

where f_0 is the system frequency prior to the incident, H is the aggregate inertia constant of the system, S_B is the total rated power of the generators [77], ΔP_g is the difference between the generation before and after the incident, and ΔP_l is the difference between the load before and after the incident. For a synchronous generator, H_g is defined as [1]:

$$H_g = \frac{\text{stored energy at rated speed (MWs)}}{\text{MVA rating}}. \quad (2.20)$$

We can use (2.20) to calculate the inertia constant of a grid that is equipped with synchronous generators only. However, as the penetration of non-synchronous generation increases, the MVA rating of the system increases, whereas the stored kinetic energy of the

system decreases. In this regard, there is no clear definition for MVA rating of the grid in (2.20). For instance, in [77] the MVA rating of all generators are included, whereas in [78] only the MVA rating of SGs are considered. Therefore, it is essential either to define the aggregated inertia of the system more precisely or to use the actual quantity of the system kinetic energy in (2.19). The kinetic energy accumulated in the rotating masses of SGs is given as:

$$I_{\text{synch}} = \sum_{i=1}^N H_{g,i} S_{B,i}, \quad (2.21)$$

where $H_{g,i}$ and $S_{B,i}$ are inertia constant, and rated MVA of generator i , respectively, and N is the number of SGs in the system. Thus, in this section, we consider the actual quantity of system kinetic energy to assess the impact of different frequency control security constraints on performance and frequency stability of the system. We simulate the system and compare the results for the four cases described below. Notice that for all cases constraints (2.5), (2.6), (2.8), (2.9), (2.10), (2.17) and (2.18) are considered.

- **NoIC**: As the base case, we do not consider the inertia constraint.
- **SgN30**: The available capacity of SGs is 30 % of total demand.

$$\sum_{g \in \mathcal{G}_{\text{synch}}} s_{g,h} \bar{S}_g \geq 0.3 S_h^{\text{load}} \quad \forall h. \quad (2.22)$$

- **Ek30**: We consider a minimum synchronous kinetic energy of 30 % compared to the situation where the system was equipped with SGs only with an average inertia constant of ($H_{\text{sys}} = 4$ s).

$$\sum_{g \in \mathcal{G}_{\text{synch}}} s_{g,h} H_g \bar{S}_g \geq 0.3 H_{\text{sys}} S_h^{\text{load}} \quad \forall h. \quad (2.23)$$

- **SgP30**: SGs should supply at least 30 % of total demand.

$$\sum_{g \in \mathcal{G}_{\text{synch}}} p_{g,h} \geq 0.3 p_h^{\text{load}} \quad \forall h. \quad (2.24)$$

For all three constraints, the model above is a MILP, which can be solved efficiently using an off-the-shelf solver.

Table 2.1 Parameters of synchronous generators.

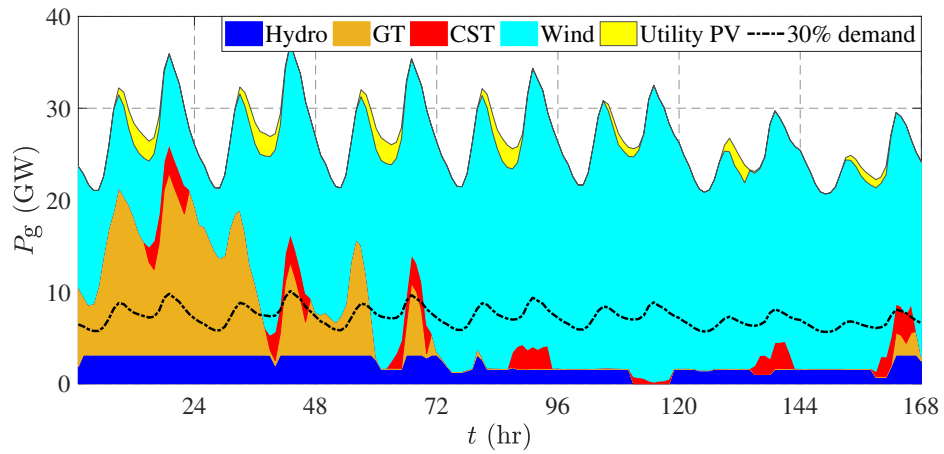
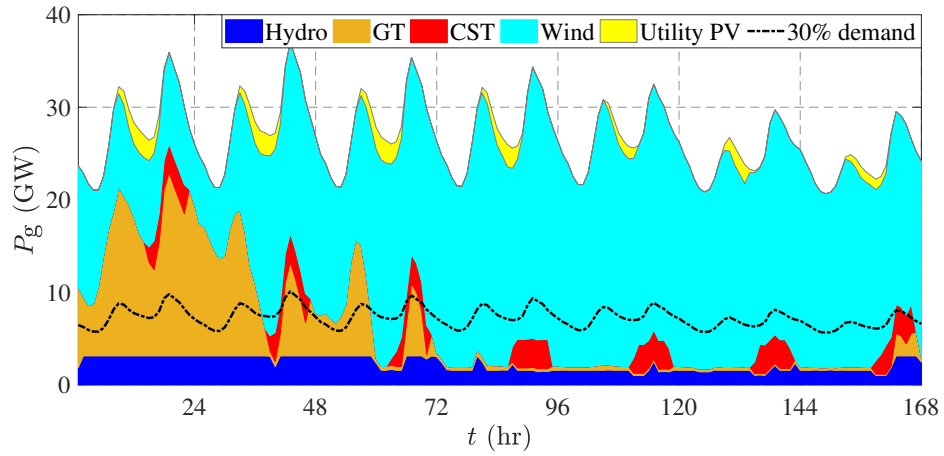
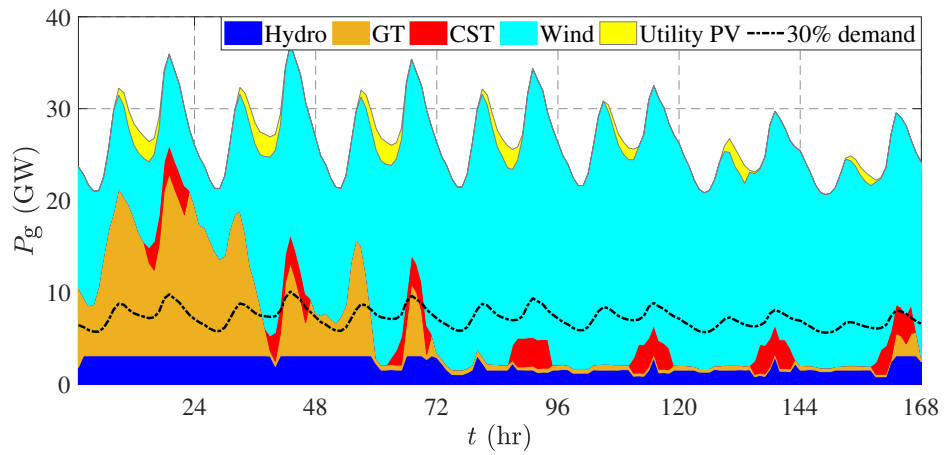
Generation Technology	Unit Size (MVA)	Max .No Units	Inertia Constant (s)	Governor Model
Hydro-1	333.3	6	4	HYGOV
Hydro-2	444.4	1	"	"
Hydro-3	333.3	2	"	"
Biogas-1	444.4	16	6	GAST
Biogas-2	333.3	16	"	"
Biogas-3	444.4	12	"	"
Biogas-4	444.4	25	"	"
Biogas-5	250	8	"	"
CST-1	300	8	6	IEEEG1
CST-2	440	3	"	"

2.3.2 Test Model

In this section, a single bus (copperplate) model of the NEM in 2020 is used as the test-bed. The system comprises non-synchronous generators (i.e. 11 WFs and 6 utility-PV plants) and SGs (as given in Table 2.1). All WFs are modelled as Type IV wind turbine generators, and all utility PV plants are modelled as full converter interface generators [4]. Also, all CSTs are modelled as SGs with governor response as presented in Table 2.1. The excitation systems and the power system stabilisers for the SGs are adopted from [69]. Because the inertia contribution of a synchronous power plant is directly related to the number of online units, the SGs' units in each power plant are modelled explicitly. Note that based on the UC results, the number of online units may vary for different hours. To assess the frequency performance of the system, we use the simulation platform presented in [10], which considers market simulation, power flow calculation, and stability assessment together. The UC results from the market model are used as the initial conditions/equilibria for frequency stability assessment. DIgSILENT PowerFactory is used for power flow calculation and dynamic simulations (frequency performance assessment).

2.3.3 Simulation Results

We solve the UC problem considering the constraints in Section 2.3.1. The UC outputs provide the initial condition/equilibrium of each generator, which are used for power flow studies. The power flow results are used as the initial conditions for the frequency performance assessment of the system.

Fig. 2.9 Dispatch results for the first week of July 2020 considering Case **NoIC**.Fig. 2.10 Dispatch results for the first week of July 2020 considering Case **SgN30**.Fig. 2.11 Dispatch results for the first week of July 2020 considering Case **Ek30**.

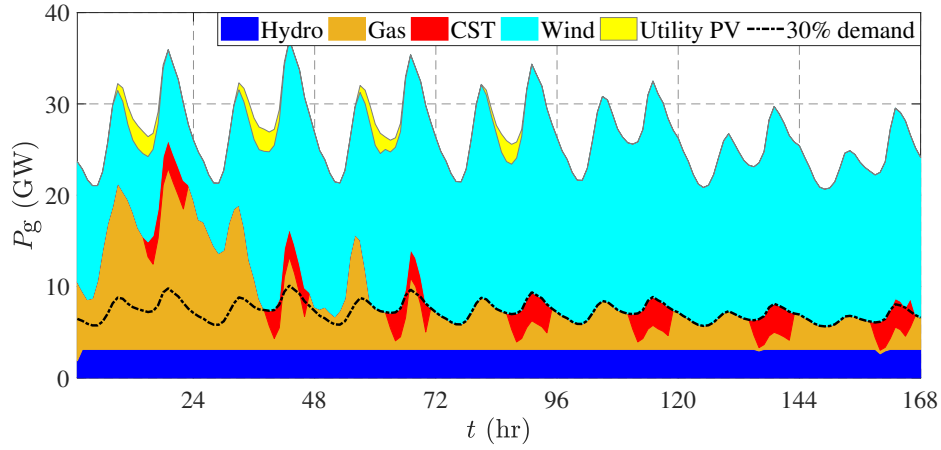


Fig. 2.12 Dispatch results for the first week of July 2020 considering Case **SgP30**.

Market Dispatch Results

We perform UC simulations for the four cases introduced in Section 2.3.1 in four representative weeks of 2020, namely, the first week of January (summer peak), April, July (winter peak with highest renewable variability), and October. In these, the market resolution is one hour (although it can be reduced to shorter duration periods for detailed studies).

First, we examine the generation mix generated by solving the four UC cases. To begin, note that the dispatch for the four representative weeks had very similar patterns. As such, for simplicity, in Figs. 2.9, 2.10, 2.11 and 2.12 we present the dispatch results, for July 2020 only, for cases **NoIC**, **SgN30**, **Ek30** and **SgP30**, respectively. The results show that different inertia constraints directly affect the market dispatch results. For instance, in **NoIC**, synchronous generation is the lowest in most hours of the test period, and it reaches a minimum of 0.7 GW at $t = 116$ h. In contrast, in **SgP30**, synchronous generators provide at least 30 % of the total demand, and synchronous generation is the highest compared to the other cases. In **SgN30** and **Ek30**, synchronous generation pattern is similar: it is higher than **NoIC**, and lower than **SgP30**.

Second, to evaluate the effectiveness of each constraint, we next assess the kinetic energy of the system. Fig. 2.13 illustrates kinetic energy of the system for the first week of July 2020. Observe that in **NoIC**, the kinetic energy of the system reaches as low as 14 GWs, whereas, in **SgN30**, **Ek30** and **SgP30**, at least a minimum of 25 GWs, 31 GWs, and 35 GWs kinetic energy is maintained, respectively. Notice that there is a discrepancy in the kinetic energy of the system in **SgN30** compared to **Ek30**, which is not obvious from the UC results (Figs. 2.10 and 2.11).

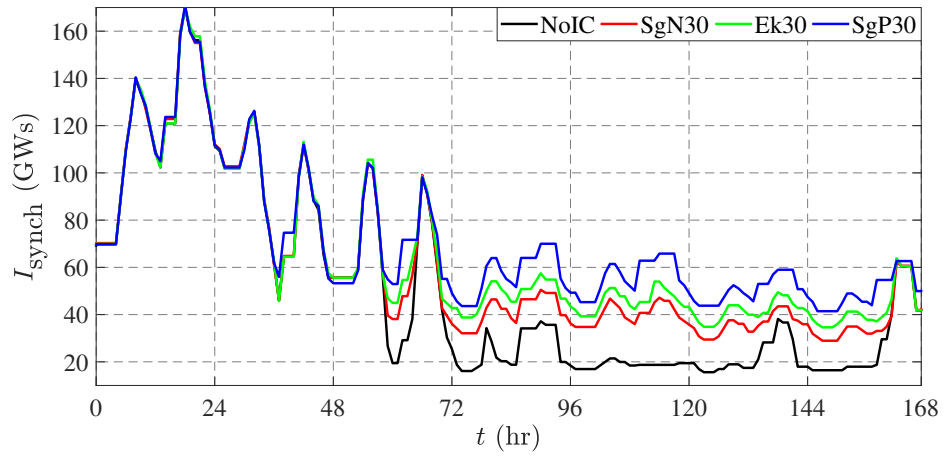


Fig. 2.13 System inertia during the first week of July 2020, for all cases.

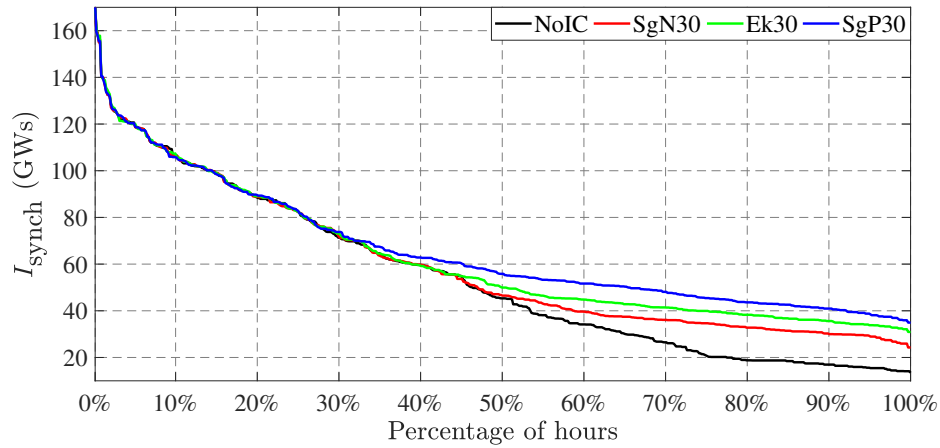


Fig. 2.14 Inertia duration curve of the system for four representative weeks of the year 2020 i.e. first weeks of January, April, July, and October.

Finally, the inertia duration curve of the system for all four representative weeks in 2020 is shown in Fig. 2.14. Observe that for more than 50 % of the hours where the generation is dominated by non-synchronous generators, the security constraints are effective, and a minimum kinetic energy is maintained. Notice that how the inertia of the system varies with the different security constraints.

System Frequency Response

We now assess the frequency performance of the system in every hour by considering the loss of the largest in-feed unit (i.e. 444.4 MW). Figs. 2.15 and 2.16 show the minimum RoCoF and the minimum frequency of the system, receptively. Note that in Case **NoIC** (no inertia constraint), both the RoCoF and the frequency nadir have the highest number of hours violating the limits [34]. In contrast, in cases **SgN30**, **EK30**, and **SgP30** both the RoCoF and the frequency nadir all improved, with different margins. We will return to these results in Section 2.3.4 when discussing the best approach. Beyond this, Fig. 2.17 shows the frequency behaviour of the system for all four cases at $t = 100$ h. Observe that the inertia constraint not only improves the RoCoF and the frequency nadir, but it also has a positive impact on the settling frequency of the system after the contingency³. It has to be mentioned that the AGC is not considered in this section. Thus, there is a steady-state error in system frequency. Looking beyond these studies, to ensure that the RoCoF is within the limits, a detailed investigation is required to identify the minimum kinetic energy requirement of the system because the RoCoF is directly related to the kinetic energy of the system as shown in (2.19).

2.3.4 Discussion

In this section, we considered that only SGs provide the kinetic energy, whereas, market modelling has suggested that this approach becomes expensive as the renewable proportion grows [79]. One alternative supply of inertia is synchronous condenser, which also provides "instantaneous" inertia in a rotating mass. These could be introduced as new installations or by retrofitting retiring thermal power stations as synchronous condensers. Moreover, other technical alternatives could contribute as a part of an efficient combined solution comprising a mix of synchronous and non-synchronous technologies, such as augmenting the transmission network, introducing flexible alternating current transmission systems (FACTS) devices with storage, or utilising synthetic inertia from WTs [8]. However, significant modelling effort is

³Mainly, because with the inertia constraints, the number of online synchronous generators increases, which results in more headroom and a better governor response.

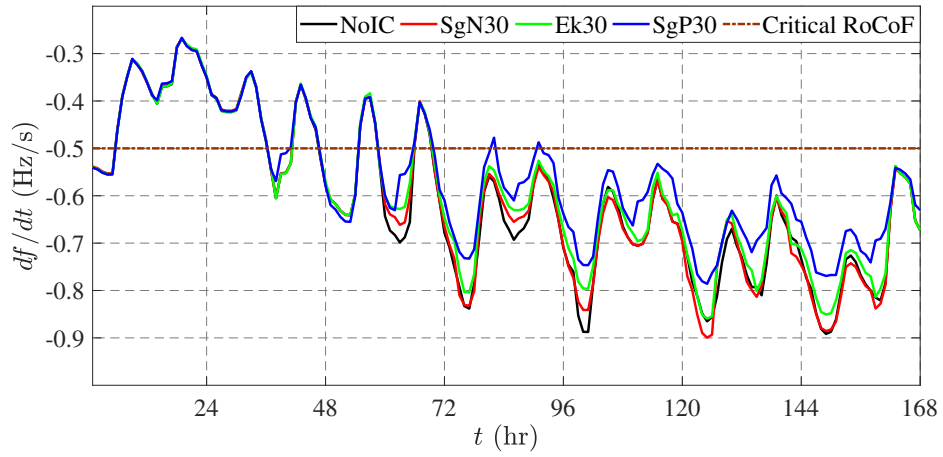


Fig. 2.15 Minimum RoCoF after the loss of the largest in-feed for the first week of July 2020.

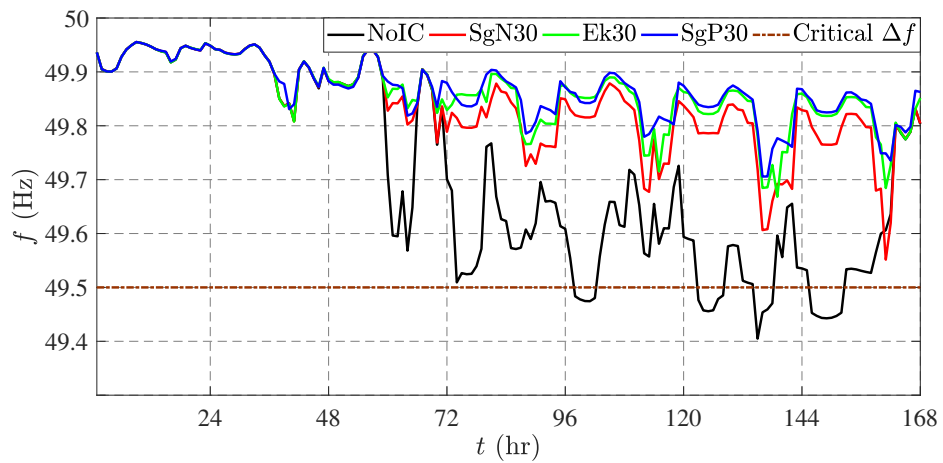


Fig. 2.16 Frequency nadir after the loss of the largest in-feed for the first week of July 2020.

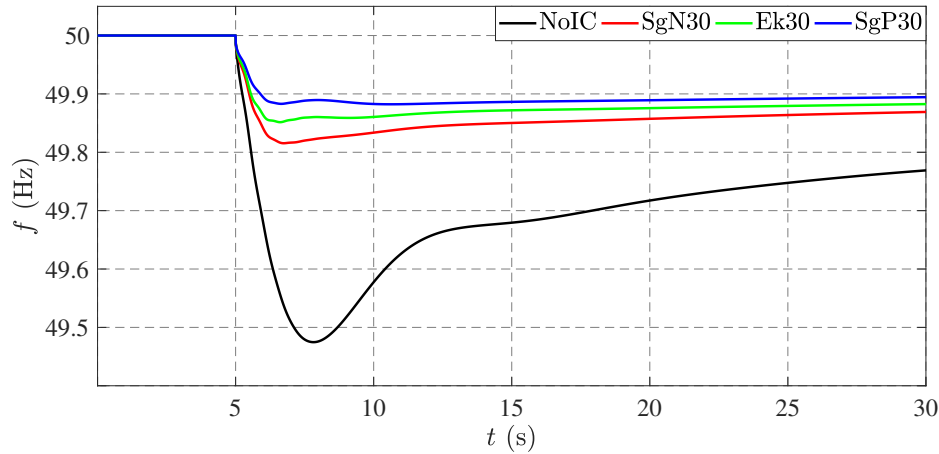


Fig. 2.17 System frequency behaviour after the loss of the largest in-feed for a typical hour in July 2020.

required to determine the efficient technical options available to address this issue, the size and scope of the interventions likely to be required, and their associated costs.

Once the least-cost technical options have been identified, a market or regulatory framework to manage the issue efficiently can be developed and implemented. This framework must be established with a solid understanding of the underlying technical requirements [80]. For example, it has been suggested that an “inertia market” could be established [81]. In the NEM, this could operate as a real-time five-minute spot market, co-optimised with the eight existing frequency control ancillary service (FCAS) markets, and the energy market. However, if there are strict locational requirements for the synchronous generation (to provide fault feed-in current in the local area, for example [8]), this may limit the number of participants able to offer capacity, limiting market competition. In this case, a framework similar to the procurement of reactive power may be more suitable (procuring the required service via a tender process, with long term contracts established). The NEM has already seen the exercise of market power in frequency control markets, causing extreme pricing outcomes, when these markets are limited to a localised area [82]. This suggests caution before implementing a new market framework of this type, without first establishing a good understanding of the technical limitations involved in operating a power system with a very high proportion of NS-RES. This section aims to provide the first steps towards that understanding.

2.4 Summary

In the first part of this chapter, we assessed the impact of high penetration of non-synchronous generation and different penetration levels of residential rooftop-PV with BS on the performance and frequency stability of the Australian FG. It was shown that a high penetration of rooftop-PV with a lower BS capacity (e.g. in Scenario **PBS-L**) can worsen the frequency response of the system because prosumers may send their excess generation back to the grid, which consequently reduces the synchronous capacity of the system. This situation improves with a higher BS capacity (e.g. in Scenario **PBS-H**). Notice that in Scenario **PBS-H** utilisation of a higher BS capacity allows prosumers to better maximise their self-consumption (minimise their energy cost), which can reduce network reinforcement and energy losses (as shown in Fig. 2.1), and improves system performance due to peak reduction and flatter net demand profile. Notice that frequency performance of the system with a high penetration of non-synchronous generation and prosumers might require a suitable market framework and/or security constraints for the system inertia and other frequency control ancillary services in which we might have to utilise non-traditional resources (e.g. WF) as well.

In the second part of this chapter, we assessed the impact of different frequency control security constraints on the market dispatch, as well as on performance and frequency stability of the system. It was shown that with the increasing penetration of non-synchronous generation, not only the system inertia reduces, but it also becomes time variant. This consequently deteriorates the frequency response of the system after a contingency (see Section 2.3.3). To cope with this issue, the concept of minimum inertia requirement was discussed. We integrated three different inertia based frequency control security constraints into the market dispatch model and showed that they have different effects on the dispatch results, as well as on performance and frequency stability of the system. To ensure that the RoCoF does not violate the limits, we introduced the minimum level of kinetic energy as a security constraint. Identifying the minimum kinetic energy requirement of a system needs an in-depth investigation because there are many important factors that have to be considered for finding the minimum kinetic energy requirement of a grid, i.e. the location of inertia, the location and size of the contingency, and the network strength. Thus, in the next chapter, we will consider these factors and perform a scenario-based sensitivity analysis to identify the minimum kinetic energy requirement of the Australian FG with high penetration of non-synchronous generation.

Chapter 3

A Frequency Performance Assessment Framework for Future Grids

3.1 Introduction

As discussed in Chapter 1, it is anticipated that the penetration of non-synchronous renewable energy sources (NS-RES), as well as prosumers, will increase in power systems around the globe. So far, studies have shown that a balance between generation and demand can be achieved using different resources, such geographical correlation of renewable resources and exploiting the flexibility of emerging technologies, e.g. battery storage (BS) and distributed resources (DR). From a technical point of view, after the balancing, priority should be given to stability and security assessment of future grids (FGs). Only a few studies have attempted to assess the stability of FGs [2, 4]. Those studies give some good insight into the effect of high penetration of NS-RES on system performance and stability; namely, frequency performance. However, it is very difficult to make general conclusions from their findings, as discussed in Section 1.2.1. Nonetheless, with high penetration levels of NS-RES, it is evident that system frequency performance is especially a serious issue for small and weakly interconnected systems, such as Ireland grid [2], and the Australian national electricity market (NEM). To deal with this issue, some studies have proposed a maximum non-synchronous instantaneous penetration (NSIP) limit, which requires a certain portion of power to be produced by the SGs at all times [2, 30]. However, before integrating any frequency control security constraint into the market dispatch model, it has to be defined precisely, and the limits for this constraint have to be identified accurately (i.e. by considering the impact of NS-RES and prosumers). As a first step, in Chapter 2, we assessed the impact of high penetration of NS-RES and prosumers on the performance and frequency performance of the Australian FG. Furthermore,

we showed that how different frequency control security constraints affect the performance and the frequency stability of the system. It was shown that to limit the RoCoF, an inertia based frequency control security constraint is very effective.

In this chapter, we take further steps to identify the maximum limits' of an inertia based frequency control security constraint as well as the maximum NSIP limits that a system can withstand without violating its frequency stability limits. Considering this, we briefly review the existing approach to address this issue in Section 3.2. Then, we propose a frequency performance assessment framework based on time-series analysis in Section 3.3. Then, in Section 3.4, we use the proposed framework to perform scenario-based sensitivity analysis, which allows us to accurately assess the frequency performance of the Australian FG for all credible contingencies (CCs; e.g. loss of largest in-feed generator). By doing this, we can identify the highest NSIP ranges that the system can withstand without violating its frequency stability limits. In Section 3.5, we employ the proposed framework to incorporate an inertia (i.e. also can be considered as RoCoF) based dynamic frequency control constraint into the market dispatch model to improve frequency performance of the system with high penetration levels of NS-RES. Further, we use conventional, such as synchronous condensers (SC) [1], and non-conventional resources, such as WF's synthetic inertia [49], and a governor-like response from WFs to improve the frequency response of the system. By doing this, we can evaluate and quantify the contribution of those resources on system frequency control, as well as identify the most effective option for system frequency control. Note that the WFs' governor-like response can be achieved by initially curtailing wind energy and operating the WFs in a de-loaded (suboptimal) mode, and changing their operation mode from sub-optimal to optimal in the inception of an event [83]. Finally, Section 3.6 summarises the chapter. The outcome of this chapter is published as a journal article in [JA2].

3.2 Background

With a high NS-RES penetration, power system frequency control becomes a challenging task and needs to be dealt with systematically. To address this issue, two distinct research approaches have emerged: system theoretic (analytical) and computational (simulation based). The system theoretic approaches [84–89] use a small signal stability (state-space) model linearised around the operating point, with suitably simplified models of power system components. Inverter-interfaced generators are modelled as generic power sources with a specified inertia and damping, with an underlying assumption that those could be synthesised using a power electronics inverter. Model reduction is used to remove algebraic equations [84–88], or to reduce the model to a second-order one [89]. The focus of system theoretic

approaches is to design optimal inertia both in terms of the amount and the location. The problem is formulated as an optimisation problem with performance metrics (e.g. oscillation damping, transient frequency overshoot, or the RoCoF) as an objective, taking advantage of the tractable mathematical model to account for time-domain constraints explicitly. Two approaches are used in the optimisation of the system performance metrics, using either numerical computation of system eigenvalues and their sensitivities [84, 85], or minimisation of a suitable system norm ($\mathcal{H}_1, \mathcal{H}_2, \mathcal{H}_\infty$), which serves as a proxy of the time-domain criteria of interest [86–88]. The two approaches are inspired by the problem of power system stabiliser tuning, using eigenvalue sensitivities [90] or robust control [91], respectively.

The main limitation of the system theoretic approaches is that the state-space system model requires several simplifications: (i) being a small-signal model, it is most suited to the analysis of power system oscillation damping but might be inaccurate for large-disturbance frequency performance analysis; (ii) the state-space power system model assumes that system dynamic matrix should remain constant; (iii) the generic inverter-interfaced generator models are simplified by necessity, so several important features that have an important impact on the system performance following a disturbance, e.g. fault-ride through capability, are omitted; (iv) given the model reduction, the location of the inertia does not properly capture the impact of power flows; and, finally, (v) the problem of optimal inertia placement cannot be separated from the market dispatch problem, given that the ability of an inverter-interfaced generator depends on its current dispatch level, which, in turn, depends on the market dispatch [70].

The simulation based approaches, on the other hand, are less restricted by modelling limitations. Their focus is typically the assessment of power system frequency performance for a particular scenario (usually a suitably augmented existing power system), which gives a good insight into the effect of high NS-RES penetration on the system frequency performance for that particular scenario [2–5], but makes general conclusions difficult. Furthermore, existing studies neglect the impact of market dynamics and emerging demand-side technologies, such as distributed generation with battery storage (i.e. prosumers) on system frequency performance. For example, the results for the US Western Interconnection [4] show that with about 50 % of NSIP, the frequency response of the system deteriorates compared to the base case, where the NSIP is approximately 4 %, which is not considered an immediate issue. In contrast, EirGrid in Ireland has limited the maximum penetration of NS-RES to 50 % to maintain the system frequency response within the permissible bounds [92]. While the existing studies [2–5] provide useful insight into the immediate challenges, they do not offer any guidance as the *maximum NS-RES limit* that a grid can accommodate from the frequency performance point of view.

Against this backdrop, we propose a data-driven computational approach based on time domain simulations to assess the impact of emerging technologies on power system frequency performance. The framework comprises market simulation, scanning tool for identifying credible contingencies (CC), load-flow analysis and frequency performance assessment. We use scenario-based sensitivity analysis, which is a pragmatic approach to capture the impact of a wide range of emerging technologies on the behaviour of future grids. Using the Australian FG as a test case with different NS-RES and prosumer penetration levels, we study the sensitivity of different parameters, including load models, contingencies' sizes and locations, inertia location and network strength on the power system frequency performance. Furthermore, we introduce a dynamic inertia based frequency control constraint in the market dispatch model to maintain system frequency response within the permissible bounds. Finally, we explore the applicability of some conventional and non-conventional resources, including synchronous condensers, and synthetic inertia and governor-like response from wind farms to improve power system frequency response and quantify their contribution to the power system frequency control. The findings provide valuable insight to power system planners and policy-makers to understand the impact of the emerging trends on future power system operation.

3.3 Frequency Performance Assessment Framework and Case Studies

Our framework is based on the stability framework proposed in [10]. Algorithm 1 summarises the proposed framework. Notice that it not only captures the most relevant aspects of power system operation that alter the frequency response of the system following a CC but also defines and identifies the CCs for a large number of scenarios using time-series approaches.

3.3.1 Inputs and Scenarios

Unlike previous deterministic studies where a few specific operation points were used to assess the frequency performance of a system [4], our framework utilises a large number of scenarios, which is crucial for identifying principal issues related to system frequency performance. For extensive time-series studies proposed in this chapter, use of a simplified network model would be sufficiently accurate and computationally efficient [5]. Although the simplified model provides an approximate result, it would be a good representation of the qualitative trend in the system dynamic behaviours. Furthermore, the Australian NEM has one of the longest transmission networks (i.e. more than 5000 km long), in which four states

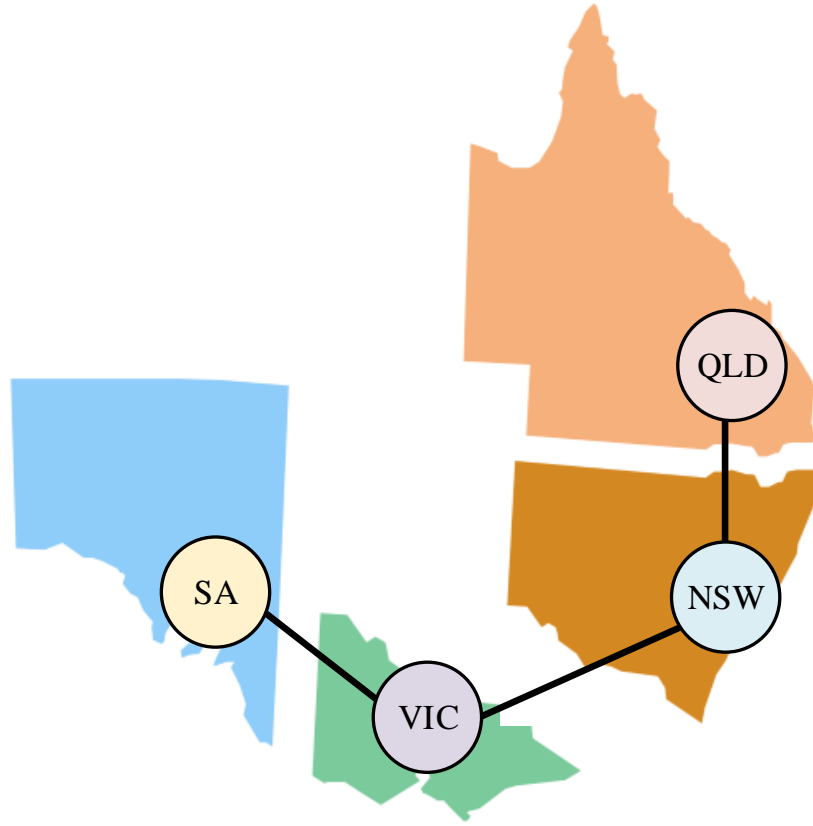


Fig. 3.1 Simplified network diagram of the Australian NEM.

are weakly connected to each other [69]. Considering these, we use a simplified four-area network model of the NEM as shown in Fig. 3.1, where each state is represented by one area (i.e. QLD, NSW, VIC and SA). The inter-state transmission lines (TLs) are augmented accordingly to accommodate the new generation and demand for the year 2040 [8]. As the base scenario, we use the current NEM generation portfolio, summarised in Table 3.1¹, with approximately 10 % non-synchronous annual penetration (NSAP), that is 10 % of annual energy is supplied by NS-RES predominantly WFs. Then, we incrementally retire the coal fired generators and increase the NSAP by 10 % up to 90 %. To do this, we use the Australian 100 % renewable studies as guidelines [7, 8, 72]; this will result in a total of nine different scenarios; $|\mathcal{S}| = 9$. In order to perform a comprehensive study, each scenario is analysed for one year at hourly resolution, $|\mathcal{T}| = 8760$, to capture a wide range of intra day and inter seasonal demand and generation variations. The hourly demand, wind and solar

¹<http://www.nem-watch.info/>

traces for each scenario are extracted from the Australian National Transmission Network Development Plan (NTNDP) [82].

Table 3.1 The assumed large-scale generation portfolio of NEM; base scenario with 10 % annual energy from NS-RES.

Plants	No.of Unit	Annual Energy (TWh)	Capacity (GW)	Inertia Constant H (s)
Hydro	7	20.2	2.3	4
Coal	77	157.6	39.4	6
CCGT	5	0.9	1.7	6
OCGT	12	1.4	3.6	6
WF	-	17.8	5.9	0

Algorithm 1 Future Grids Frequency Performance Assessment Framework

Inputs: Network data, generation data, ancillary service requirements (e.g. spinning reserve), wind, solar and demand traces for each scenario $s \in \mathcal{S}$ in the studied year.

```

1: for  $s \leftarrow 1, |\mathcal{S}|$  do
2:   for  $t \leftarrow 1, |\mathcal{T}|$  do
3:     Market simulation (generation dispatch);
4:     Identify credible contingencies;
5:     Load-flow analysis;
6:   end for
7:   for  $c \leftarrow 1, |\mathcal{C}|$  do
8:     for  $t \leftarrow 1, |\mathcal{T}|$  do
9:       Assess frequency performance for all CC;
10:    end for
11:  end for
12: end for

```

Outputs: Frequency stability indices (i.e. minimum RoCoF and frequency nadir) for each time slot $t \in \mathcal{T}$, for each sensitivity case $c \in \mathcal{C}$, and for each scenario $s \in \mathcal{S}$.

3.3.2 Market Simulation (Line 1-6, Algorithm 1)

In restructured power systems, market dynamics can affect system operation, and consequently, system frequency stability and performance [93]. Furthermore, system frequency dynamics can be influenced by several factors as follows [1]:

$$\frac{df}{dt} = \frac{f_0}{2I_{\text{synch}}} p^{\text{cc}} - \frac{f_0}{2I_s D_{\text{load}}} f, \quad (3.1)$$

where f_0 is the reference frequency of the system prior an incident, p^{cc} is the size of the CC, D_{load} denotes the frequency damping of the system load, f is the system frequency, and I_{synch} represents the level of system synchronous inertia, given in (2.21).

Note that the above parameters, as well as system governor response, and system primary reserve would change from one period to the following; therefore, to capture the effect of market dynamics and other changes on system frequency performance, we run the market dispatch model. We use the same market dispatch model introduced in Sections 2.2.1 and 2.3.1, which is based on a modified unit-commitment (UC) problem that aims to fulfil the demand requirement while minimising generation cost by considering fixed, start-up, shut-down and fuel cost of all generators. In addition, the dispatch decisions are constrained by the minimum thermal stable limits, ramp rates, minimum up/down time of SGs, renewable resource availability and thermal limits of transmission lines [94]. In the market dispatch model, it is assumed that the conventional SGs, such as coal fired power plants, open cycle gas turbines (OCGT) and combined cycle gas turbines (CCGT) bid at their respective short-run marginal cost (SRMC), estimated using the predicted fuel price, thermal efficiency, and variable operation and maintenance (O&M) cost in 2040 [95]; while, the NS-RES generators (e.g. WFs and PV plants) bid with zero SRMC. Notice that the NS-RES would push the conventional SGs out of the merit order. This, in turn, can significantly reduce the size and the operation point of CCs (e.g. largest in-feed units). Therefore, during the market simulation, we identify the size and operating point of the CCs as follows²:

$$p_h^{\text{cc}} = \max(p_{g,h}) \quad g \in \mathcal{G}_{\text{synch}}, \quad (3.2)$$

where, $p_{g,h}$ represents the dispatch level of generator g during time period h , and $\mathcal{G}_{\text{synch}}$ is the set of all SGs. Once the dispatch results for a specific hourly scenario are generated and the CCs are identified, we perform load flow analysis, which provides the initial condition for dynamic simulations.

3.3.3 Sensitivity Cases and Frequency Performance Assessment (Line 7-12, Algorithm 1)

For a comprehensive frequency performance assessment, we consider the sensitivity of some of the most relevant parameters given in (3.1) including the load model, as well as the size and the location of contingencies as shown in Fig. 3.2. The static load model (L_s)

²Due to high simulation burden, we consider only the largest in-feed unit as a CC and find its operation point. For more detail studies, we can monitor the in-feed power at every node to find the node with the highest in-feed power, and consider it as a CC.

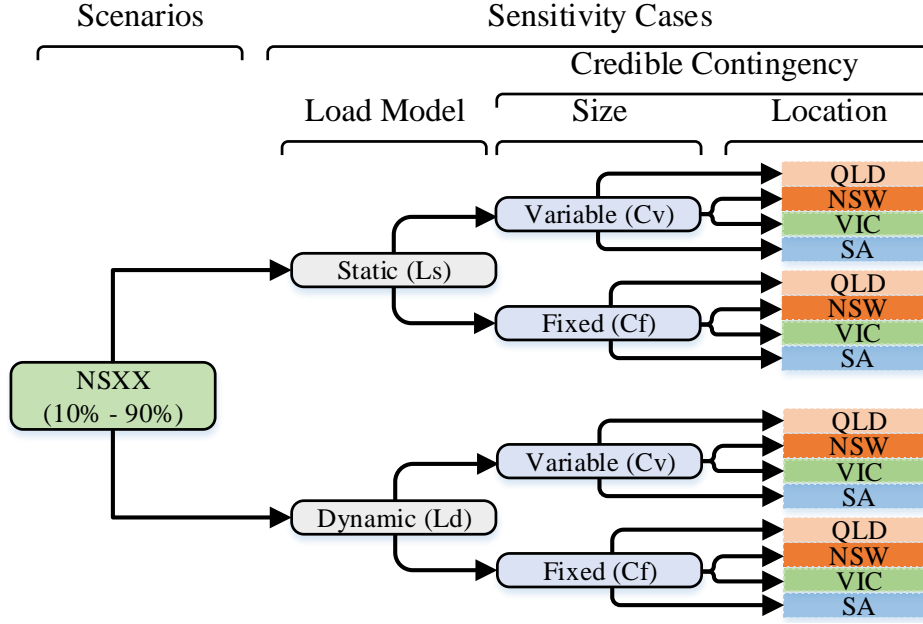


Fig. 3.2 A summary of scenarios and sensitivity cases, NSXX is the NSAP and varies from 10 % to 90 %.

is a constant impedance, current and power (ZIP) model [96]; whereas, the dynamic load model (L_d)³ consists of 40 % induction machines [99], and 60 % ZIP. For the size of the variable contingency (C_v), we use the values obtained from (3.2); whereas, for the size of the fixed contingency (C_f), we use the size of the largest in-feed generator that currently operates in the NEM, i.e. 666 MW [69]. We consider the above cases in all areas; namely, QLD, NSW, VIC and SA. So, considering the number of scenarios $|\mathcal{S}| = 9$, and sensitivity cases $(2 \times 2 \times 4) = 16$, we will assess a total of 144 cases in a year; $|\mathcal{C}| = 144$, with $|\mathcal{T}| = 8760$ in a year; resulting in 1261440 simulation runs. Based on Fig. 3.2, we use the following convention to present the results;

- **NSxx-Ls/d,Cv/f,Location-Metre**: **NSxx** is the NSAP, i.e. 10 % to 90 %; **Ls/d** represents the load model, i.e. **Ls** and **Ld**; **Cv/f** shows the contingency size, i.e. **Cv** and **Cf**; **Location** provides information regarding the location of the CC, and **Metre** is the bus where the measurements were taken.

³There is no report to confirm the portion of induction machine load in the Australian system. However, by considering the WECC load portion (i.e. 20-30 % induction machine [97]), as well as the CIGRE working group report on Japan load portion (i.e. 53 % induction machine [98]) as references, and comparing the socio-economic situation of the above mentioned jurisdictions with Australia, we have selected 40 % induction machine for the dynamic load model. Note that by considering 40 % induction machine for the dynamic load model and 0 % induction machine for the static load model, all the cases with induction machine load between 0 % and 40 % are covered.

An example is given as follows:

- *NS40-LdCvNSW-SA*; the NSAP is 40 %; dynamic load model is used; contingency size is obtained from equation (3.2); contingency location is NSW, and the measurement is taken from the SA's bus.

3.3.4 Outputs

The proposed framework provides a set of outputs for every simulated hour; namely, the minimum RoCoF and frequency nadir. We use these output indicators to estimate the critical range of NSIP that the Australian FG can accommodate from a system frequency performance point of view. The NSIP for every period t is defined as follows:

$$\text{NSIP} = \frac{p_h^{\text{NS-RES}}}{p_h^{\text{NS-RES}} + p_h^{\text{synch}}}, \quad (3.3)$$

where $p_h^{\text{NS-RES}}$ and p_h^{synch} are the power contribution of NS-RES and SGs, respectively.

3.4 Frequency Performance Assessment Results

The framework proposed in Section 3.3 is used for the frequency performance assessment of the Australian FG. Similar to Chapter 2, all SGs are modelled with their governor, excitation system and power system stabilisers [69, 70]. Also, all WFs are modelled as Type IV wind turbine generators (WTG), and all utility PV plants are modelled as full converter interface generators.

3.4.1 Market Dispatch Results

We perform UC simulation for the nine scenarios introduced in Section 3.3.1. First, we examine the generation mix generated by solving the nine UC scenarios. To deal with the unpredictability of load and generations, we considered a minimum of 10 % spinning reserve from SGs for scenarios *NS10* to *NS80* in each region. With such a constraint, it was infeasible to increase the NSAP to above 83 %; therefore, in scenario *NS90* we dropped the spinning reserve constraint. Notice that behind scenario *NS80* the system is predominantly renewable based with some biofuel fired OCGTs in each region that provide operational flexibility for the system [72]; hence, scenario *NS90* can be considered as a 100 % renewable based network with a generation mix of WFs, Hydro, concentrated solar thermal (CST), PV-plants and OCGTs. Second, we evaluate the impact of high penetration of NS-RES on the amount

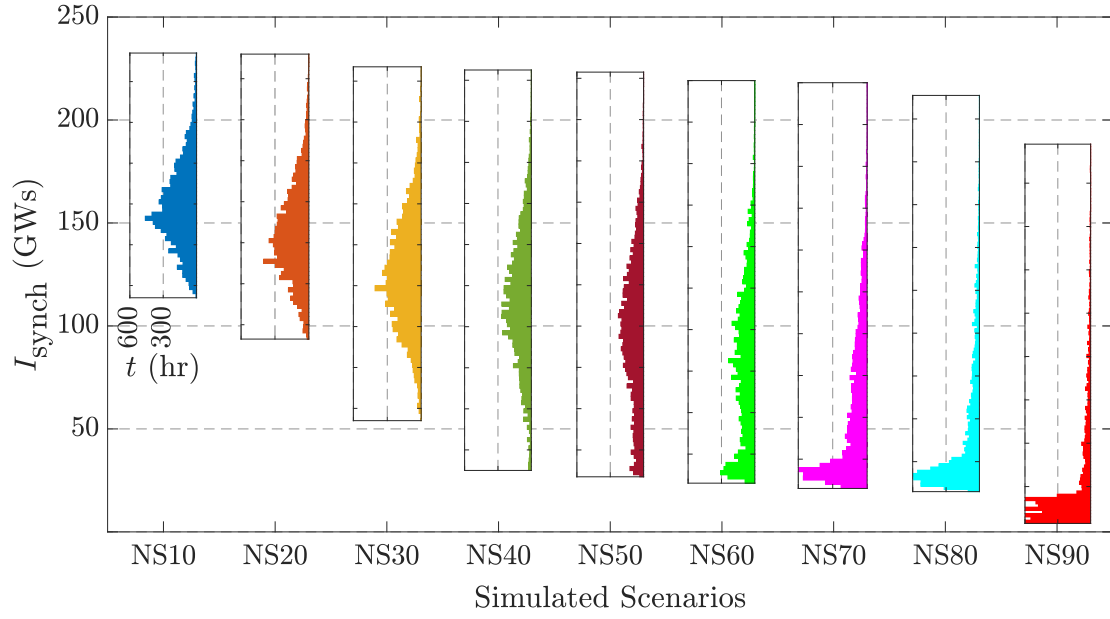


Fig. 3.3 Histograms of system synchronous inertia for all scenarios; for consistency all histograms are plotted on the same scale.

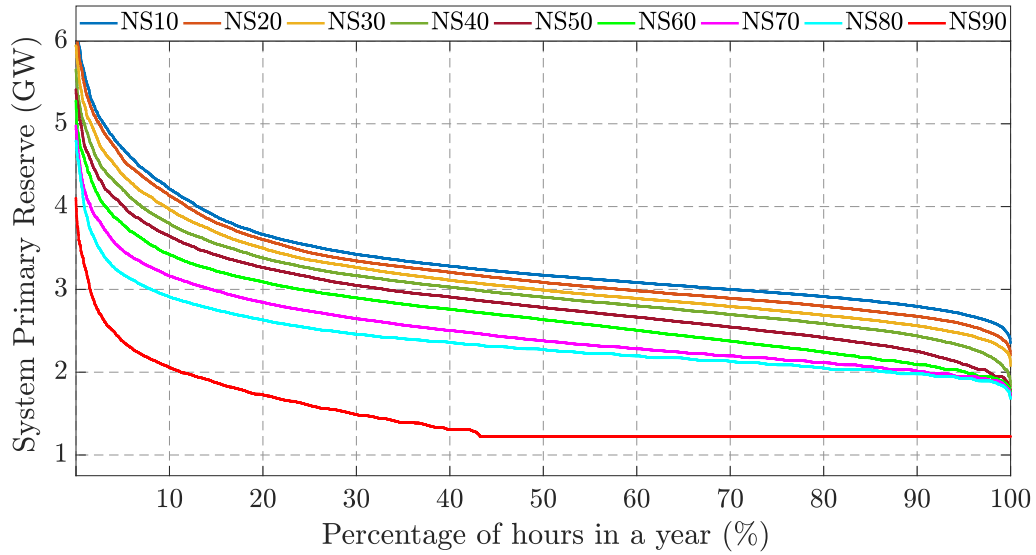


Fig. 3.4 System primary reserve for all scenarios; $\bar{P}_g(t) - P_g(t)$, $g \in \mathcal{G}_{\text{synch}}$.

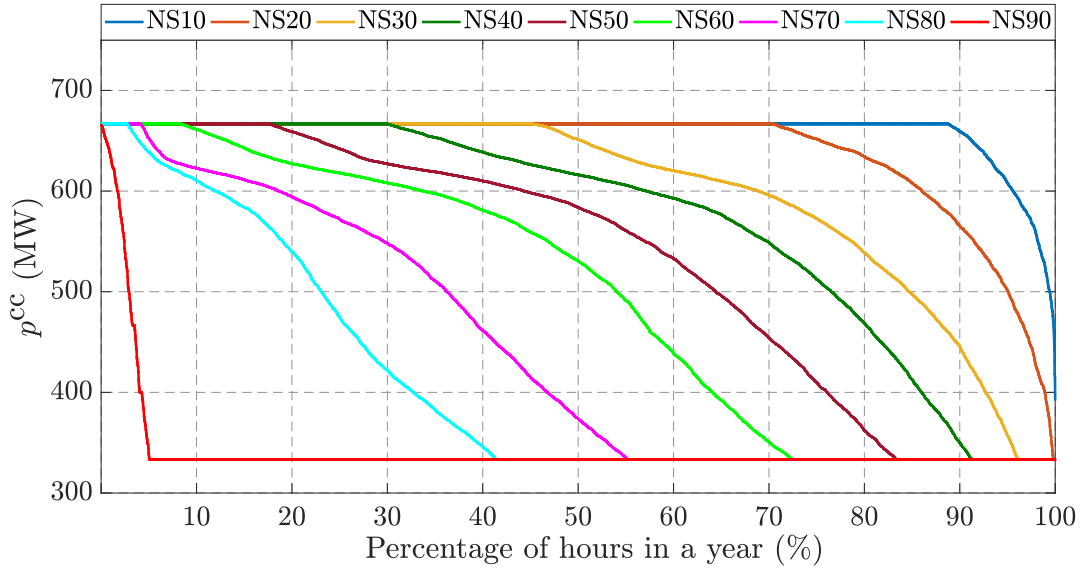


Fig. 3.5 Size of credible contingency (i.e. C_v) based on Algorithm 1.

of available synchronous inertia and system primary reserve, which can be directly linked to the RoCoF and frequency nadir [1]. As illustrated in Fig. 3.3, with the increasing penetration of NS-RES, not only the system synchronous inertia reduces, but it also becomes more time variant. For instance, in scenario *NS10*, the synchronous inertia varies between 114GWs and 234GWs with a mean value of 159GWs; whereas, in scenario *NS90*, the variation is between 4GWs and 178GWs with a mean value of 18GWs. The system primary reserve follows a similar trend, as shown in Fig. 3.4. The combined reduction of synchronous inertia, as well as system primary reserve can have significant detrimental impacts on system frequency performance, which will be analysed in the next subsection. Third, we evaluate the changes in the size of CCs. As shown in Fig. 3.5, there is a significant discrepancy in the sizes of CCs in different scenarios, e.g. in scenario *NS10*, the size of CC falls below 666 MW approximately 10 % of the time; whereas, in scenario *NS80*, this time increases to more than 95 %. This might have a positive impact on system frequency performance. Therefore, it is very important to consider these changes and assess their implication on system frequency performance. Finally, we use the UC results to perform load flow analysis. The load flow results are used as the initial conditions for the frequency performance assessment of the system in the following subsection.

3.4.2 Frequency Performance Results

We analyse the frequency behaviour of the system for the first 50 s following a CC for all simulation runs introduced in Section 3.3.3. This will allow us to quantify the impacts of

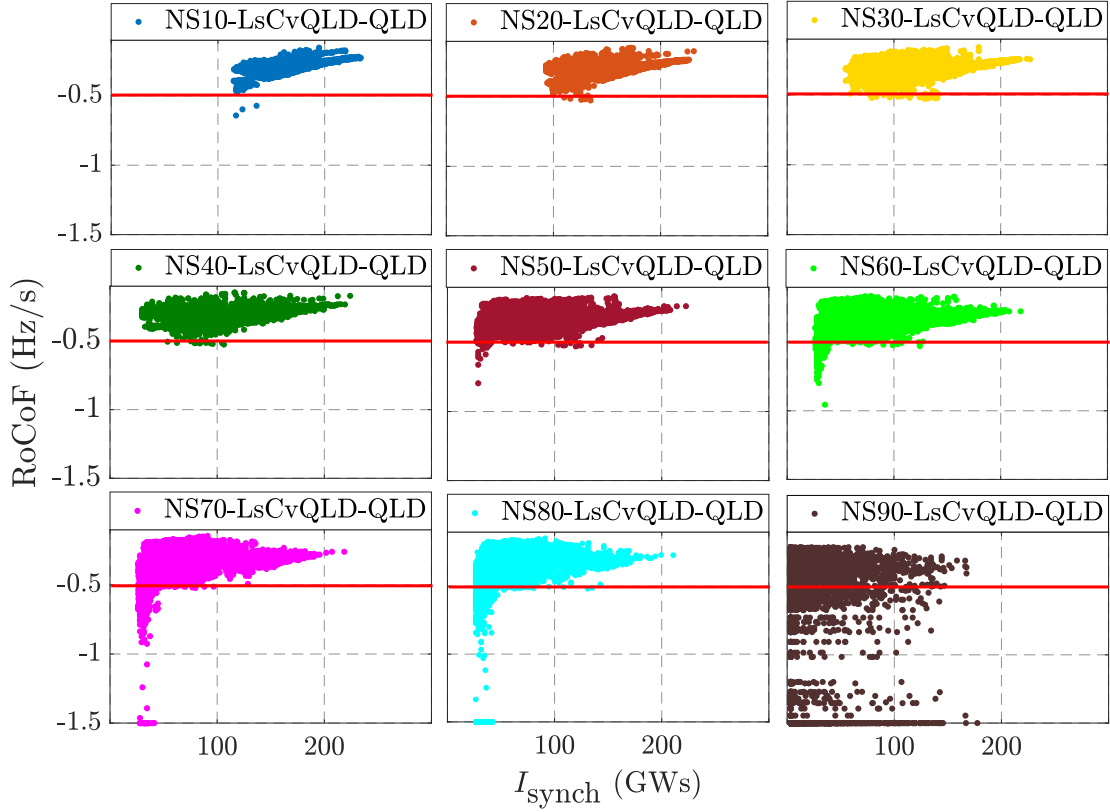


Fig. 3.6 Minimum RoCoF following the loss of CC for the simulated year; the red line shows the critical RoCoF.

reduced inertia, and primary reserves on system frequency performance; namely RoCoF and frequency nadir. Fig. 3.6 summarises the minimum RoCoF for all scenarios of *NSxx-LsCvQLD-QLD*. Observe that how the minimum RoCoF decreases with the reduced amount synchronous inertia, and for the NSAP of 60 % and above the minimum RoCoF starts violating the critical RoCoF (i.e. -0.5 Hz s^{-1} [2]). The frequency nadir follows a similar trend as shown in Fig. 3.7; where above 60 % NSAP, the number of hours that the frequency nadir drops below 49.5 Hz (i.e. minimum allowable frequency during a contingency [100]) increases significantly, and for scenario *NS90* even the mean value of frequency nadir is close to 49.5 Hz. Notice that the exclusion of spinning reserve in scenario *NS90* resulted in low system inertia. Also, in some situations, despite a high level of system inertia, some regions had very low or even zero inertia. As a result, in these situations even with high level of system inertia, we have noticed a high RoCoF for regions with low inertia as shown in Fig. 3.6, case *NS90-LsCvQLD-QLD*. This demonstrates the importance of inertia location on system frequency performance. We will return to this point in Section 3.5 when discussing the technical options for improving system frequency performance.

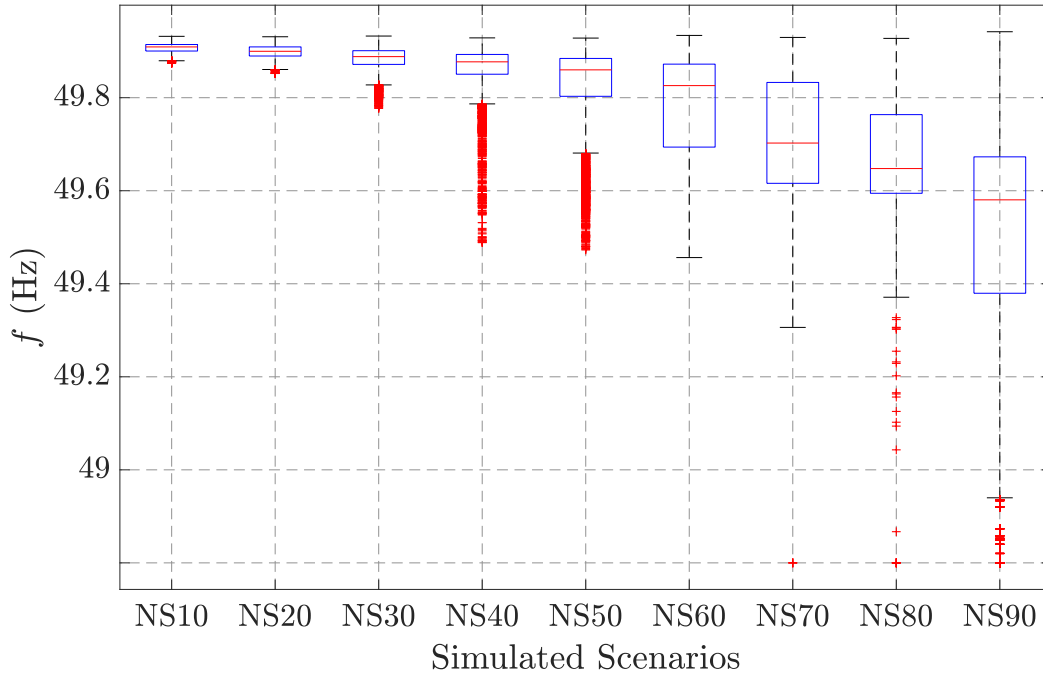


Fig. 3.7 Frequency nadir following the loss of CC for cases NS_{xx} - $LsCvQLD$ - QLD .

Notice that how the reduced amount of synchronous inertia and primary reserve in Figs. 3.3 and 3.4 affect the RoCoF and the frequency nadir of the system in Figs. 3.6 and 3.7, respectively. Although inertia level is one of the most relevant indicators of system frequency characteristic, it is not the sole parameter that influences the frequency behaviour of a system. There are other factors that need to be considered while defining the critical level of system inertia as discussed in Section 3.3. For instance, observe in Fig. 3.6, for scenarios $NS60$, $NS70$ and $NS80$, that for a wide range of inertia level (i.e. $I_s = 30 \text{ GW s}$ to 50 GW s) the RoCoF might violate its limit in some hours but not in the others. Therefore, based on the above results, it would be impractical to define a single accurate critical inertia level, and consequently, NSIP. Thus, to accurately estimate the critical NSIP of the system from the system frequency performance point of view, we analyse the impact of different parameters that influence the frequency behaviour of the system; namely, load model, CC size, CC location and prosumers in the following subsections.

The Impact of the Load Model

The effect of the load model on the system frequency stability performance is significant. As an example, Fig. 3.8 illustrates the RoCoF considering static load model (i.e. $NS20$ - $LsCvVIC$ - VIC , and $NS80$ - $LsCvVIC$ - VIC) and dynamic load model (i.e. $NS20$ - $LdCvVIC$ - VIC

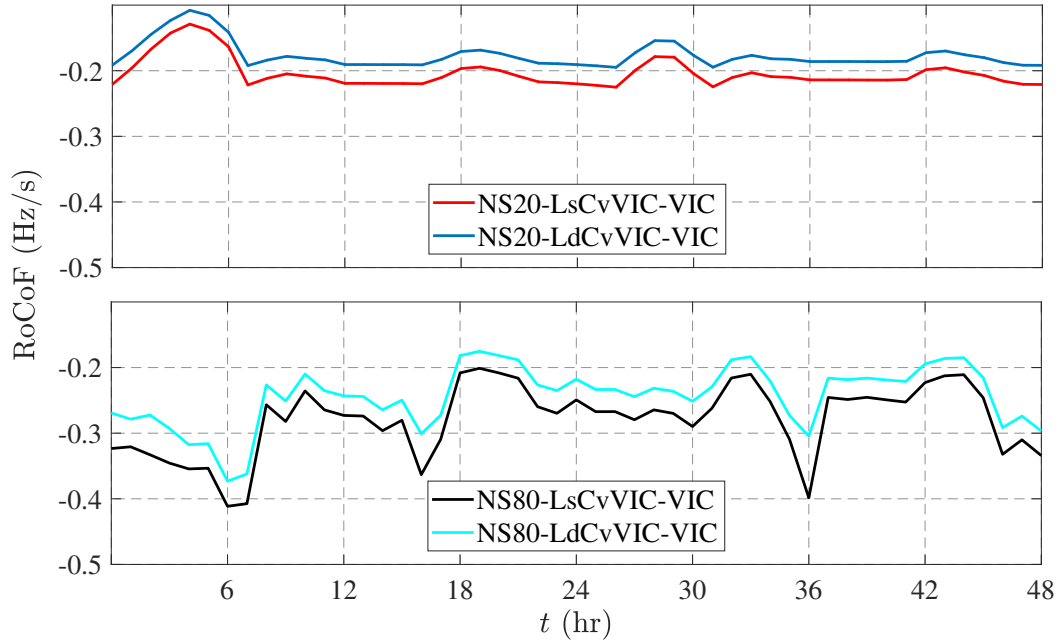


Fig. 3.8 RoCoF for two typical days considering the sensitivity of load model, for a low NSAP scenario (i.e. NS20) and a high NSAP scenario (i.e. NS80).

and *NS80-LdCvVIC-VIC*). Observe that with the *Ls*, the RoCoF deteriorates compared to *Ld* in both scenarios. Overall, it was observed that the impact of load model is more evident with a high NSIP and load level, e.g. Fig. 3.8, scenario *NS80*, $t = 6$ h and $t = 36$ h. This is because, with a high NSIP and load level, the system inertia decreases, while the frequency damping of the system load (D_{load}) increases. Therefore, the term including D_{load} in equation (3.1) becomes more dominant; as a result, the contribution of load dynamic becomes more significant.

The Impact of Contingency Size

The impact of contingency size is evidently significant on system frequency performance indices. For instance, observe in Fig. 3.9 that the RoCoF is notably better in cases *NS20-LsCvVIC-VIC* and *NS80-LsCvVIC-VIC*, where the CC size was identified during the market simulation using equation (3.2), compared to cases *NS20-LsCfVIC-VIC* and *NS80-LsCfVIC-VIC*, where a fixed CC size was assumed. Observe how the size of CC in Fig. 3.5 affects the RoCoF in Fig. 3.9. As shown in Fig. 3.5 for scenario *NS20* only about 10 % of the year the CC size obtained from (3.2) is smaller than C_f ; whereas, in scenario *NS80* only less than 5 % of the time the CC size obtained from Algorithm 1 (i.e. C_v) is the same as the assumed CC size (C_f); while, in about 60 % of the time the C_v size can be as small as half size of the

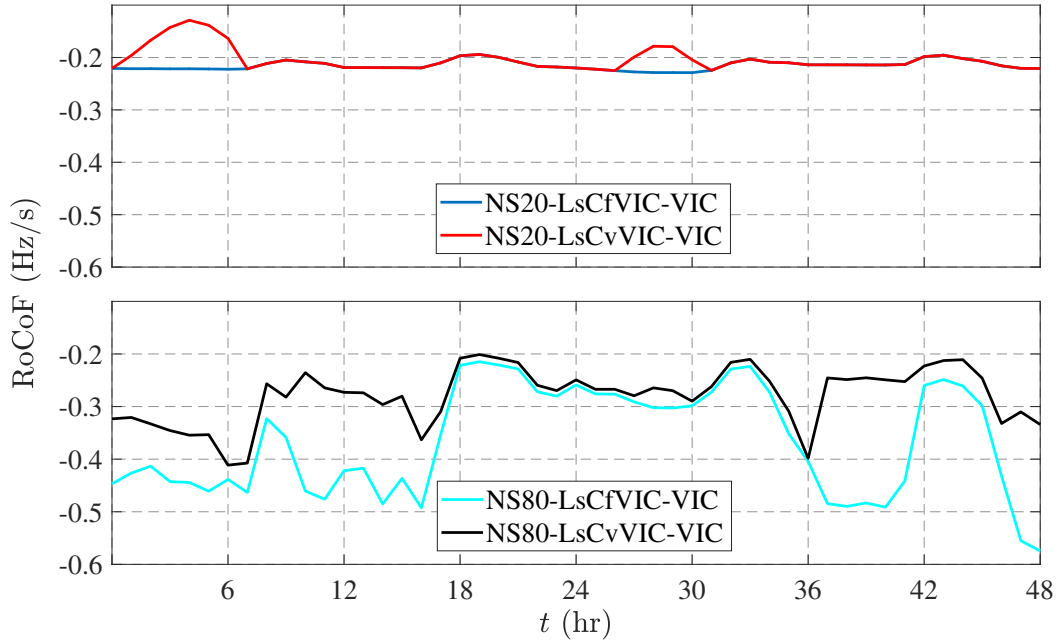


Fig. 3.9 RoCoF for two typical days considering the sensitivity of contingency size, for a low NSAP scenario (i.e. NS20) and a high NSAP scenario (i.e. NS80).

Cf. Fig. 3.9 clearly illustrates this discrepancy. As shown in equation (3.1) the size of CC is directly proportional to RoCoF. As a result, the RoCoF is considerably better in case *NS80-LsCvVIC-VIC*, with variable contingency size compared to case *NS80-LsCfVIC-VIC*, where the contingency size is fix. This clearly demonstrates the importance of CC size; therefore, accurate identification of CC size would be crucial for frequency performance assessment of FGs.

The Impact of Contingency and Inertia Location

The effect of contingency location on the RoCoF is shown in Fig. 3.10. Observe that the RoCoF in case *NS20-LsCvQLD-SA*, where the contingency is occurring in QLD, is not as severe as in case *NS20-LsCvSA-SA*, where the incident is in SA. Note that in scenario *NS20*, all the areas have very high inertia as shown in Fig. 3.3, thus, the discrepancy between the RoCoF in those two situations is mostly related to the network strength than the inertia. Hence, this illustrates the impact of network strength on frequency stability performance. Again, note that the RoCoF in case *NS80-LsCvQLD-SA*, where the contingency is occurring in QLD, is not as severe as in case *NS80-LsCvSA-SA* in most of the hours, where the incident is in SA. Nonetheless, in this scenario difference between RoCoF in cases *NS80-LsCvQLD-SA* and *NS80-LsCvSA-SA* is not as high as it is in cases *NS20-LsCvQLD-SA* and *NS20-LsCvSA-SA*.

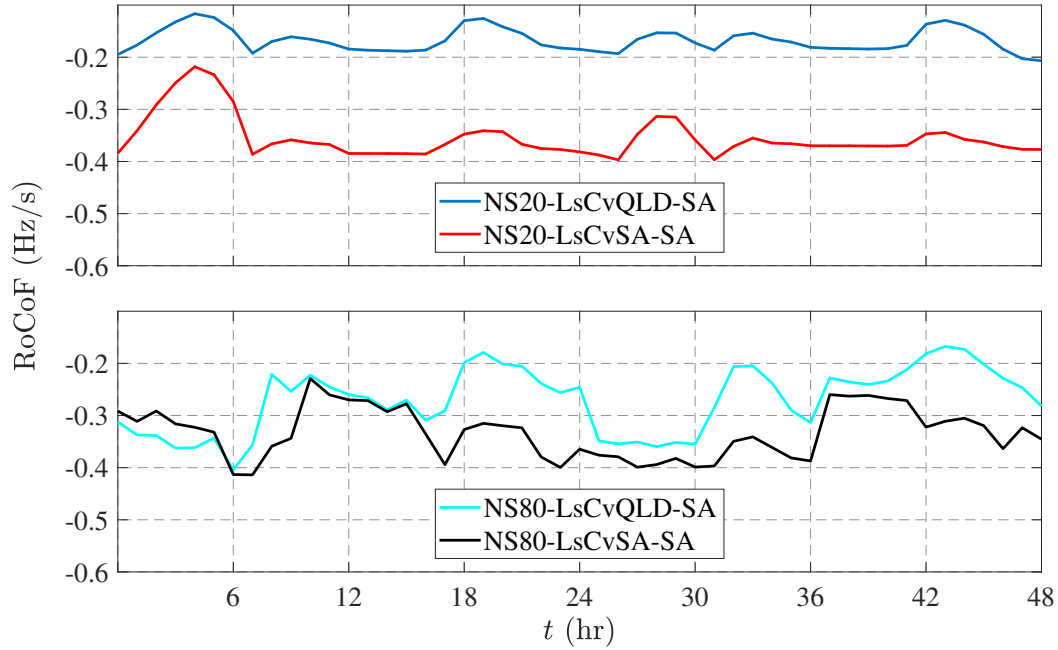


Fig. 3.10 RoCoF for two typical days considering the sensitivity of contingency location, for a low NSAP scenario (i.e. NS20) and a high NSAP scenario (i.e. NS80).

SA. This is because in scenario *NS80* all the areas; namely, QLD and SA, have very little inertia. As a result, with higher penetration levels of NS-RES, the impact of both inertia location, as well as network strength, becomes more significant on the frequency stability performance. Overall, it was observed that inertia location, as well as network strength, play a crucial role on frequency performance behaviour. For instance, the end regions of the NEM that are weakly connected to the system, QLD and SA, were more vulnerable to an incident than the middle regions that are strongly connected to the system, NSW and VIC.

The Impact of Prosumers

To study the impact of prosumers on system frequency performance, we use the generic demand model proposed in [12] and used in Section 2.2. This model aims to capture the aggregated effect of prosumers for market modelling and stability studies. Notice that of the total demand on each state, the percentage of prosumers with battery storage (BS) for NSW, VIC, QLD, and SA are 6.3 %, 8.6 %, 16 %, and 22 %, respectively inspired by AEMO [73]. Further, to assess the sensitivity of BS capacity, BS capacities of 1.8 kWh [73], and 3 kWh per 1 kW of rooftop-PV are considered. Observe that with the increased penetration levels of prosumers, the net demand profile of the system becomes smoother as shown in Fig. 3.11a. This is because prosumers utilise their rooftop-PV and exploit the flexibility of their BS

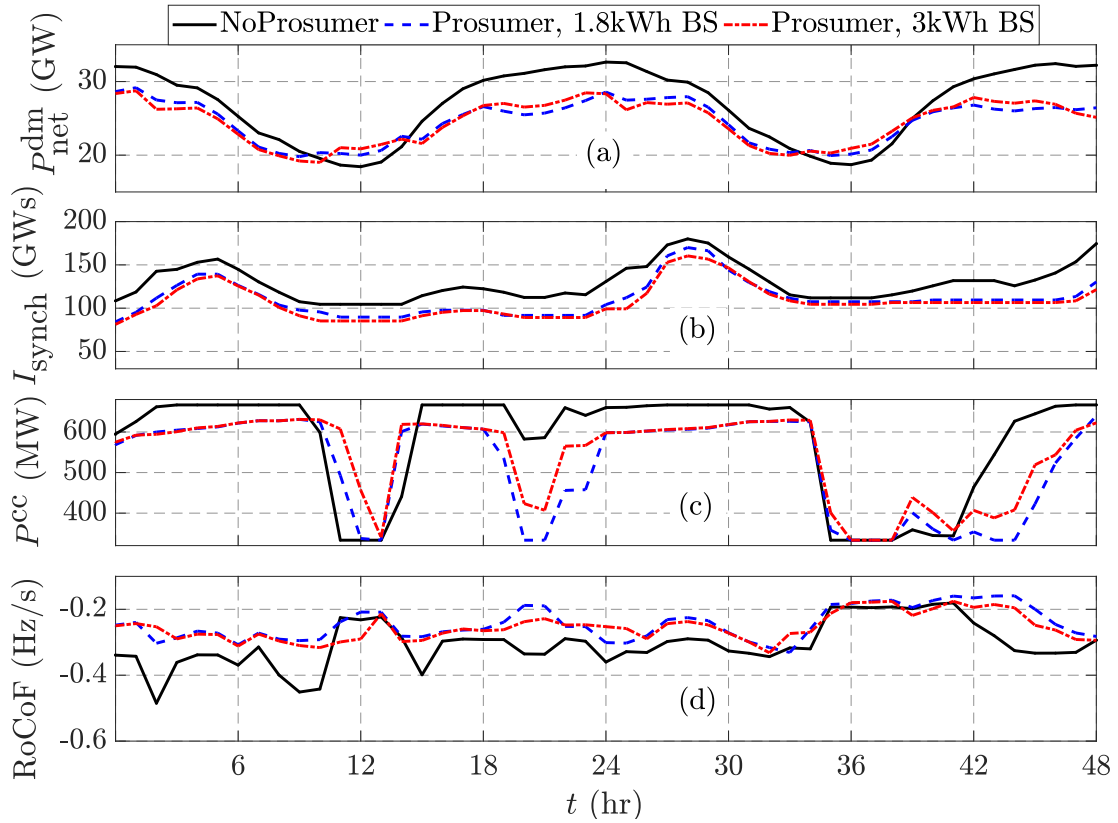


Fig. 3.11 The impact of prosumers with different battery storage capacity on (a) the net demand level (P_{net}^{dm}), (b) level of system inertia (I_s), (c) size of CC (P^{cc}), and (d) RoCoF for two typical days for case *NS80-LsCvVIC-VIC*.

system to shift their consumption from peak hours to non-peak hours by maximising their self-consumption [12]. This, in turn, has an implication on the amount of available inertia as well as the size of CC as shown in Fig. 3.11b and c, respectively. Notice that with high penetration of prosumers not only the net demand of the system but also the system inertia and the size of CC reduces in most hours (e.g. $t = 18$ h to 24h). The reduction of system inertia, as well as CC size, result in a situation where the system RoCoF improves as illustrated in Fig. 3.11d. This is because the impact of CC size on the RoCoF is more significant on those situations as also discussed earlier. Overall, it was observed that BS cases had the least number of hours that the RoCoF violated its limits, and with a higher BS capacity of prosumers (i.e. 3 kWh), the results are even better, which confirms the findings of Chapter 2.

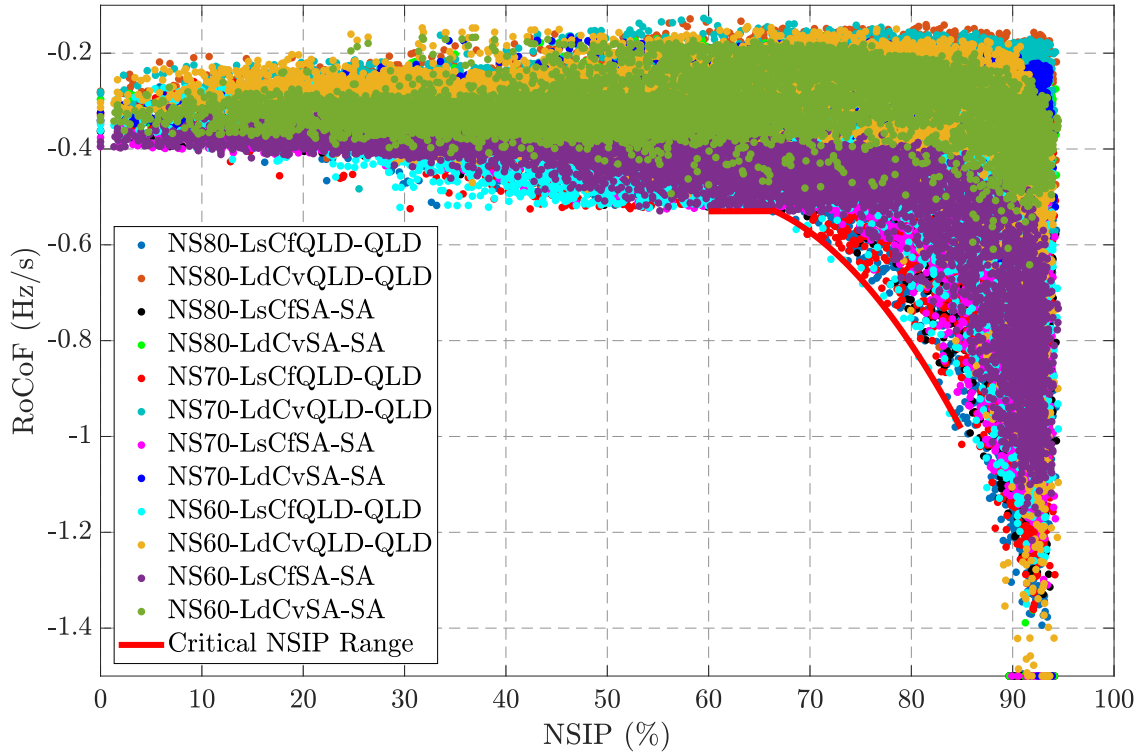


Fig. 3.12 Minimum RoCoF following a credible contingency based on NSIP.

Summary

The results suggest that the system frequency response is sensitive to many parameters that can change from one period to the following, which makes it difficult to define a single NSIP that would ensure the stable operation of the system. Therefore, instead of defining a single critical NSIP, a critical NSIP range has to be defined as shown in Fig. 3.12. After analysing the sensitivity of different parameters, we identify the most vulnerable cases, i.e. those with the highest number of hours that the RoCoF violates its limits, and present the results in Fig. 3.12. Observe that for a critical RoCoF, $\frac{df_{\text{crit}}}{dt} = -0.5 \text{ Hz s}^{-1}$, the system critical NSIP range would be 60 % to 67 %, which can increase up to 84 % for a critical RoCoF, $\frac{df_{\text{crit}}}{dt} = -1 \text{ Hz s}^{-1}$. To ensure that the RoCoF is within its permissible bounds in all operation conditions, we will introduce a dynamic inertia constraint in the next section.

3.5 Improving Frequency Response of the System with High Penetration of NS-RES

To improve the frequency response of the system with high penetration of NS-RES following a contingency, we explore following approaches: 1) adding a dynamic inertia based frequency control security constraint to the market dispatch model, 2) using other resources, such as WFs and SCs.

3.5.1 Dynamic Inertia Based Frequency Control Security Constraint

Initially, we implemented a global inertia constraint for the whole system; however, for the NEM, which has a very long transmission network (over 5000 km from QLD to SA), as shown in Fig. 3.1, the global inertia constraint was ineffective because inertia location is also very important as demonstrated in Section 3.4.2. Therefore, in the time domain simulations, the RoCoF violated its limits due to uneven distribution of inertia in different regions. To assure that each region has sufficient amount of inertia that would prevent the RoCoF from violating its limits, we consider regional RoCoF constraints for each region. To do this, first we identify the size of CC, $p_{r,h}^{cc}$, in each region as follows:

$$p_{r,h}^{cc} = \max(p_{g,h}) \quad g \in \{\mathcal{G}_{\text{synch}} \cap \mathcal{G}_r\}, \quad (3.4)$$

where \mathcal{G}_r is set of all generators in region $r \in \mathcal{R}$. Then, we incorporate the regional inertia constraint in the UC problem. Note that at the inception of an incident, we can assume that the contribution of the load damping on the RoCoF is insignificant; thus, by rearranging equation (3.1), we can consider the following inertia based constraint for each region:

$$I_{\text{synch},r} \geq \frac{f_0 p_{r,h}^{cc}}{2 \left| \frac{df_{\text{crit}}}{dt} \right|}, \quad (3.5)$$

where $I_{\text{synch},r}$ represents the total inertia of region $r \in \mathcal{R}$, which is determined considering status (i.e. on/off), inertia constant H_g and MVA rating of each SG, as given in equation (3.6), with N_r being the number of total SG in region $r \in \mathcal{R}$. f_0 is system frequency at the inception of the event, $p_{r,h}^{cc}$ is the size of CC in region $r \in \mathcal{R}$ identified from equation (3.4), and $\frac{df_{\text{crit}}}{dt}$ is the critical RoCoF (i.e. considered as -0.5 Hz s^{-1}). Note that implementation of such approaches ensure that each state will have sufficient inertia without relying on the neighbouring state. For a more detail study, one can consider the contribution of neighbouring

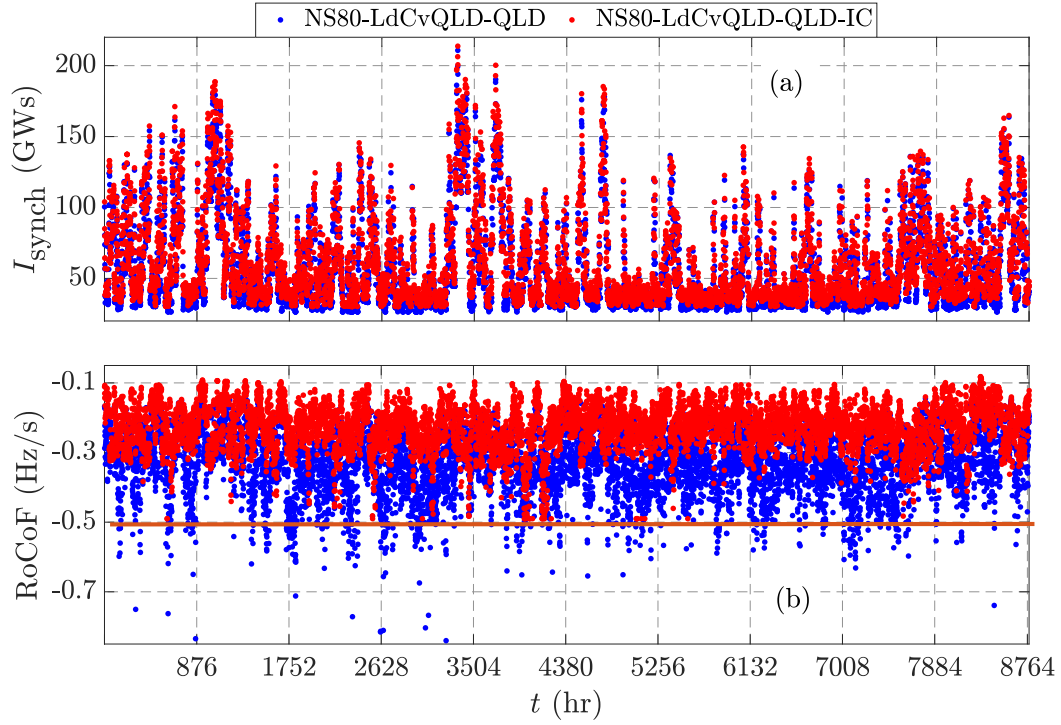


Fig. 3.13 Impact of dynamic inertia constraint on (a) synchronous inertia of the system and (b) RoCoF for QLD.

states through the inter-area connections.

$$I_{\text{synch},r} = \sum_{i \in N_r} H_{g,i} S_{B,i}. \quad (3.6)$$

The effectiveness of regional inertia constraints on system synchronous inertia level as well as RoCoF is illustrated in Fig. 3.13. Observe that with no inertia constraint in case *NS80-LdCvQLD-QLD* the system synchronous inertia can reduce to below 26 GW s. Whereas, with the inertia constraint in case *NS80-LdCvQLD-QLD-IC* a minimum synchronous inertia of $I_s \approx 30$ GW s is maintained. As a result, with the inertia constraint, the RoCoF does not violate its limits as shown in Fig. 3.13b. Nonetheless, incorporation of inertia constraint in the UC problem results in curtailment of 380 GWh energy per annum from WFs. Note that by curtailing wind energy in a coordinated way, we might be able to add more flexibility to the system, which will be explored in the next subsection.

3.5.2 Utilisation of Other Sources for Frequency Control

To improve system frequency response, we use three different techniques and perform time-series analysis for a whole year. This will allow us to compare and quantify the contribution of each option. To do this, we use case *NS80-LdCvQLD-QLD* as the base case and explore the following options:

- **Normal:** This is the reference option and no additional source is used for improving system frequency response.
- **SC:** In every region, we consider one synchronous condenser (SC), with ($S = 400 \text{ MV A}$) and ($H = 6 \text{ s}$). This would add a total synchronous inertia of ($I_s = 9.6 \text{ GW s}$) to the system around the clock.
- **IE:** Since the contingency is located in QLD, we consider one of the QLD's WFs that operates at near its rated capacity and provides $P_{WF,h} = 600 \text{ MW}$ all over the year. We apply the inertia emulation (IE) technique [49] to exploit the rotational kinetic energy of this WF for frequency control.
- **DL:** We use the same WF introduced earlier and de-load (DL) it by 5 %, which results in $P_{WF,h} = 570 \text{ MW}$. The de-loading is achieved by pitching the blade angles and increasing the rotor speeds of the wind turbines [83]. Note that the total curtailed energy of the WF over the year would be 263 GWh compared to 380 GWh resulted from implementation of inertia based constraint.

Fig. 3.14 summarises the minimum RoCoF and the frequency nadir of the system for all options. Observe that in the *Normal* option the RoCoF violates its critical value (i.e. -0.5 Hz s^{-1}) in many hours; whereas, in the other options, i.e. *SC*, *IE* and *DL*, the RoCoF does not violate its critical value and falls between -0.5 Hz s^{-1} and -0.1 Hz s^{-1} . Thus, from the RoCoF perspective, the most effective option is *SC* followed by *DL* and *IE*, as shown in Fig. 3.15 as well. This is because in option *SC* the amount of synchronous inertia is considerably high compared to other options. Further, in contrast to *DL* and *IE* options that require control action to provide inertial response, *SC* provides a natural response in harmony with the system RoCoF, which is more effective. Note that the available kinetic energy of the WF in option *DL* is more than option *IE* because the de-loading is achieved by increasing the rotor speed of the wind turbines, as well as pitching of the wind turbines' blades [20].

The frequency nadir, however, has been affected differently as shown in Fig. 3.14b. For instance, in option *SC*, since the SC provides inertial response but not governor response, it reduces the minimum RoCoF and delays the frequency nadir, but has an insignificant

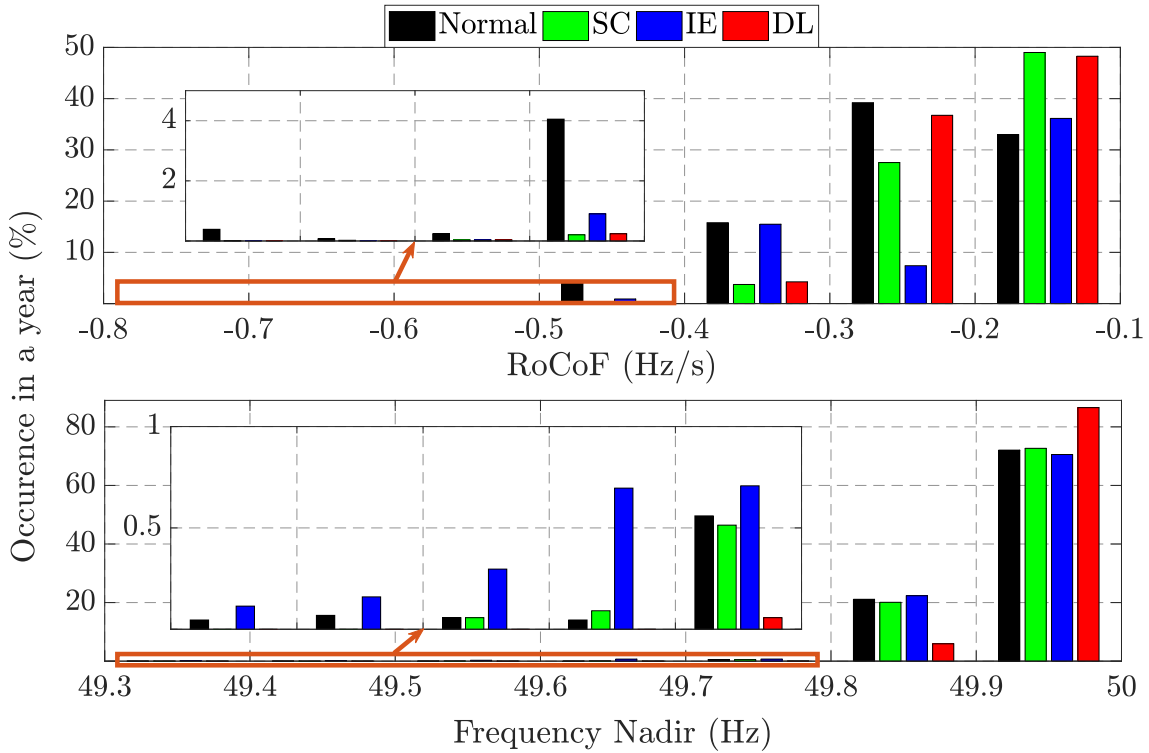


Fig. 3.14 Distribution of (a) RoCoF, and (b) frequency nadir for Case *NS80-LdCvQLDQLD*; considering cases **Normal**, **SC**, **IE**, and **DL**.

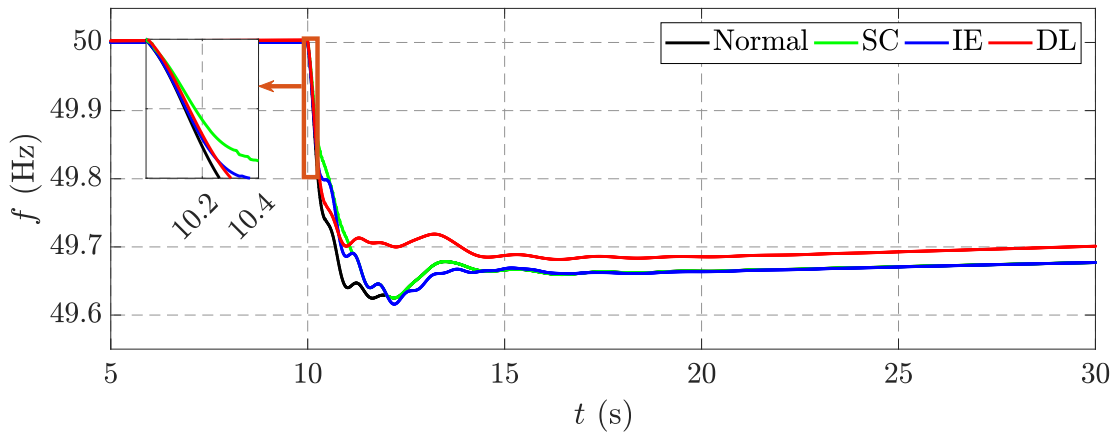


Fig. 3.15 System frequency behaviour for a typical hour considering cases **Normal**, **SC**, **IE**, and **DL**.

impact on the value of the frequency nadir. In option *IE*, the RoCoF improves; however, the frequency nadir might deteriorate compared to the base case in some hours as shown in Fig. 3.14b. This is because extraction of kinetic energy from a wind turbine reduces

its rotor speed, and in turn, its coefficient of performance. Recovery of the coefficient of performance following inertia emulation requires kinetic energy that should be provided by the grid. In some situations, this would result in a second frequency nadir as shown in Fig. 3.15. As a result, in option *IE*, the number of hours that the frequency nadir falls between 49.3 Hz and 49.8 Hz slightly increases compared to the base case. Nonetheless, option *DL* not only improves RoCoF and frequency nadir, but it also has a positive impact on the settling frequency; because in this option, in addition to kinetic energy, the wind turbines release additional power to the grid using a governor-like control.

3.6 Summary

This chapter introduced a framework for frequency performance assessment of future grids. By utilising this framework, we performed a comprehensive scenario-based sensitivity analysis on the Australian future grid and identified a critical range of non-synchronous instantaneous penetration that the system can accommodate without violating its frequency stability limits. Further, it was shown that there are many parameters that affect the frequency performance of the system that change from one period to the following. Therefore, to consider those changes, and to maintain system frequency response within its permissible bounds at all time, we proposed a dynamic inertia based frequency control security constraint and incorporated it into the market dispatch model. It was shown that by the implementation of such constraint the frequency response criteria can be satisfied. Nonetheless, enforcement of this constraint resulted in the curtailment of wind energy. We showed that by curtailing wind energy in a coordinated way, we can add more flexibility to the system. This was done by de-loading the wind farms and engaging them to frequency control using a governor-like response, which not only improved the RoCoF and the frequency nadir but also improved the settling frequency following a contingency. Moreover, by performing extensive time-series simulation, we quantified the contribution of synchronous condenser and wind farm synthetic inertia on system frequency response. So, from a technical point of view, de-loading the wind farms and engaging them to frequency control can be considered as one of the most promising options for systems with high penetration levels of NS-RES; thus, in the next chapter, we work further on this concept not only to quantify the contribution of wind farms in frequency control by considering a more realistic model of a wind farm, but also to optimise the contribution of a wind farm in frequency control.

Chapter 4

Participation of Wind Generation in Frequency Control

4.1 Introduction

As explained in Chapter 1, it is anticipated that wind technologies would provide a large share of future electrical energy. Furthermore, in Chapters 2 and 3, it was shown that with a high penetration of non-synchronous renewable energy sources (NS-RES), such as wind generation, system frequency control becomes a challenging task. To address the aforementioned issues, it is suggested that either the wind farms (WFs) should provide ancillary services similar to the conventional synchronous generators (SGs), or the flexibility of the system should be enhanced, which would allow power systems to adapt to variable resources e.g. wind generations [43]. So far, a concept called "Delta Control" has been implemented in Denmark. In this strategy, WFs operate below their maximum capacity, which allows them to increase or decrease their output similar to conventional generators [101]. Implementation of this strategy also allows WFs to provide frequency control services. Although technically "Delta Control" concept is considered as a very suitable solution for the system frequency control, financially it has to be justified because of the constant curtailment of wind energy in the de-loaded operation mode.

Nonetheless, as shown in Chapter 3, with higher penetrations of NS-RES, maintaining system frequency performance indices within their permissible bounds, requires some technical and possible policy measures (e.g. integration of a dynamic inertia based frequency control security constraint into the market dispatch model, as discussed in Section 3.5.1). Such measures, in turn, limits the instantaneous penetration of NS-RES (i.e. results in curtailment of NS-RES). Considering these, to improve the frequency performance of the

system with high penetration of NS-RES, WFs should participate in frequency control. One of the most effective ways to engage WFs in frequency control is to initially operate them in a de-load (sub-optimal) mode, as also illustrated in Section 3.5.2. Hence, in this chapter, we extend that concept by optimising contribution of WFs in frequency control by considering a more realistic model of a WF. To do these, in the first part of this chapter, we explicitly model the wake interaction among the wind turbines (WTs) within a WF and maximise the rotational kinetic energy of the WF for a specific de-loading margin. The outcome of this part is published as a conference paper in [CP1]. In the second part of this chapter, we propose an optimal control strategy for the participation of WFs in frequency control. In this strategy, we inject the optimised kinetic energy of the WF into the system in a controlled manner based on system's RoCoF and frequency nadir. The outcome of this part is published as another conference paper in [CP2]. By doing these, we reduce the need for frequency control services from the conventional SGs in systems with higher penetrations of wind generations.

4.2 Exploring Wake Interaction for Frequency Control

In this section, we propose an optimised operation strategy for the wind farms. In this strategy, we maximise the kinetic energy of wind turbines by an optimal combination of the rotor speed and the pitch angle. We exploit the wake interaction in a wind farm and de-load some of the up-wind turbines. We show that the kinetic energy accumulated in the rotating masses of the WTs can be increased compared to the base case without compromising the efficiency of the wind farm. In a specific system, we show that by implementing this strategy and injecting the stored kinetic energy of the WTs' rotors into the system during a frequency dip, we can delay the system frequency nadir.

4.2.1 Participation of Wind Power in Frequency Control

As discussed in Section 1.2.2, there are mainly two options for control of frequency by WTs: *inertial response* and *de-loaded operation* [102]. Since the stator and the rotor of a variable speed wind turbine (VSWT) are decoupled by the power electronic converter, an additional control loop is required to make the WT inertia available to the system, which is referred to as synthetic inertia in some references [49]. The addition of this new loop can provide up to 20 % extra power to the system for up to 10 s during a frequency dip [53]. Nonetheless, this inertial response decreases the rotor speed which consequently reduces the coefficient of performance. To recover the coefficient of performance, the kinetic energy of the rotor

should be restored, which can result in another frequency event [53]. In some situations, the second frequency dip can be worse than the first one [54].

Unlike synthetic inertia where no wind energy is spilled, in the de-loading strategy a WT needs to be permanently de-loaded for frequency control, and operate with a lower coefficient of performance [18]. The output power of a VSWT in the sub-optimal operation mode depends on its power in the optimal operation mode and the de-loading margin (δ) as follows:

$$P^{\text{sub}} = (1 - \delta)P^{\text{opt}}, \quad (4.1)$$

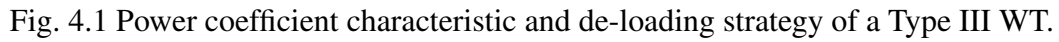
when the power in the sub-optimal operation mode and the wind speed are known, the coefficient of performance in the sub-optimal operation mode can be calculated as follows:

$$C_P^{\text{sub}} = \frac{P^{\text{sub}}}{0.5\rho\pi R^2 v^3}, \quad (4.2)$$

where ρ is the air density, R denotes the rotor of the WT blades, and v is the wind speed.

There are different de-loading strategies for a VSWT. For wind speeds below the rated wind speed, the de-loading can be achieved by changing the reference values of (A) the rotor speed [103], (B) the pitch angle [19], and (C) a combination of both the rotor speed and the pitch angle [20]. Once the rated wind speed is reached, de-loading is possible only by changing the reference value of the pitch angle because at this point the rotor speed is maximum. It has been demonstrated that below the rated wind speed, the last strategy (i.e. C) is the most efficient de-loading strategy both from technical as well as economical point of views [102]. Because in this strategy, by a combined optimisation of both the rotor speed and the pitch angle, not only a certain amount of power reserve can be achieved, but also a considerable amount of kinetic can be achieved, which can be used for the primary frequency control. Therefore, in this strategy, for the same power reserve margin, the amount of spilled energy is reduced significantly. For instance, a comparison of strategy C with A and B reveals that by keeping the same marginal electrical power reserve in all cases, the annual production of a WF can increase by up to 2.79 % in strategy C [102].

Between the cut-in wind speed and the wind speed where the rotor speed reaches its maximum value, de-loading can be achieved by changing the rotor speed in proportion to the de-loading margin, δ , and keeping pitch angle constant. Once the maximum rotor speed is reached, de-loading is possible only by changing the pitch angle, β . Fig. 4.1 shows the performance coefficient, C_p , as a function of the tip speed ratio λ defined as $\lambda = \frac{R\omega}{v}$, where



4.2.2 Stationary Wake Model

As explained in Section 1.2.2, A *Stationary Wake Model* [65], which was recently developed for control purposes is very suitable for the purpose of this thesis. This wake model requires minimum data, and its parameters have a clear interpretation, which makes it suitable for control purposes. Thus, in this chapter, we use the stationary wake model for modelling the aero-dynamical interaction of WTs within a WF. The stationary wake model is a suitable interaction model for a single row of WTs with the wind speed parallel to a row of the WTs. It maps the coefficient of thrust, which is directly linked to the wind speed deficit, the wind speed and the turbulence level of the up-WTs to identify their effect on the down-WTs [65].

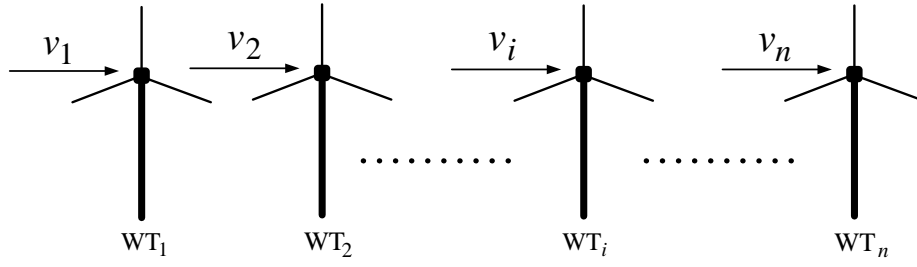


Fig. 4.2 A row of wind turbines in a wind farm for wake modelling.

Considering the configuration of Fig. 4.2, we can calculate the wind speed that reaches WT_{i+1} as:

$$v_{i+1} = v_i + k'(v_1 - v_i) - kv_1 C_{t,i} , \quad (4.3)$$

where $0 < k' < 1$ corresponds to the recovered wind speed, $0 < k < k'$ accounts the effect of the previous WT and $0 < C_{t,i}(\lambda, \beta) < 1$ is the thrust coefficient of the nearest up-WT. Distance parameters k' and k are selected based on actual WF data. In the simplest approach, we need the data from three WTs. k can be set based on $C_{t,1}$ and v_2 , and then k' can be set by having k , $C_{t,2}$ and v_3 . It is assumed that $k' = 0.35$ and $k = 0.1$. The coefficient of performance $C_p(\lambda, \beta)$ and the coefficient of thrust $C_t(\lambda, \beta)$ are defined as follows:

$$C_p = \frac{2P_{mec}}{\rho \pi R^2 v^3} , \quad (4.4)$$

$$C_t = \frac{2T_F}{\rho \pi R^2 v^2} , \quad (4.5)$$

where P_{mec} is the wind power transferred into mechanical power in the WT's rotor, ρ is the air density, R is the radius of the WT's rotor, wind speed is v and T_F is the rotor thrust. Considering (4.4) and (4.5), and the power and torque relations, $P = \omega T$, a direct relationship between $C_p(\lambda, \beta)$ and $C_t(\lambda, \beta)$ in all operation regions where $C_t < \frac{8}{9}$ can be derived as follows [104]:

$$C_p = \frac{1}{2} \left(1 + \sqrt{1 - C_t} \right) C_t , \quad (4.6)$$

where C_p can either be given in a look-up table [105], or it can be approximated using curve-fitting [106]. The above equations show that any changes in $C_p(\lambda, \beta)$ results in changes to $C_t(\lambda, \beta)$. Reducing $C_p(\lambda, \beta)$ for de-loaded operation results in a lower value of $C_t(\lambda, \beta)$, which results in less energy being extracted from the wind. This, in turn, increases the wind downstream and reduces the turbulence. By doing this, up-WTs would produce less power;

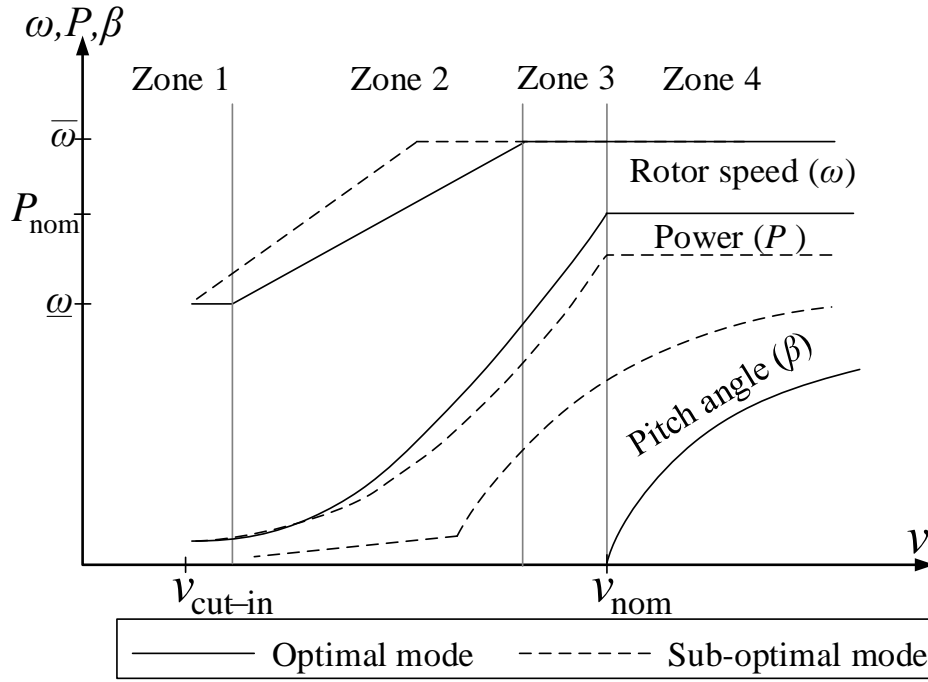


Fig. 4.3 Power, rotor speed and pitch angle characteristics of a Type III WT.

whereas, down-WTs produce more power because of higher wind speed. Overall, there might be some operation points, where the total output power of the WF might remain the same, while optimising the rotational kinetic energy of the WF for frequency control services. We can formulate this as an optimisation problem to maximise the rotational kinetic energy of the WF without compromising its output power in the following subsection.

4.2.3 Wind Farms Optimal Operation Strategy for Frequency Control

Fig. 4.3 illustrates the rotor speed, the pitch angle and the power characteristics of a Type III WT under the optimal and the sub-optimal (de-loaded) operation modes in four different zones. Under the optimal operation mode, the rotor speed is constant in Zones 1 and 3, and C_p is not optimal. In Zone 2, any changes in the wind speed causes the rotor speed to change in order to maximise C_p . In Zone 4, the rotor speed is at its maximum limit. Therefore, the pitch control operates to limit the input mechanical power to its rated value. Under the optimised sub-optimal operation mode [20] in Zones 1 and 2, both the rotor speed, ω , and the pitch angle, β , vary to optimise the kinetic energy of the rotor, defined as:

$$E_k^{\text{opt}} = \frac{1}{2} J (\omega^{\text{sub}})^2, \quad (4.7)$$

where J is the VSWT inertia, and ω^{sub} is the rotor speed in the sub-optimal operation mode. The kinetic energy can also be expressed in per unit system as follows:

$$E_k^{\text{opt}} = H(\omega_{\text{pu}}^{\text{sub}})^2, \quad (4.8)$$

where $\omega_{\text{pu}}^{\text{sub}}$ is the per unit rotor speed of the VSWT in the sub-optimal operation mode, and H is the normalised inertia of the WT. A typical value for H is $3 \frac{\text{MWs}}{\text{MW}}$ to $5 \frac{\text{MWs}}{\text{MW}}$.

In Zones 3 and 4, since the rotor speed is maximum $\bar{\omega}$, the only control variable is β , and no additional kinetic energy can be achieved. In Zone 2 under the sub-optimal mode, $\omega_{\text{high}}^{\text{sub}} > \omega^{\text{opt}}$, so Zone 2 becomes narrower as the δ increases, and this limits the available margin of de-loading, δ [20]. Considering the above-mentioned constraints, we formulate the optimisation problem in the following section.

The Optimisation Problem

We optimise the total kinetic energy of a WF by de-loading some of the up-WTs by jointly optimising the rotor speed, ω , and the pitch angle, β . We consider a WF with a single row of identical Type III WTs, so the wake effect of the neighbouring rows is not considered. Additionally, we assume that the wind direction is parallel to the string of WTs. Optimisation problem for a WF with N WTs in a row is formulated as follows:

$$\underset{\omega, \beta}{\text{maximise}} \quad \sum_{i=1}^N E_{k,i}, \quad (4.9)$$

the optimisation problem is subjected to (4.3), as well as the following constraints:

$$P_i \leq \bar{P}_i \quad \forall i \in \{1 \dots N\}, \quad (4.10)$$

$$0 \leq \beta_i^{\text{sub}} \leq \bar{\beta}_i \quad \forall i \in \{1 \dots N\}, \quad (4.11)$$

$$P_i^{\text{sub}} = (1 - \delta)P_i^{\text{opt}} \quad \forall i \in \{1 \dots N-1\}, \quad (4.12)$$

$$\underline{\omega}_i \leq \omega_i^{\text{opt}} \leq \omega_i^{\text{sub}} \leq \bar{\omega}_i \quad \forall i \in \{1 \dots N\}. \quad (4.13)$$

The optimisation variables are ω_i and β_i , so the number of variables is $2N$, where N is the number of WTs in the WF. In a Type III WT, $\underline{\omega}$ and $\bar{\omega}$ are limited by the size of the power electronic converter. Furthermore, the minimum rotor speed in the sub-optimal operation mode is further limited by the minimum rotor speed in the optimal mode. As shown in Fig. 4.1, to increase the stored kinetic energy of the rotor, its speed in the sub-optimal mode should be higher than its speed in the optimal mode, $\omega^{\text{sub}} \geq \omega^{\text{opt}}$.

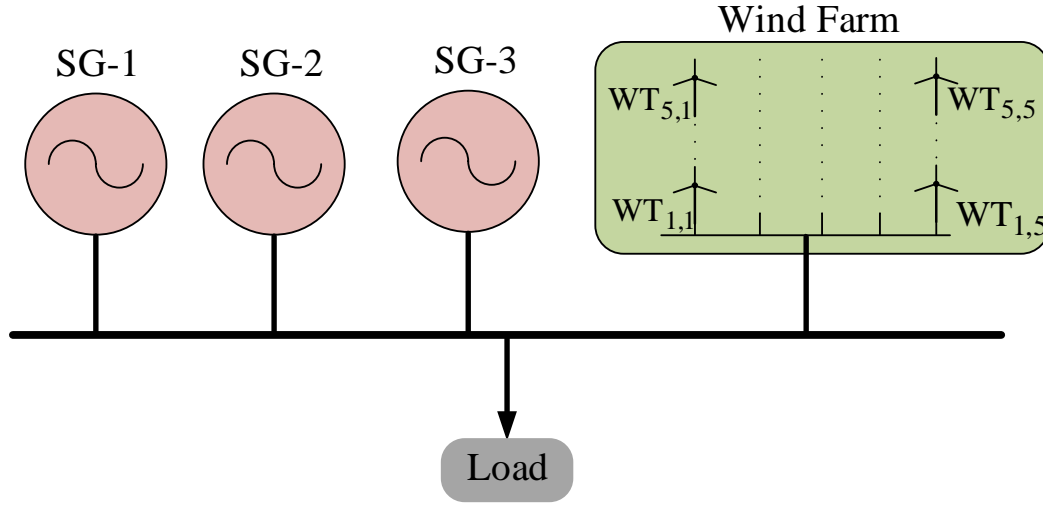


Fig. 4.4 One-line diagram of the power system for simulation.

The resulting constrained non-linear optimisation problem is non-convex and global, having several local optima. We solve it with the pattern search algorithm using MATLAB Global Optimisation Toolbox [107]. Although the optimisation problem has multiple optima, we were able to solve it efficiently with a good-quality solution (i.e. increasing the KE while maintaining the active power output of the WF as shown in Fig. 4.6). For a small system used in this section, the computational efficiency was not an issue. For a larger system, the optimisation can be performed off-line and solutions stored in a look-up table, which can then be readily implemented in a control algorithm.

4.2.4 Case Study

We evaluate the efficacy of the proposed operation strategy on a small test system with high penetration of wind generation shown in Fig. 4.4. The system consists of three SGs, a WF with 5 rows of WTs, each consisting of five 5 MW Type III WTs, and a 140 MW constant load. We assume that the distance between the rows is large enough so we can ignore the wake interaction between the neighbouring rows, which enables us to perform the optimisation for each row independently.

We consider the 5 MW NREL reference WT [105]. Using the pattern-search algorithm with the above constraints, we can maximise the total kinetic energy of a WF with N WTs by a combined optimisation of ω and β in Zones 1 and 2. In Zones 3 and 4, the rotor speed is at its maximum limit; therefore, the only control variable is β , so the kinetic energy cannot be increased further.

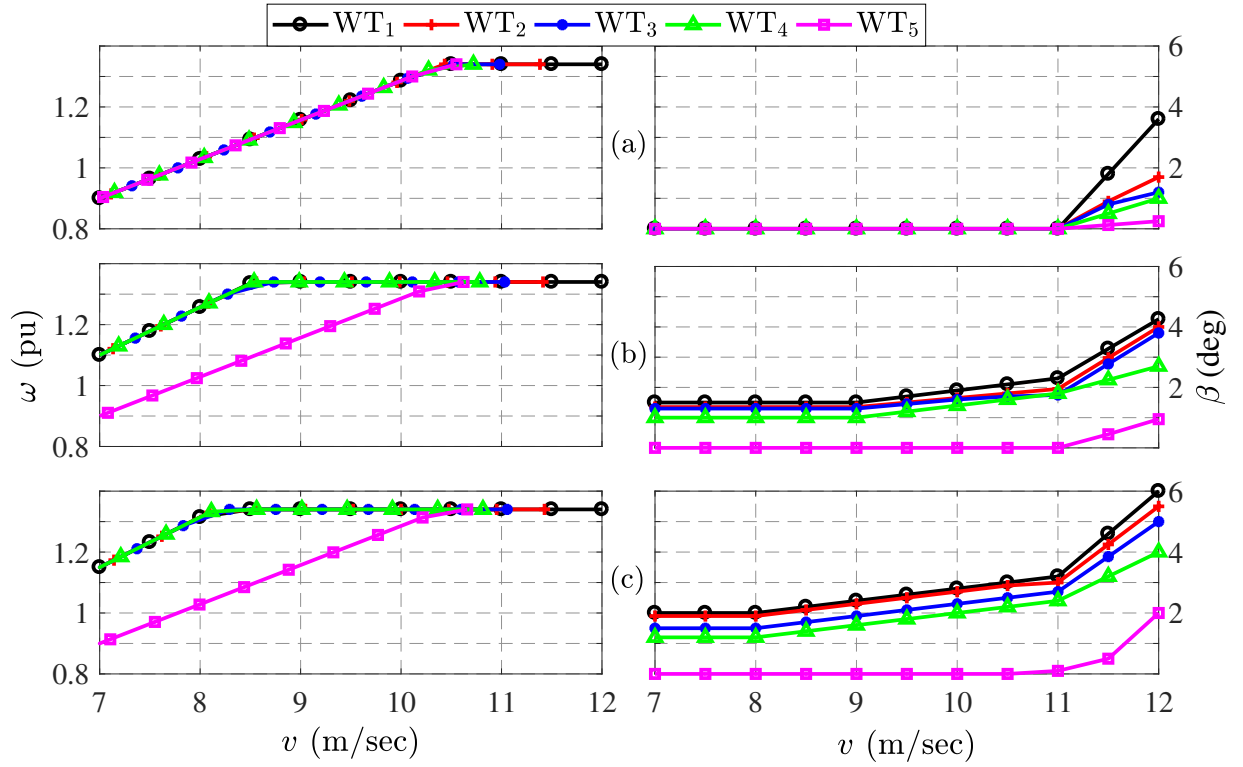


Fig. 4.5 The pitch angle and the rotor speed of the wind turbines in the wind farm: a) Case I, $\delta = 0\%$, b) Case II, $\delta = 5\%$, c) Case III, $\delta = 10\%$.

Optimisation Results

The optimisation of the kinetic energy was performed for a WF with five Type III WTs in a row. As per (4.1 and 4.12), we run the simulation for three cases:

- **Case I:** $\delta = 0\%$, all WTs operate in the optimal mode,
- **Case II:** $\delta = 5\%$, the de-loading margin is applied only to WT₁ – WT₄,
- **Case III:** $\delta = 10\%$, the de-loading margin is applied only to WT₁ – WT₄.

Note that WT₅ which is the last WT in the WF is not de-loaded. By doing this, we maximise WT₅'s power production and capture the spilled wind energy of the other up-WTs. For all three cases, the optimisation was performed for a wind speed range of $7 \frac{\text{m}}{\text{s}} \leq v \leq 12 \frac{\text{m}}{\text{s}}$, where the rotor speed varies between $\underline{\omega} \leq \omega \leq \overline{\omega}$. Fig. 4.5 shows the optimal rotor speeds and the pitch angles of WT₁ – WT₅ in all cases. The optimised kinetic energy and the total power of the WF are shown in Fig. 4.6. In Case I, all WTs operate in the optimal mode, and no additional kinetic energy can be stored as shown in Figs. 4.5a and 4.6a. In Cases II and III, the results are similar for lower wind speeds (Zones 1 and 2), and we can store considerable

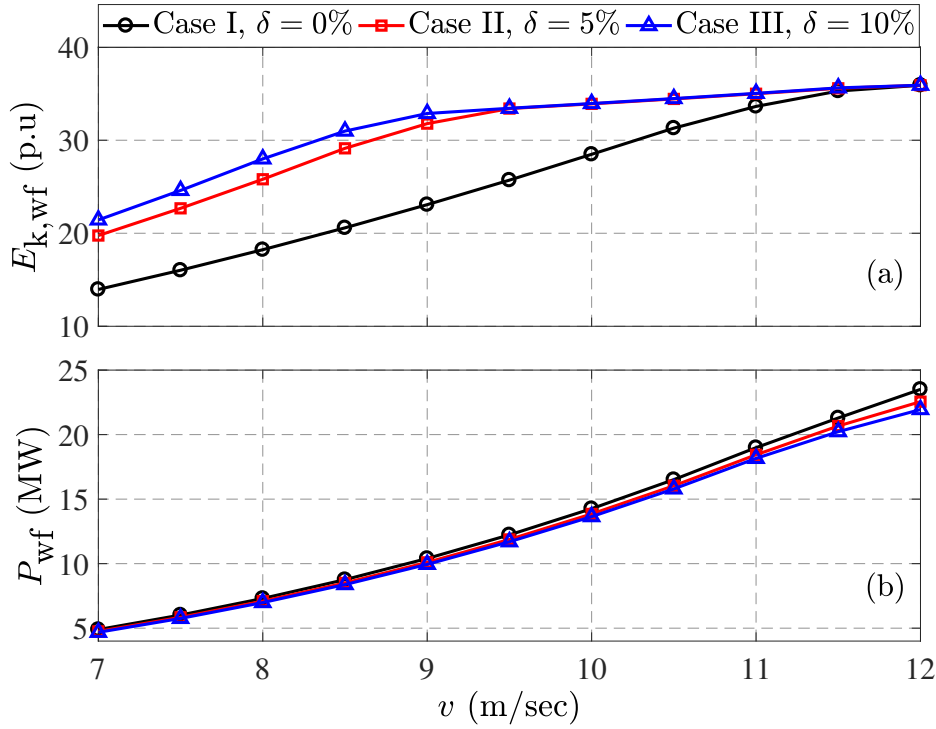


Fig. 4.6 The optimised kinetic energy in p.u, based on the ratings of the wind turbine, and the power of the wind farm with different de-loading margins.

amount of kinetic energy by varying both the rotor speed and the pitch angle as shown in Figs. 4.5b and 4.5c. Since both C_p and C_t are functions of the rotor speed and the pitch angle, and the operation of the down-WTs is linked to the operation of the up-WTs by the wake equation, i.e. (4.3), we can vary both the rotor speed and the pitch angle of the WTs and not affect the total power of the WF, but still be able to store considerable amount of kinetic energy in the rotating masses of the WTs, as shown in Fig. 4.6a.

In Cases II and III, the rotor speed and the pitch angles of $WT_1 - WT_4$ follow similar trends (i.e. Zones 1 and 2) until the rated rotor speed is reached (i.e. in Zone 3). In these regions, setting the pitch angle approximately between 1° and 2° , and maintaining the total power of the WF close to optimal, the rotor speed increases more rapidly, thus increasing the total amount of stored kinetic energy. As shown in Fig. 4.6a, we can increase the total kinetic energy of the WF by increasing the, δ . However, once the rated rotor speed is reached, no further kinetic energy can be stored. Fig. 4.6a shows that for wind speeds, $v \geq 9.5 \frac{m}{s}$, the rotor speeds are at their respective maximal limits in both cases. Therefore, no additional kinetic energy can be stored in Cases II and III, and in this region, the optimisation of the kinetic energy is independent of the δ . For wind speeds, $v \leq 9.5 \frac{m}{s}$, on the other hand, the available kinetic energy of the rotor is directly proportional to the, δ , as shown in Fig. 4.6a.

Table 4.1 Settings and characteristics of synchronous generators

SG	Type	P_{out} (MW)	\bar{P} (MW)	Governor Type[108]	Droop
1	Steam	25.5	45	IEEEG1	20 %
2	Gas	45	50	TGOV1	5 %
3	Gas	20	25	TGOV1	5 %

Observe that for lower wind speeds the cumulative output power of the WF is almost the same in all three cases. In higher wind speeds, on the other hand, as the δ increases, the total output power decreases. In lower wind speeds, we can take advantage of the wake interaction to partly recuperate the power which we lose by de-loading. For higher wind speeds, we are unable to do this because the power that we lose by de-loading of the up-WTs is comparatively higher, which negatively impacts the efficiency of the WF, as shown in Fig. 4.6b. A better strategy for higher wind speeds would be to de-load fewer WT's with a higher δ , which would allow down-WTs not only to recuperate the power which we lose by the de-loading of the up-WTs but would also possibly improve the overall efficiency of the WF. Indeed, it has been shown in [65] that in a WF with 10 WT's in a row, de-loading the first WT by 10 % improves the row efficiency of the WF by 3 %.

Time-Domain Simulations

To validate the optimisation results, we use time-domain simulation to simulate a frequency disturbance in the simple test system shown in Fig. 4.4. Unlike voltage, frequency is a global variable. Hence, for the purpose of validating our results using of a copperplate model is sufficient. Note that for the time-domain simulation, we extend the optimisation results from a single row of WT's in the WF to five rows of WT's in the WF, as shown in Fig. 4.4. We do this by considering a large distance between the neighbouring rows of the WT's perpendicular to the direction of the wind speed. We assume that the free wind speed v_1 reaching $\text{WT}_{1,1} - \text{WT}_{1,5}$ is uniform and $v_1 = 8 \frac{\text{m}}{\text{s}}$, which results in an overall output power of $P_{\text{wf}} = 47 \text{ MW}$ from the WF in all three cases. The characteristics and the settings of the SGs are given in Table 4.1.

Simulation was performed for the three cases described in Section 4.2.4. For all cases, we disconnect SG-3 from the system at $t = 10 \text{ s}$. Meanwhile, in Cases II and III, we change the operation mode of $\text{WT}_{1,x} - \text{WT}_{4,x}$ from sub-optimal to optimal to release the stored kinetic energy into the system. The system frequency response is shown in Fig. 4.7 and the rotor speeds are shown in Fig. 4.8. Since all rows of WT's in the WF are identical, only the rotor speeds of the $\text{WT}_{1,1} - \text{WT}_{1,5}$ are shown.

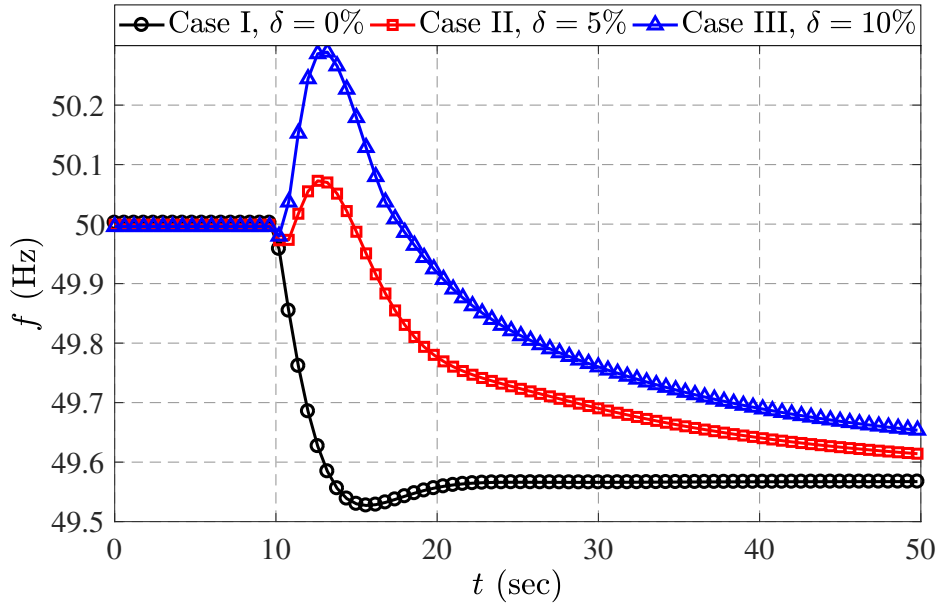


Fig. 4.7 System frequency behaviour during the generation loss.

In Case I, all WTs operate in the optimal mode, so there is no additional kinetic energy. Hence, after disconnecting SG-3, the system frequency drops rapidly and the frequency nadir of 49.52 Hz is achieved after 6 s. It takes about 13 s for the frequency to plateau as shown in Fig. 4.7. The rotor speeds are shown in Fig. 4.8a. Since the wind speed is constant, and the WTs operate in the optimal mode, the rotor speeds after the incident remain constant.

In Cases II and III, considerable amount of kinetic energy is available as shown in Fig. 4.6a. Therefore, after disconnecting SG-3, we inject this kinetic energy to the system. As a result, for the first few seconds, the system frequency not only does not drop, but it also rises, as shown in Fig. 4.7. Since in Case III the δ is higher than in Case II, WF contribution on the primary frequency response is even higher. Fig. 4.7 shows that in these two cases too much of kinetic energy is released too soon, which resulted in a frequency over-shoot. A better strategy would be to inject this energy into the system gradually, either by using the control strategy developed in [102] or by reducing the rate of change of the rotor speed. Figs. 4.8b and c illustrate the rotor speeds of WTs in Cases II and III. Observe that there is a significant discrepancy between the rotor speeds of WT₁ – WT₄ in the sub-optimal and the optimal operation modes, which results in a positive contribution of the WF to the primary frequency control. Note that WT₅ is not de-loaded, so it does not participate in the frequency control, and has a constant rotor speed during the frequency event. To control the rate of change of the rotor speed and release the rotational kinetic energy of the WF into the system in a controlled manner, we propose an optimal frequency control strategy in the following section.

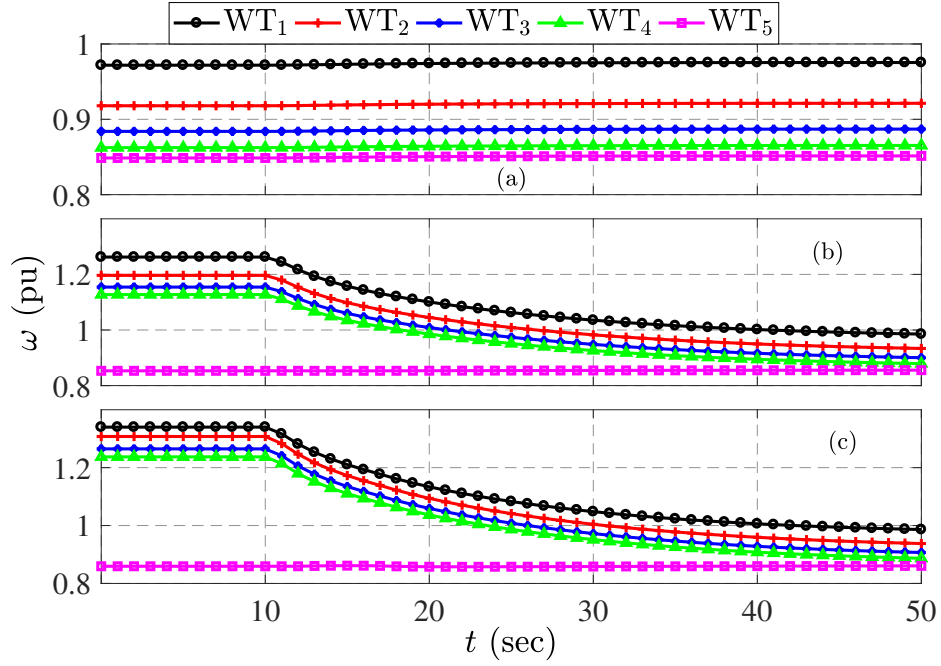


Fig. 4.8 The rotor speed of wind turbines during the generation loss: a) Case I, $\delta = 0\%$, b) Case II, $\delta = 5\%$, c) Case III, $\delta = 10\%$.

4.3 An Optimal Control Strategy for Participation of Wind Farms in Frequency Control

In Section 4.2, we exploited wake interaction in a WF to maximise the total kinetic energy of the WTs' rotating masses in the WF. Nonetheless, it was noticed that the deployment of WTs' rotational kinetic energy into the system in an uncontrolled manner might result in frequency over-shoot in some situations. To deal with that issue, we propose an optimal control strategy for the participation of WFs in primary frequency control. The aim of this strategy is to optimally deploy the rotational kinetic energy of the WF into the system after a frequency event. By doing this, we improve both the RoCoF and the frequency nadir. In this strategy, we control the rate of change the WTs' rotor speed. Hence, the amount of power injected, from the WF rotational kinetic energy, into the system by the controllers is proportional to the RoCoF and the frequency deviation after the contingency. By implementing this strategy in a test system shown in Fig. 4.4, the stored kinetic energy of the WTs in the WF is gradually injected into the system during a frequency excursion. The results show that not only the system frequency nadir is reduced, but also it is kept relatively uniform for up to 50 s.

4.3.1 Proposed Control Strategy

Considering the optimised sub-optimal operation strategy discussed in Section III, the total electrical power supplied by a de-loaded WT during a frequency event is given as:

$$\hat{P} = P_{\text{mec}} + P_{E_k} , \quad (4.14)$$

where P_{mec} is the mechanical part as follows:

$$P_{\text{mec}} = \frac{1}{2} C_p(\lambda, \beta) \rho \pi R^2 v^3 , \quad (4.15)$$

and P_{E_k} is the inertial part and can be expressed as follows:

$$P_{E_k} = H \frac{d}{dt} (\omega_{\text{pu}}^{\text{sub}})^2 , \quad (4.16)$$

the total amount of kinetic energy that a WF can release into the system during a frequency excursion is given as:

$$\Delta E_k = \sum_{i=1}^N H \left((\omega_{\text{pu},i}^{\text{sub}})^2 - (\omega_{\text{pu},i}^{\text{opt}})^2 \right) , \quad (4.17)$$

where N is the number of de-loaded WTs in the WF, H is the normalised inertia of the WTs, $\omega_{\text{pu},i}^{\text{sub}}$ and $\omega_{\text{pu},i}^{\text{opt}}$ are the per unit rotor speed of the WT_{*i*} in the sub-optimal and optimal operation mode, respectively. Notice that in Zones 1 and 2, the rotor speed in the sub-optimal mode is always higher than the rotor speed in the optimal operation mode ($\omega^{\text{sub}} \geq \omega^{\text{opt}}$), as shown in Figs. 4.1 and 4.8.

As shown in Fig. 4.6, in Zones 1 and 2, the WF has the same output power both in the sub-optimal operation mode as well as the optimal operation mode. However, the kinetic energy of the WF in the sub-optimal operation mode is considerably higher compared to the optimal operation mode. Therefore, it can be concluded that during a frequency event when the operation modes of the up-WTs are changed from the sub-optimal to the optimal, only a small portion of extra mechanical power is provided by the WF. Whereas, according to (4.17) and Fig. 4.6, considerable amount of kinetic energy can be injected into the system. In small systems with high penetration of wind generation similar to the one shown in Fig. 4.4, this can sometimes result in a frequency overshoot, as shown in Fig. 4.7. Therefore, our focus is to control the injection of the kinetic energy into the system during a frequency excursion. This can be controlled by various system variables including the frequency deviation, the RoCoF, and the rate of change of the rotor speed. By doing this, not only we can prevent

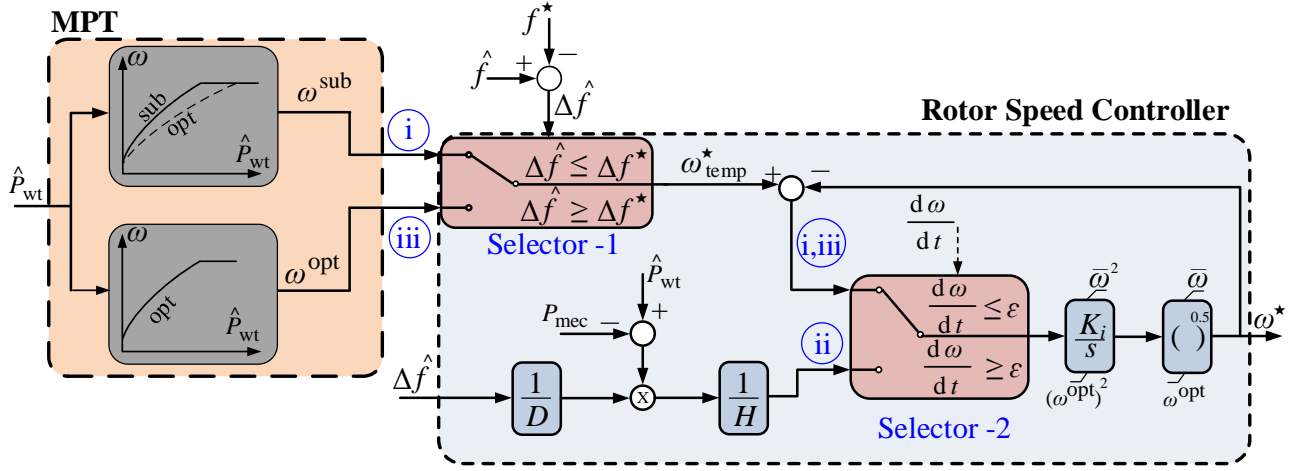


Fig. 4.9 The proposed rotor speed controller diagram.

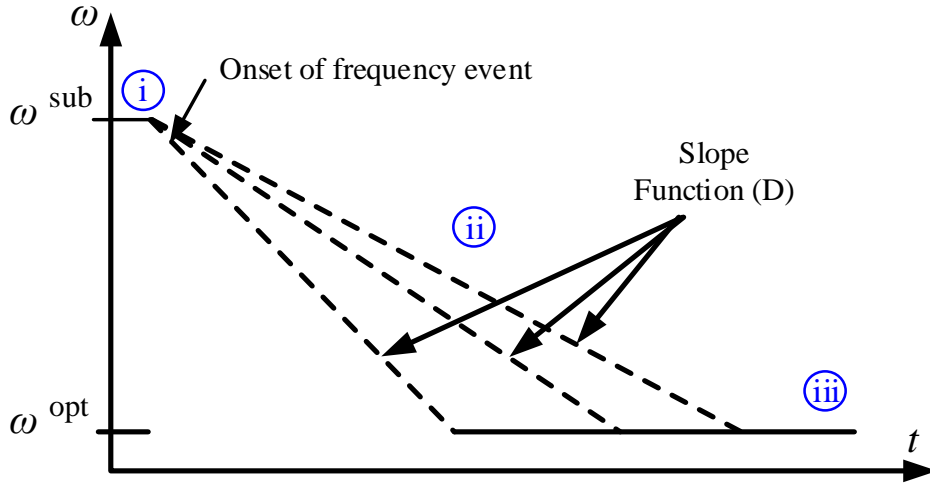


Fig. 4.10 The rotor speed transition representation from the sub-optimal to the optimal operation mode during the system frequency excursion.

the system frequency overshoot, but also provide primary frequency response for a longer period.

The proposed rotor speed controller is shown in Fig. 4.9, which has three operation modes, as shown in Fig. 4.10:

- (i) the sub-optimal operation mode,
- (ii) the transition from the sub-optimal to the optimal operation mode during a frequency event, and
- (iii) the optimal operation mode.

The system frequency is an input to the controller. As the system frequency drops below the reference frequency ($|\Delta\hat{f}| \geq |\Delta f^*|$), *Selector 1* switches the operation mode from (i) to (iii), as shown in Fig. 4.9. Here, the rotor speed starts to decrease. As the rotor speed decreases, the total output power of the WF (4.14) increases, mainly due to an increase in the inertial part (4.16) because the mechanical output power of the WF is mostly the same in the optimal and the sub-optimal operation modes as discussed in Section 4.2.4. The variation in the rotor speed activates *Selector 2*, which changes the operation mode from (iii) to (ii). The reference speed in (ii) is derived from (4.16) and (4.18), as illustrated in Fig. 4.9. The parameters of (4.18) and Fig. 4.9 were determined heuristically. At this stage, based on the system frequency deviation, the controller regulates the rate of change of the rotor speed until $\frac{d}{dt}\omega$ becomes very small, or until the secondary controller is activated which reverses the process. As the $\frac{d}{dt}\omega$ converges to zero, *Selector 2* switches the operation mode from (ii) to (iii). At this point, there is no more kinetic energy to be injected into the system, and the WTs operate in the optimal operation mode. As shown in Fig. 4.10, the rate of change of the rotor speed in (ii) is a function of D , as also shown in (4.18). In (4.18), the faster the RoCoF and/or the higher the frequency deviation the faster the rate of change of the rotor speed and vice versa, as also illustrated in Fig. 4.10.

$$D = K_{df} \frac{df}{dt} + K_f \Delta\hat{f}. \quad (4.18)$$

The proposed pitch angle controller is illustrated in Fig. 4.11. Observe that the pitch angle controller has two operation modes. At the onset of the frequency event, the controller instantly switches the operation mode from the sub-optimal to the optimal to release part of the mechanical power (4.15). This results in an increase in the mechanical output power of individual WTs. However, it does not change the mechanical output power of the WF significantly because of the wake effects. The mechanical output power of the WTs is still not optimal at this stage because the rotor speed is sub-optimal. Note that the optimised pitch angles are stored in look-up tables and then provided to each individual WTs, as shown in Fig. 4.11.

Note that with the above control strategy in a system with high penetration of wind energy, we can control the rate at which the kinetic energy of the WF is released into the system during a frequency event based on the actual requirement of the system. This is achieved by measuring the RoCoF as well as the frequency deviation of the system and controlling the injection of the kinetic energy based on those measurements. This not only significantly reduces the system frequency nadir, but it also prevents the system frequency overshoot in

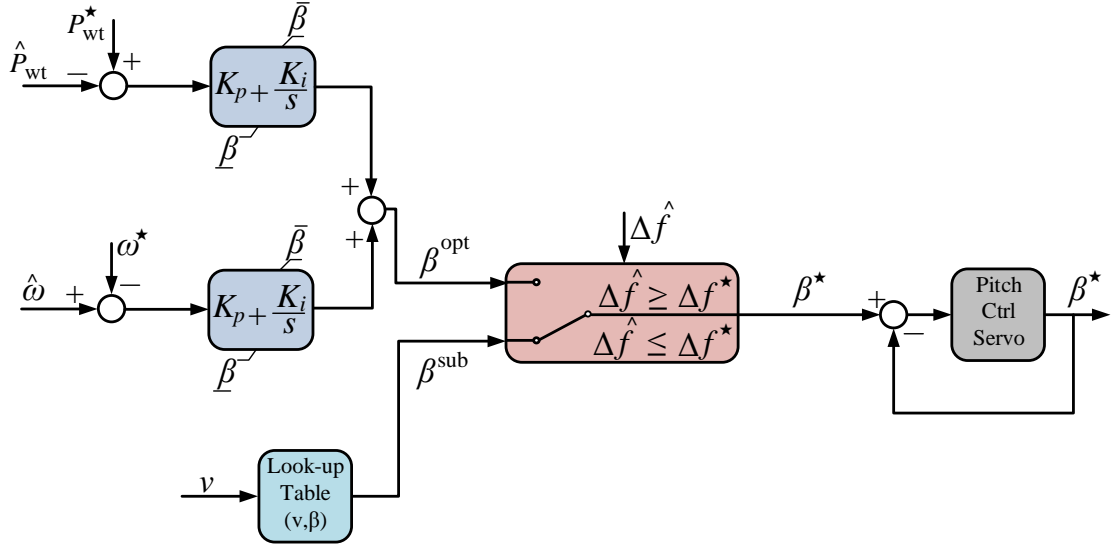


Fig. 4.11 The proposed pitch angle blade controller diagram.

the first few seconds after the operation mode of the WTs is changed from the sub-optimal to the optimal. We will return to this in the following subsection when discussing the results.

It has to be mentioned that operation of both *Selectors 1 and 2* are initiated by the system frequency deviation only when $|\Delta \hat{f}| \geq |\Delta f^*|$, which prevents the controller to operate on the small changes of the rotor speed caused by the changes in the wind speed, or small frequency disturbance. In the following subsection, we perform some time-domain simulation to evaluate the efficacy of the proposed control strategy.

4.3.2 Time-Domain Simulation Results

The control strategy presented in the previous section is implemented on the test system shown in Fig. 4.4. For the sub-optimal operation mode, the optimisation results of Case III where $WT_{1,N} - WT_{4,N}$ were initially de-loaded by 10 % is considered. Simulation was performed for the same situations explained in Section 4.2.4, where the free wind speed entering the WF is $v_1 = 8 \frac{m}{s}$, and at $t = 10s$ the SG-3 with $P_{out} = 20MW$ was disconnected from the system. We run the simulation for different operation scenarios:

- **a** - $\Delta f^* = 150mHz$,
- **b** - $\Delta f^* = 200mHz$,
- **c** - no controller is used in this scenario.

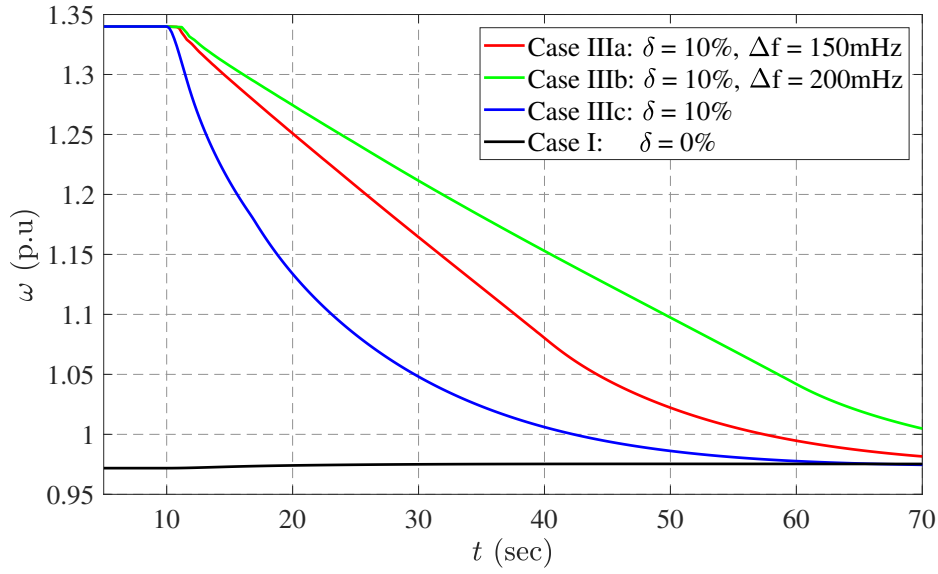


Fig. 4.12 Rotor speed of $WT_{1,1}$ in the WF under different operation scenarios.

We use the above scenarios considering the results of Case III from Section 4.2.4, and compare the results with Case I. The rotor speed of the $WT_{1,1}$, the system frequency, and the total output power of the WF are illustrated in Figs. 4.12, 4.13, and 4.14, respectively.

Observe that under the optimal operation mode, the rotor speed of the WT does not change during the system frequency event (i.e. Case I), and the output power of the WF is also constant. Therefore, the WF does not participate in the primary frequency control. As a result, the RoCoF is very high and the system frequency nadir is below 49.55 Hz as shown in Fig. 4.13. On the other hand, by utilising the operation strategy discussed in Section 4.2.4, without appropriate controller (i.e. Case IIIc), the rotor speed changes from the sub-optimal to the optimal operation mode in a very short time, which results in injection of too much power from the rotating masses of the WTs into the system in a very short time as shown in Fig. 4.14. As a result, in the first few seconds after the incident, not only the system frequency does not drop, but it also rises as shown in Fig. 4.13.

With the proposed rotor speed and pitch angle controllers, after an incident, the $\frac{d}{dt}\omega^*$ is a function of the RoCoF and system frequency deviation. For instance, in Case IIIa, with $\Delta f^* = 150\text{mHz}$, it takes about 50 s for the rotor speed controller to release the stored kinetic energy of the rotor, and move from the sub-optimal operation mode to the optimal operation mode. Whereas, in Case IIIb, with $\Delta f^* = 200\text{mHz}$, this time is more than 60 s as shown in Fig. 4.12. This consequently affects the total output power of the WF, as well as the system frequency response, as shown in Figs. 4.13, and 4.14, respectively. Observe that without the appropriate control strategy, the kinetic energy of the WTs is released in a very short time,

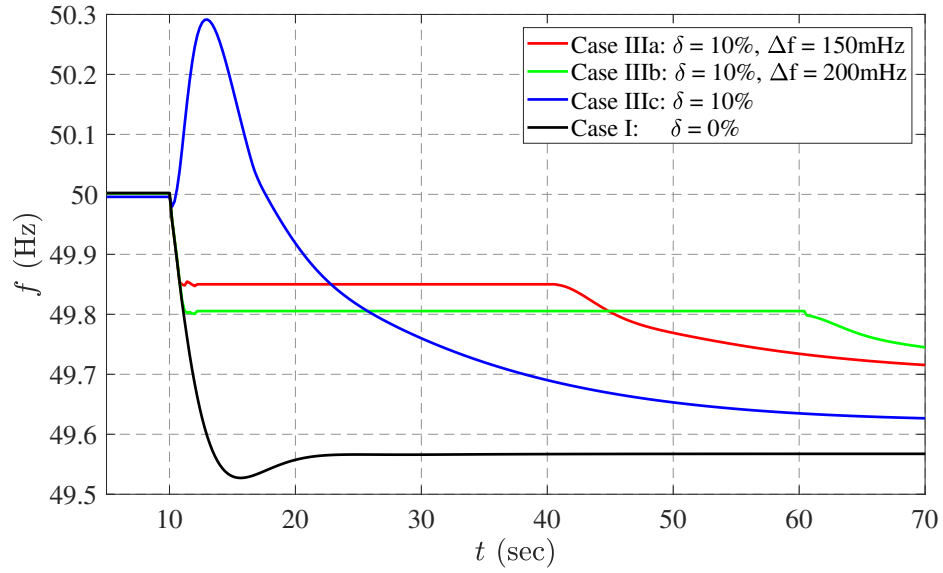


Fig. 4.13 System frequency under different operation scenarios.

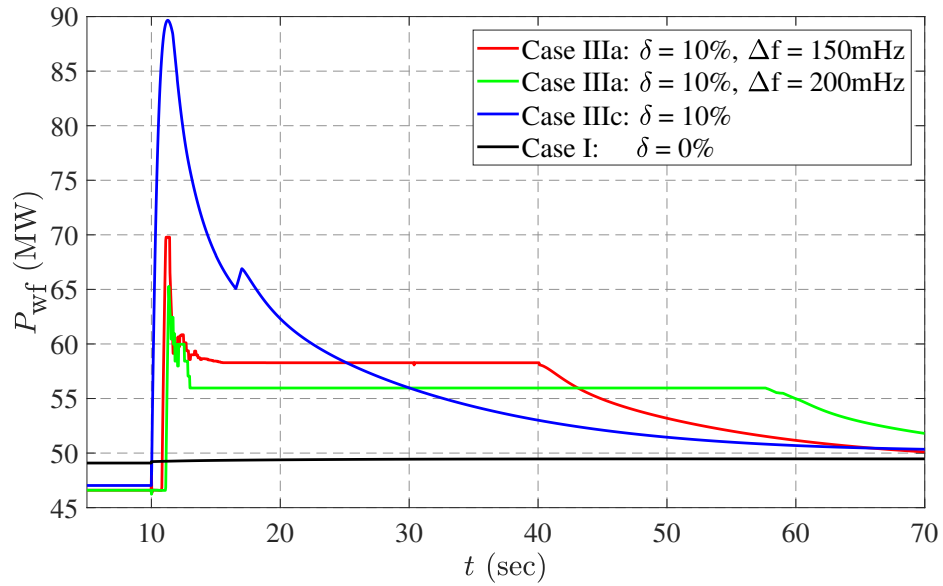


Fig. 4.14 Total output power of the WF under different operation scenarios.

which cannot be used efficiently. With the proposed control strategy, on the other hand, we can manage to use the kinetic energy of the WT's more efficiently, and keep the total output power of the WF as well as the system frequency relatively uniform from the onset of the frequency event until the rotor speed reaches its optimal value.

4.4 Summary

In the first part of this chapter, we proposed an optimised operation strategy for the WFs in the sub-optimal operation mode. In this strategy, we maximised the total stored kinetic energy of the WT's rotors, which can be released into the system during a frequency dip. We did this by optimising the rotor speeds and the pitch angles of some of the up-WTs within the WF. In contrast to the traditional WF operation, which is based on optimally operating every individual WT, we model the whole WF as a single optimisation problem by taking advantage of the wake interaction within the WF. We showed that not only a WF can provide primary frequency response, but it also can possibly deliver more power. It has been shown that by using WT's rotational kinetic energy, we can delay the system frequency nadir. We have, however, observed that in some cases too much kinetic energy could be released into the system too soon, which indicated that more intricate control strategies might be needed to achieve an optimal system performance.

Therefore, in the second part of this chapter, an optimal control strategy for the participation of VSWT based WFs in primary frequency control was proposed. In this strategy, we controlled the injection of the WT's rotational kinetic energy into the system during a frequency excursion by controlling the rate of change of the rotor speed to reduce the system frequency nadir. The results showed that with the proposed operation and control strategy, WFs can provide valuable primary frequency control service. It was shown that considerable amount of rotational kinetic energy can be stored in the rotating masses of WT's, which can be used for the primary frequency control. The simulation results show that in a test system with high penetration of wind energy it takes about 50 s - 60 s to deploy the rotational kinetic energy of the WT's, and keep the system frequency relatively uniform during this period.

Chapter 5

Coordinated Operation of Wind Farms for Frequency Control

5.1 Introduction

In this chapter, we further develop the WFs' operation and control strategy proposed in Chapter 4 and propose a coordinated WF operation strategy that exploits the wake interaction within a WF. In contrast to the conventional WF operation strategy, where each WT is optimised individually, three operation strategies are suggested:

1. Maximisation of the WF's power while maintaining WF's rotational kinetic energy;
2. Maximisation of the WF's rotational kinetic energy while maintaining WF's output power; and
3. A de-loaded strategy whereby the WF's rotational kinetic energy is maximised for a fixed de-loading margin.

The three operation strategies are formulated as non-linear optimisation problems and solved in a central wind farm controller. The optimal rotor speeds and pitch angles are used as reference values in the individual WTs. The optimisation results for the three respective operation strategies show that: 1) up to 3 % increase in the WF's output power; 2) up to 23 % increase in the WF's rotational kinetic energy; and 3) up to 28 % increase in the WF's rotational kinetic energy and 8 % reserve power while operating the WF in a 5 % de-loaded mode with respect to the conventional operation strategy. Time-domain simulations show that the proposed operation strategy noticeably improves the WF's performance in frequency control.

In this chapter, we advance the work of Chapter 4 in the following aspects:

- The aim of Section 4.2 was to optimise the rotational kinetic energy of a WF with a simplified optimisation algorithm, whereas, in this chapter, we introduce three different algorithms, i.e. optimisation of WF's rotational kinetic energy, optimisation of WF's power, and optimisation of WF's rotational kinetic energy while de-loading the WF. Furthermore, we have improved the performance of the optimisation algorithm by introducing new decision variables (e.g. de-loading margin) and new constraints. We have also proposed a central wind farm controller (CWFC) that coordinates the operation of individual WTs within a WF. Further, we study the variability of the wind speed, as well as the wind speed time delay due to wake effect on the performance of the proposed CWFC.
- In Section 4.3, we introduced a frequency controller for individual WTs to regulate the injection of WTs' rotational kinetic energy into the system during a frequency event. In this chapter, we integrate those controllers into the CWFC to optimise the performance of the WF as a whole. The outcome of this chapter is published as journal article in [JA1]

The rest of the chapter is organised as follows: In Section 5.2, we briefly review the WF controllers. Section 5.3 presents the optimisation algorithm, as well as the proposed CWFC. In Section 5.4, the performance of the proposed operation strategy is evaluated in a case study, and Section 5.5 concludes the chapter.

5.2 Wind Farm Controllers

As discussed in Section 1.2.2, although both the electrical interconnection of the WTs, as well as the wake interaction within a WF have been studied extensively [21, 58–60, 68, 109], less work has been done on the coordinated operation of WTs within a WF [62]. The authors in [64] studied coordinated operation of WFs by considering the wake effects. They demonstrated that by intelligently selecting the operation point of the up-WTs, it is possible to improve the overall efficiency of the WF, which confirms the finding of [65].

WFs typically have a hierarchical control structure with a CWFC and individual WT controllers. The CWFC regulates the output power of the WF, P_{wf} and Q_{wf} , by defining the active and reactive power set-points of the individual WTs, $P_{wt,i}^*$ and $Q_{wt,i}^*$ [109]. Other requirements, i.e. ramp rate limiters, delta control and reactive power control can also be integrated into the CWFC [110]. The individual WT controllers achieve the operation points provided by the CWFC by regulating their ω and β . Because of the wake interaction, the operation point of the up-WTs has a direct effect on the wind speed reaching the down-WTs,

and, in turn, the output power of the down-WTs. To optimise the output power or kinetic energy of a WF for frequency control, and to operate a WF in a coordinated manner, we should optimally select ω_i^* and β_i^* rather than $P_{wt,i}^*$. Since the CWFC already communicates with the individual WTs, the capability of defining ω_i^* and β_i^* can easily be integrated into the CWFC. Therefore, in the CWFC by considering the wake interaction among the WTs and using an optimisation algorithm, we can determine the optimal values of ω_i^* and β_i^* .

5.3 Coordinated Operation of Wind Farms

We assume Type III WTs but the proposed operation strategy is applicable to Type IV machines too. The mechanical power of a Type III WT is given as:

$$P_{mec} = \frac{1}{2} \rho \pi R^2 v^3 C_p(\lambda, \beta), \quad (5.1)$$

where ρ is the air density, R is the radius of the WT blade, v is the wind speed and $C_p(\lambda, \beta)$ is the performance coefficient of the WT that varies with the blade pitch angle, β , and the tip speed ratio, λ , expressed as:

$$\lambda = \frac{\omega R}{v}, \quad (5.2)$$

The kinetic energy of a WT in per unit system is given as:

$$E_k = H \omega^2, \quad (5.3)$$

where ω is the rotor speed of the WT in per unit, and H is the normalised inertia of the WT. Typical values of H are between 3 s and 5 s. Ignoring the wake effect of the neighbouring rows of WTs by considering a large distance between the WTs perpendicular to the direction of the wind speed, the wind speed v_{i+1} reaching the WT_{i+1} can be calculated as follows [65]:

$$v_{i+1} = v_i + k'(v_1 - v_i) - kv_1 C_{t,i}, \quad (5.4)$$

where v_i is the wind speed at the nearest up-WT, WT_i , v_1 is the free wind speed entering the WF (at the first WT in the WF), k' corresponds to the recovered wind speed, k accounts for the effect of the previous WT, and $C_{t,i}(\lambda, \omega)$ is the thrust coefficient of the nearest up-WT. The distance parameters k' and k are selected based on the actual WF data. In the simplest approach, we need data from three WTs. Both C_t and C_p can be either given in look-up tables [105] or approximated using curve fitting [111]. Fig. 5.1 illustrates C_t and C_p

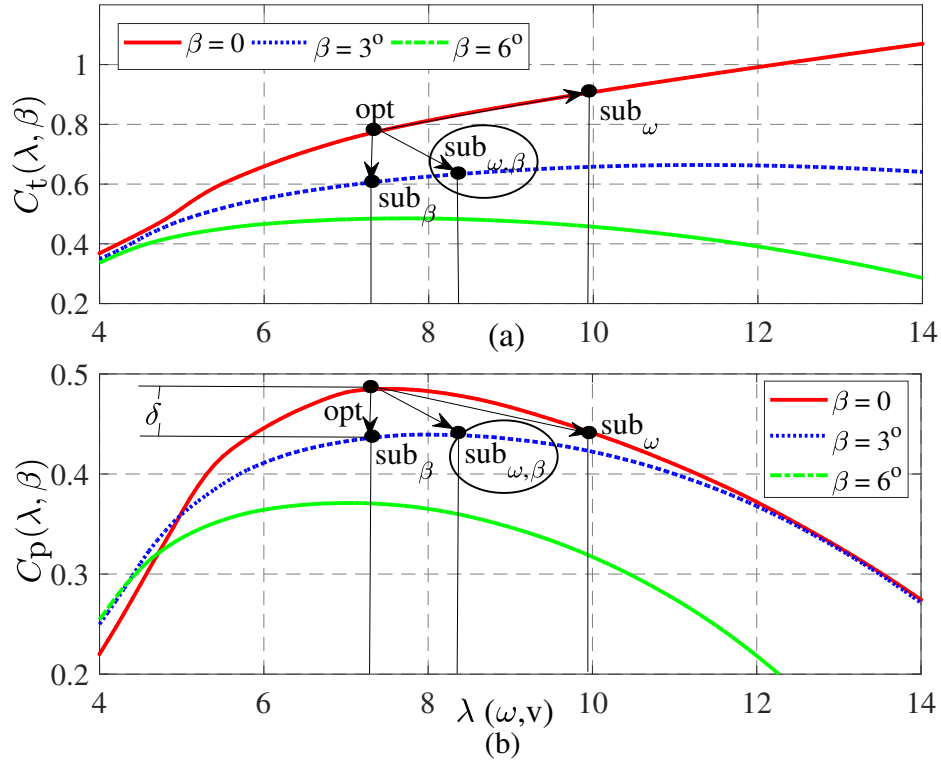


Fig. 5.1 Thrust and power coefficient of the NREL's 5 MW Type III wind turbine.

characteristics of the NREL 5 MW Type III WT [105] that was used as a reference in this study.

Normally, WTs operate in an optimal mode in order to maximise the power extraction as shown in Fig. 5.1b. However, to participate in primary frequency control, a WT has to operate in a sub-optimal mode with a lower coefficient of performance, C_p^{sub} . As shown in Fig. 5.1b, there are three feasible sub-optimal regions with a de-loading margin δ : (1) over speeding of the rotor, sub $_\omega$; (2) pitching of the rotor blades, sub $_\beta$; and (3) a combination of both, sub $_{\omega, \beta}$. According to (5.4) and (5.1), in a WF, the operation of up-WTs affects the wind speed reaching down-WTs, and, in turn, the output power of the down-WTs. Hence, to exploit the wake interaction in a WF, and to operate a WF in a coordinated manner, the up-WTs should be de-loaded in a way not only to increase kinetic energy in the rotating masses of the up-WTs, but also to reduce C_t of the up-WTs. This, in turn, increases the wind speed reaching the down-WTs (5.4). By reducing C_t , the fatigue load on the down-WTs also decreases [65]. As shown in Fig. 5.1, to achieve both of these objectives, the up-WTs should operate near the point, sub $_{\omega, \beta}$.

The rotor speed, the pitch angle and the power characteristic of a Type III WT in the optimal and sub-optimal operation modes, sub $_{\omega, \beta}$, in four different zones is shown in Fig. 4.3.

Note that in the optimal operation mode, the WT is partially loaded in Zones 1, 2 and 3; whereas, it is fully loaded in Zone 4. Zone 1, a start-up zone, is a transition between cut-in wind speed and Zone 2. In Zone 1, the rotor speed is at its minimum, and $C_p(\lambda, \beta)$ is not optimal. In Zone 2, the aim is to optimise the power capture of the WT. Hence, in this zone, the pitch angle is kept at its minimum, and the rotor speed is controlled in a way to maximise $C_p(\lambda, \beta)$. Zone 3 is a transition zone between partially loaded and fully loaded regimes. Notice that fluctuation of wind speed around its rated value may result in torsional torque variations and power overshoots. To deal with this issue, in [112] and [113] an optimal control strategy and a model predictive control were proposed, respectively. Zone 3 is normally required to limit the tip speed at rated power, and prevent torsional torque variations. In Zone 4, the WT is fully loaded and the rotor speed is at its limit, so the pitch control operates to limit the input mechanical power to its rated value. As shown in Fig. 4.3, in the proposed sub-optimal operation mode, $\text{sub}_{\omega, \beta}$, in Zones 1 and 2, both ω and β vary to maximise WF's kinetic energy. In Zones 3 and 4, the rotor speed is maximum, $\omega = \bar{\omega}$, so the only control variable for the de-loading will be β , and additional kinetic energy cannot be attained in these zones. In the following subsection, we formulate the optimisation problem.

5.3.1 The Optimisation Problem

The aim of the optimisation problem is to maximise either the total kinetic energy of the WF, $E_{k, \text{wf}}$, or the total output power of the WF, P_{wf} . This can be achieved by operating some of the up-WTs in a sub-optimal operation mode, and capturing the spilled energy of these WTs by the down-WTs.

Optimisation of Kinetic Energy

In a WF with N WTs in a row, the objective function is given as:

$$\underset{\omega, \beta}{\text{maximise}} \quad \sum_{i=1}^N E_{k,i}(\omega, \beta, v), \quad (5.5)$$

where $E_{k,i}(\omega, \beta, v)$ is given in (5.3). The objective function is subject to the following constraints:

a) *Converter rating*: The rotor speed is constrained as follows for all $i \in 1 \dots N$:

$$\underline{\omega}_i \leq \omega_i^{\text{opt}} \leq \omega_i^{\text{sub}} \leq \bar{\omega}_i, \quad (5.6)$$

the minimum and the maximum rotor speeds are limited by the rated power of the power electronic converter that is 30 % to 40 % of the nominal power of the generator. As shown in Fig. 5.1, to ensure that the WT's do not operate with a lower rotor speed than the optimal rotor speed, the minimum rotor speed in sub-optimal operation mode is further limited by the minimum rotor speed in optimal operation mode.

b) *Generator and turbine rated power* for all i :

$$P_i \leq \bar{P}_i, \quad (5.7a)$$

$$0 \leq \beta_i^{\text{opt}} \leq \beta_i^{\text{sub}} \leq \bar{\beta}_i, \quad (5.7b)$$

where in (5.7a), the output power of each WT is limited by its rated capacity. In higher wind speeds, pitch angle operates to limit the mechanical input power of the WT as given in (5.7b) and shown in Fig. 4.3. The pitch angle in the sub-optimal operation mode is also limited by the minimum pitch angle in optimal operation mode as shown in Fig. 5.1.

c) *Wake effect*: In a WF, operating points of up-WT's affect the wind speed reaching down-WT's as stated in (5.4) and Fig. 5.1. We consider (5.4) as the wake effect constraint for all i up to $N - 1$.

The constraints (5.6) and (5.7b) assure that the de-loaded WT's operate near the point $\text{sub}_{\omega, \beta}$ in Fig. 5.1. By doing this, we reduce C_t of up-WT's which consequently increases the wind speed reaching down-WT's as indicated in (5.4).

d) *Performance*: To ensure that the optimisation of kinetic energy does not reduce the output power of the WF, following constraint is enforced:

$$\sum_{i=1}^N P_i^{\text{sub}} = \sum_{i=1}^N P_i^{\text{opt}}. \quad (5.8)$$

After performing a number of simulations, we found that de-loading the WT's in the lower part of the WF (with respect to the wind direction) results in inferior local optima. Similarly, we found that the de-loading margin for an individual WT should not exceed 10 %. Therefore, we pruned the feasible region by enforcing the following two constraints:

$$P_i^{\text{sub}} = (1 - \delta) P_i^{\text{opt}} \quad \forall i \in \begin{cases} 1 \dots \frac{N}{2}, & N \text{ even} \\ 1 \dots \frac{N-1}{2}, & N \text{ odd} \end{cases} \quad (5.9a)$$

$$0 \leq \delta_i \leq 0.1 \quad \forall i \in \begin{cases} 1 \dots \frac{N}{2}, & N \text{ even} \\ 1 \dots \frac{N-1}{2}, & N \text{ odd.} \end{cases} \quad (5.9b)$$

Constraint (5.9a) assures that only the up-WTs are de-loaded; this will allow down-WTs to capture the spilled energy of the up-WTs. Constraint (5.9b) limits the maximum de-loading margin, δ , of the up-WTs to 10 %.

Optimisation of Kinetic Energy while De-loading the WF

The total kinetic energy of a WF can be maximised while operating the WF in a de-loaded mode. In this case, the objective function and all other constraints are the same as in Section 5.3.1.a except constraint (5.8), which needs to be modified as follows:

$$\sum_{i=1}^N P_i^{\text{sub}} = (1 - \Delta) \sum_{i=1}^N P_i^{\text{opt}}, \quad (5.10)$$

where Δ is the de-loading margin of the WF.

Optimisation of Power

It is also possible to maximise the total output power of the WF. In a WF with N WT's in a row, the objective function is as follows:

$$\underset{\omega, \beta}{\text{maximise}} \quad \sum_{i=1}^N P_i(\omega, \beta, v). \quad (5.11)$$

The objective function is subject to all other constraints presented for the optimisation of kinetic energy, except constraint (5.8) which changes to constraint (5.12). The constraint (5.12) ensures that the optimisation of power does not reduce WF's kinetic energy that might be used for inertial responses:

$$\sum_{i=1}^N E_{k,i}^{\text{opt}} = \sum_{i=1}^N E_{k,i}^{\text{sub}}. \quad (5.12)$$

The resulting constrained non-linear optimisation problem is non-convex, having several local optima. However, by pruning the feasible region by imposing constraints (5.9a), we were able to solve the problem more efficiently than Section 4.2.3. For a small system used in this section, the computational efficiency was not an issue, so it can be performed on-line. However, for larger systems, the optimisation can be performed off-line and solutions stored in look-up tables, which can then be readily implemented in a control algorithm. The implementation of the control algorithm is discussed in detail in the next subsection.

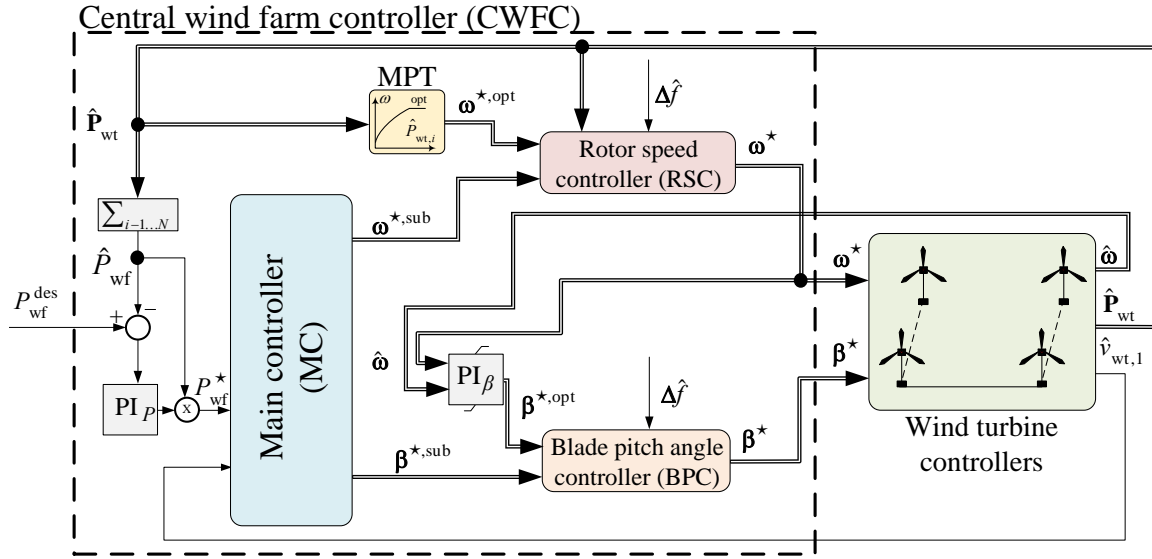


Fig. 5.2 The proposed CWFC for coordinated operation of wind farms with frequency control capability. Double lines show vector signals.

5.3.2 The Central Wind Farm Controller

The CWFC regulates the injection of WF's active and reactive power to the grid through the active and reactive power control loops, respectively. To implement the proposed operation strategy, we need to modify the active power control loop of the CWFC, as shown in Fig. 5.2. The proposed optimisation algorithm is implemented in the main controller (MC). The CWFC receives $\hat{\omega} \in \mathbb{R}^N$ and $\hat{\mathbf{P}}_{wt} \in \mathbb{R}^N$ of individual WTs to calculate the maximum available power of the WF, \bar{P}_{wf} . Then, the maximum available power is reported to the system operator to ensure that the desired power is not more than the maximum available power, $P_{wf}^{des} \leq \bar{P}_{wf}$. The desired value of the WF power, P_{wf}^{des} , is provided as an input from the grid to the CWFC. To ensure a correct power reference for the WF, a PI controller is considered. The PI_P sets the reference power of the whole WF, P_{wf}^* . To ensure that the WF power reference is achieved, constraint (5.8) should be modified as follows:

$$P_{wf}^* = \sum_{i=1}^N P_i^{sub}. \quad (5.13)$$

The wind speed for individual WTs can be calculated either from $\hat{\omega}$, $\hat{\beta}$, and $\hat{\mathbf{P}}_{wt}$ using (5.1), or from $\hat{\omega}$, $\hat{\beta}$, and $\hat{v}_{wt,1}$ using the wake equation (5.4) in the MC. In this chapter, we use the latter method. Note that for large systems the optimisation can be performed off-line and the results for different cases can be stored in the MC in the form of look-up tables. The outputs of the MC are the optimisation variables, $\omega^{*,sub} \in \mathbb{R}^N$ and $\beta^{*,sub} \in \mathbb{R}^N$.

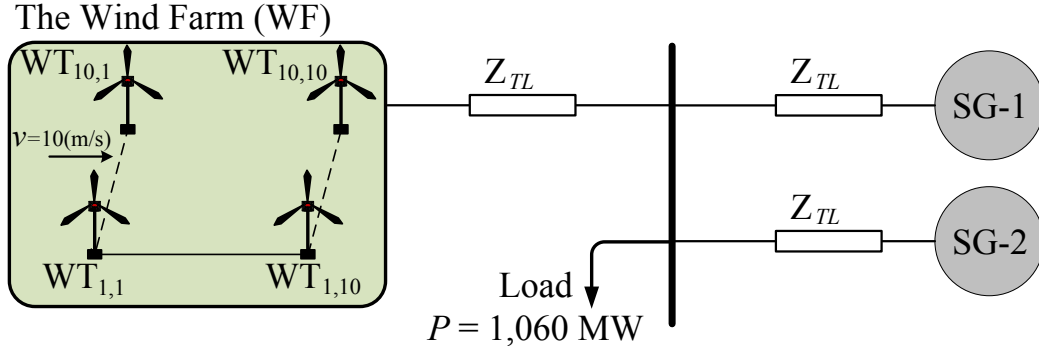


Fig. 5.3 One-line diagram of test power system for simulation.

The frequency control capability is achieved through the rotor speed controller (RSC) and the blade pitch angle controller (BPC) blocks (each WT has one RSC and one BPC in the CWFC, as shown in Figs. 4.9 and 4.11, receptively). When the WF participates in frequency control, a frequency event with $|\Delta \hat{f}| \geq |\Delta f^*|$ activates the RSC and BPC of each WT to change the operation mode of the WF from sub-optimal (proposed operation strategy) to optimal (conventional operation strategy). By doing this, we release the stored kinetic energy, as well as the available reserve power of the WF to the grid in a controlled way. In the conventional operation strategy, the optimal rotor speeds, $\omega^{*,\text{opt}}$, are obtained from a quadratic equation as a function of measured power in the maximum power tracker (MPT) block. Whereas, the optimal pitch angles, $\beta^{*,\text{opt}}$, are obtained using a proportional integral (PI) controller, and the error between the rated rotor speed and the measured rotor speed. Note that in this chapter, we use the PI control parameters of the GE's Type III WT's pitch controller [114], which results in a satisfactory performance.

The outputs of RSC and BPC blocks are reference rotor speeds, $\omega^* \in \mathbb{R}^N$, and reference blade pitch angles, $\beta^* \in \mathbb{R}^N$, of individual WTs, respectively. The objective of the individual WT controllers are to obtain the ω^* and β^* provided by the CWFC, and, therefore, the active power set point.

5.4 Case Study

We evaluate the performance of the proposed operation strategy on a test system shown in Fig. 5.3. The system consists of two SGs, a WF with 10 rows of WTs, each consisting of ten NREL 5 MW Type III WTs [105], and a 1060 MW constant power load. Simulation parameters for the SGs, WTs and WF are provided in Tables 5.1, 5.2 and 5.3, respectively.

First, we solve the optimisation problem for different cases, as described below. Second, we perform time domain simulations to observe and evaluate the contribution of the WF in

Table 5.1 Settings and characteristics of synchronous generators.

SG	Turbine Type	P_{nom} (MW)	H (s)	Governor Type	Droop (%)
1	Steam	600	4	IEEEG1	12.5
2	Gas	600	6	TGOV1	5

Table 5.2 The parameters and settings of the reference wind turbine.

Parameters	Values with units
P_{nom}	5 MW
H	4 s
R	63 m
$\underline{\omega}$	0.722 pu
$\overline{\omega}$	1.267 pu
C_p^{opt}	0.485
λ	7.5
G	1:97
$v_{\text{cut-in}}$	$3 \frac{\text{m}}{\text{s}}$
v_{nom}	$11.4 \frac{\text{m}}{\text{s}}$
$v_{\text{cut-out}}$	$25 \frac{\text{m}}{\text{s}}$

frequency control and evaluate the effectiveness of proposed operation strategies. Finally, we assess the dynamic performance of the CWFC with variable wind speeds generated by a suitable wind speed model.

5.4.1 Optimisation Results

We assume that the distance between the rows of WTs is large enough, which enables us to perform the optimisation for each row independently. The distance between each WT in a row, in the wind speed direction, is $L = 14R$. Notice that when the distance between the WTs or the wind speed direction changes, the parameters k and k' in (5.4) need to be modified accordingly (the values for typical wind directions can be stored in a look-up tables in the MC block). We simulate the system and compare the results for the four cases described below:

1. **MaxPwt:** Every individual WT within the WF operates in the optimal operation mode to locally maximise the energy capture. This is the conventional WFs' operation strategy.

Table 5.3 The wind farm characteristics and the central wind farm controller parameters.

Parameters	Values with units
$K_{p,P}$	1
$K_{i,P}$	0.1
$K_{p,\beta}$	150
$K_{i,\beta}$	25
Δf^*	−200 mHz
L	882 m
k	0.12
k'	0.37

2. **MaxEk:** Kinetic energy of the WF, $E_{k, \text{wf}}$, is maximised as discussed in Section 5.3.1.a.
3. **MaxEk5:** We maximise kinetic energy of the WF and consider a 5 % de-loading margin for the WF. In this case, as discussed in Section 5.3.1.b, constraint (5.10) changes to: $\sum_{i=1}^N P_i^{\text{sub}} = 0.95 \sum_{i=1}^N P_i^{\text{opt}}$.
4. **MaxPwf:** We maximise the power of the wind farm, P_{wf} , as explained in Section 5.3.1.c.

The optimisation was performed for cases MaxPwf, MaxEk and MaxEk5 with a wind speed range of $6 \frac{\text{m}}{\text{s}} \leq v \leq 12 \frac{\text{m}}{\text{s}}$, where the rotor speed of the WTs varies between $\underline{\omega} \leq \omega \leq \bar{\omega}$. The rotor speed and the pitch angle of up-WTs (the de-loaded WTs) show similar trends. Whereas, their quantities vary depending on the available wind speed. As an example, Fig. 5.4 illustrates the rotor speed and the pitch angle of WT_{1,1} in all four cases. A comparison of rotor speeds and pitch angles in different cases reveals that in cases MaxPwf, MaxEk and MaxEk5 de-loading of the up-WTs were achieved by an increase in the reference values of the rotor speed and pitch angle. This confirms that the de-loaded WTs operate near the point $\text{sub}_{\omega, \beta}$ in Fig. 5.1.

Fig. 5.5 illustrates the relative changes in the output power of the individual WTs in case MaxEk compared to case MaxPwt. Notice that the up-WTs operate in a de-loaded mode, whereas the down-WTs capture the spilled energy of the up-WTs and generate more power compared to the base case. It is notable that because of the constraint (5.8), the total output power of the WF is the same in both cases.

The wind speed profile of the WF for an initial wind speed of $v_{1,1} = 10 \frac{\text{m}}{\text{s}}$ is shown in Fig. 5.6. In Fig. 5.7, the wind speed profile of the WF in case MaxEk is compared to case MaxPwt. From Figs. 5.6 and 5.7, it can be seen that by de-loading the up-WTs, the available wind speed reaching the down-WTs increases considerably. This is due to the wake

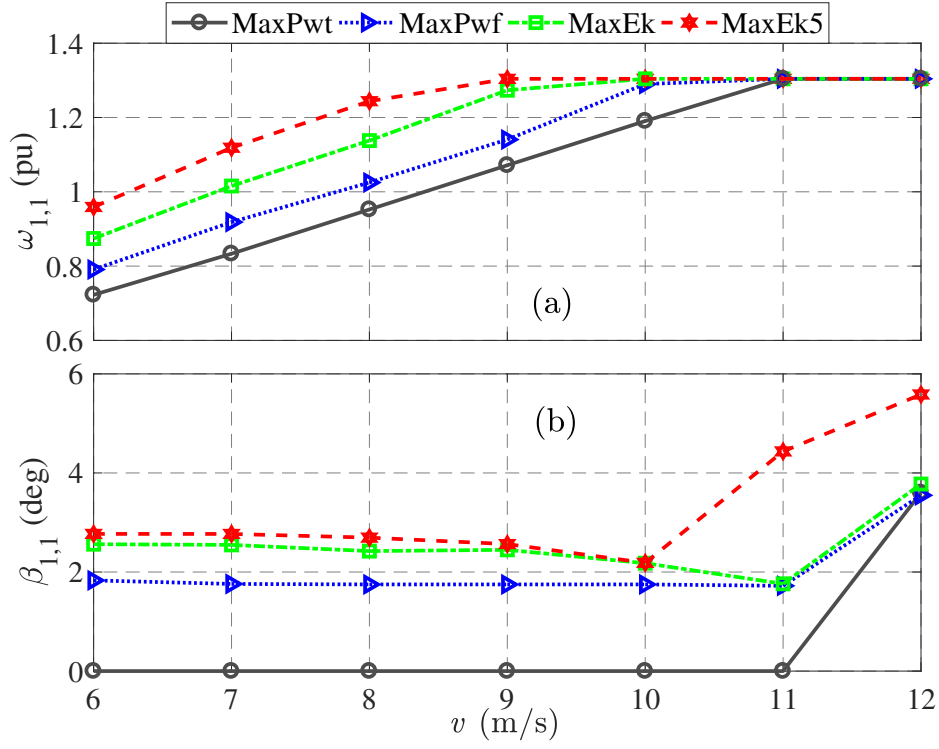


Fig. 5.4 The rotor speed and the pitch angle of WT_{1,1} in different operation cases.

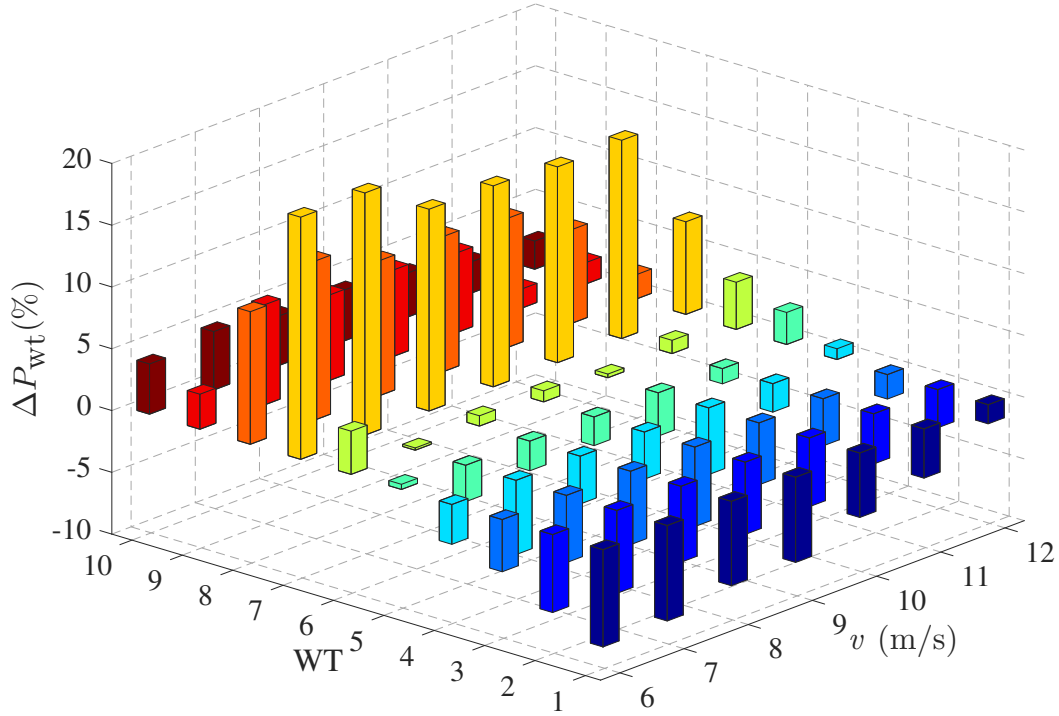


Fig. 5.5 The relative changes in the output power of wind turbines in Case MaxEk compared to Case MaxPwt.

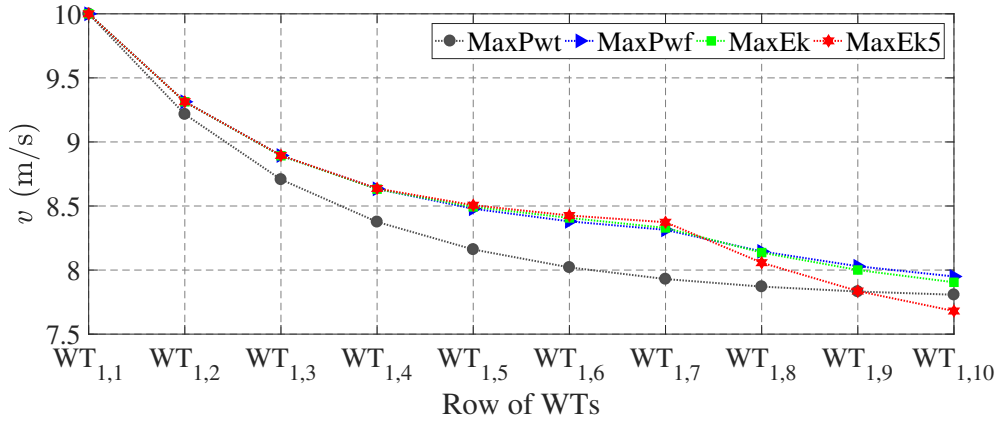


Fig. 5.6 Wind speed profile of the wind farm for an initial wind speed of $v_{1,1} = 10 \frac{\text{m}}{\text{s}}$.

interaction and the correlation of C_p and C_t , as shown in Fig. 5.1 and (5.4). Observe how the wind speed in the proposed operation strategies reduces more gradually compared to the conventional operation strategy. Nonetheless, in all cases, the wind speeds leaving the WF have similar values, which indicates that no energy is lost.

Fig. 5.8 illustrates the WF's kinetic energy and power for all four cases. In case MaxPwf, the WF output power is improved by up to 3 % for wind speeds in Zones 2, 3 and 4, while kinetic energy remains the same as in case MaxPwt. This implies that we can improve the output power of the WF while still being able to provide a similar inertial contribution as in case MaxPwt. In case MaxEk, kinetic energy increases by 23 % for wind speeds in Zones 2 and 3. In Zone 4, however, the marginal contribution of kinetic energy reduces because in this region most of the WTs operate with a maximum rotor speed. In case MaxEk5, where the WF is de-loaded by 5 %, the amount of additional kinetic energy in the rotating masses of

in Zone 4, the improvement is the same as in case MaxEk because in this region most of the WTs operate with a maximum rotor speed. It can be seen that the optimisation of WF's power is independent of the rotor speed range, and, therefore, the output power of a WF can be optimised over a wide range of wind speeds. On the other hand, optimisation of kinetic energy is only possible for the wind speeds where the rotor speed varies between $\underline{\omega} \leq \omega \leq \overline{\omega}$. Notice that in case MaxEk5, with a 5 % de-loading margin (with respect to the conventional operation strategy where each WT's power is optimised individually, case MaxPwt), the WF provides 8 % reserve power for frequency control (by changing the operation mode of the WF from MaxEk5 to MaxPwf). This, in turn, reduces the need for further de-loading of WFs for frequency control services and provides valuable financial incentives for the WF operators. In the following subsection, we perform time-domain simulation to evaluate the efficacy of the proposed operation strategies, as well as the CWFC.

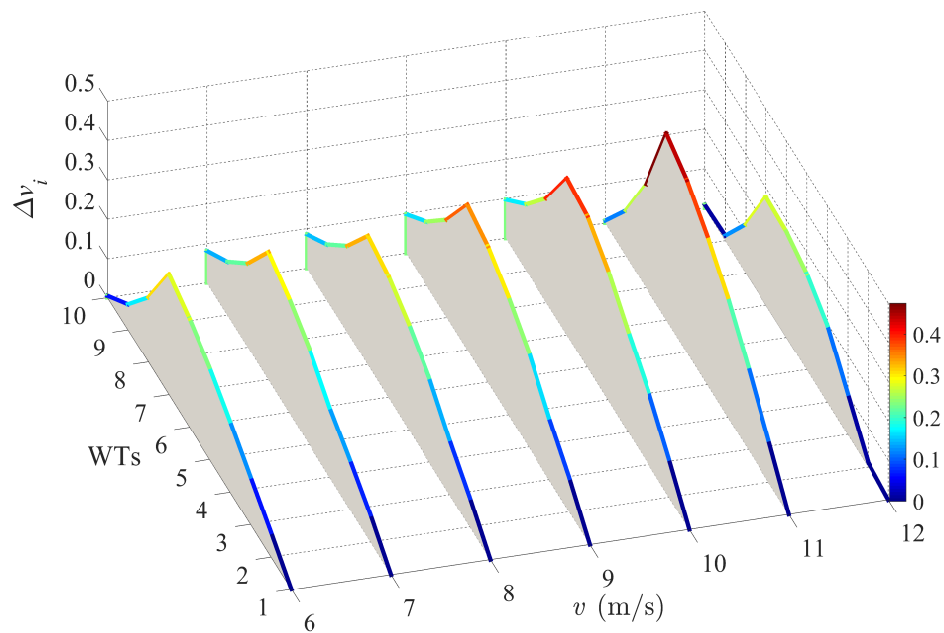


Fig. 5.7 The relative changes in the available wind speed " Δv_i " in Case MaxEk compared to Case MaxPwt.

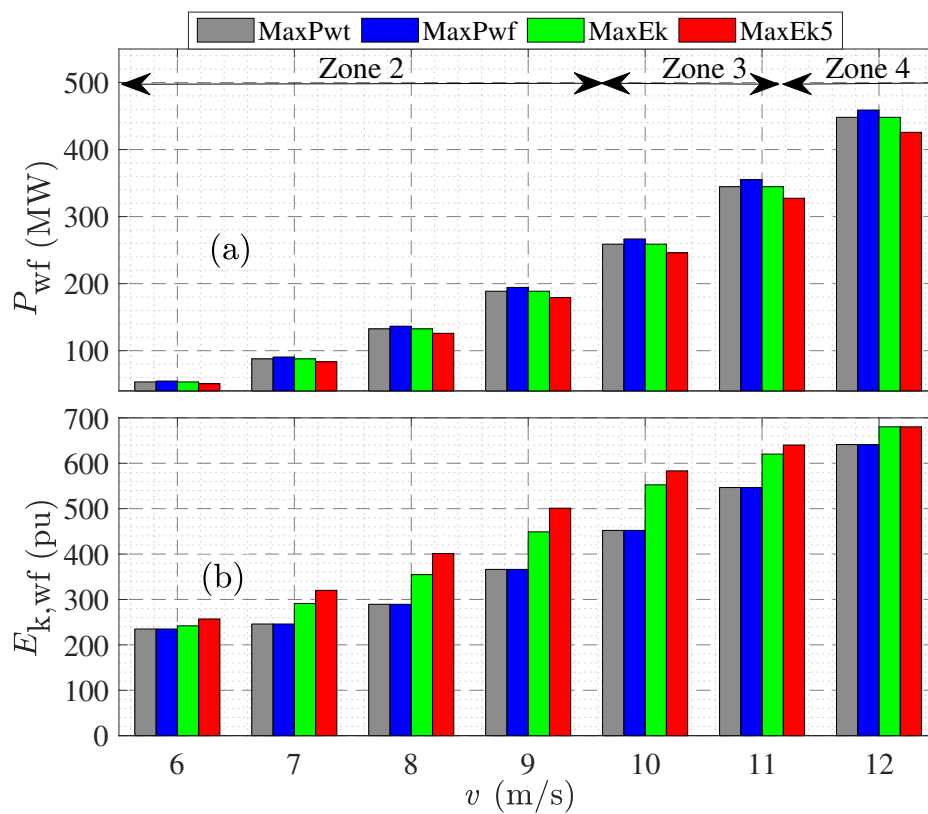


Fig. 5.8 Power and kinetic energy of the wind farm in all four cases.

5.4.2 Contribution of Wind Farm in Frequency Control

The effectiveness of the proposed operation strategies in frequency control is assessed using the test system shown in Fig. 5.3. Time-domain simulations were performed for five cases shown in Table. 5.4. In all cases, the load is 1060 MW, and a frequency event was considered by a 12 % step increase of the load at $t = 300$ s. In case SGs, the WF does not operate, so the load is entirely supplied by two SGs. Hence, we consider case SGs as a benchmark to evaluate the frequency response of the system with and without the WF contribution to frequency control in four other cases. In all four cases where the WF operates, the incoming wind speed is $v_{N,1} = 10 \frac{\text{m}}{\text{s}}$, and the WF output power is shown in Table. 5.4.

Table 5.4 Simulation cases for wind farm contribution in frequency control.

Simulation case	WF participates in frequency control	P_{wf} (MW)	P_{SG1} (MW)	P_{SG2} (MW)
SGs	N/A	0	560	500
MaxPwt	No	259	301	500
MaxEk5	Yes	246	314	500
MaxEk	Yes	259	301	500
MaxPwf	Yes	266	294	500

Fig. 5.9 shows the frequency behaviour of the system for all five cases. In case MaxPwt, the WF does not participate in frequency control. Thus, frequency nadir is larger than case SGs. In cases MaxEk5, MaxEk and MaxPwf, the WF participates in frequency control by shifting its operation mode to MaxPwt at the inception of the frequency event. In case MaxEk5, by releasing power from 28 % additional kinetic energy and 5 % reserved power of the WF into the system in a controlled manner, both system frequency nadir, as well as system steady state frequency, improves considerably, and frequency response is even better than case SGs. Fig. 5.10 illustrates kinetic energy and output power of the WF in case MaxEk5. Notice that after the injection of power from additional kinetic energy to the system at $t = 340$ s, WF's power should be approximately 259 MW. However, due to the wake effect time delay, which will be discussed in the next subsection, it is approximately 264 MW. In case MaxEk, WF provides power from its additional kinetic energy. Thus, the frequency response of the system is better than case MaxPwt. In case MaxPwf, there is no additional kinetic energy and output power of the WF reduces from 266 MW to 259 MW. However, due to the wake effect time delay, the WF has an insignificant contribution to frequency response. It is worth mentioning that in this case because of WF's power reduction, the frequency nadir is lower than other cases but still higher than the case MaxPwt, where the WF does not participate in the frequency control.

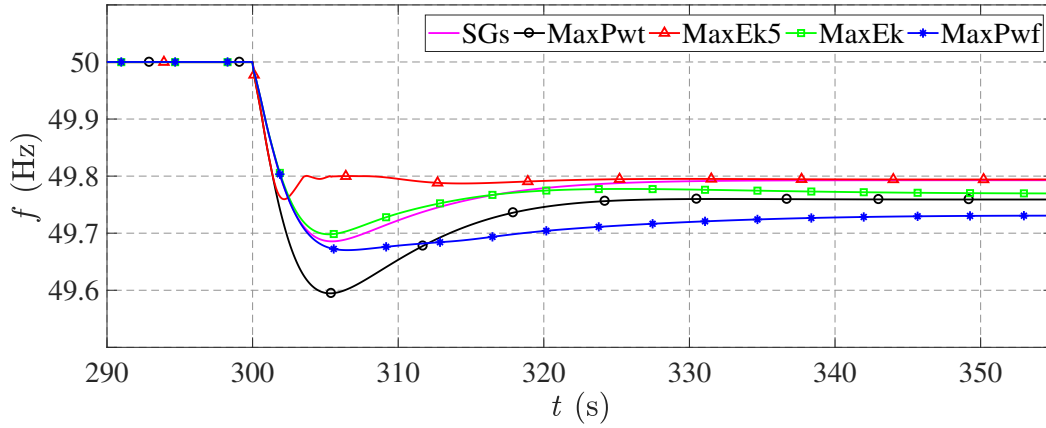


Fig. 5.9 System frequency behaviour after a 12% step increase in the load.

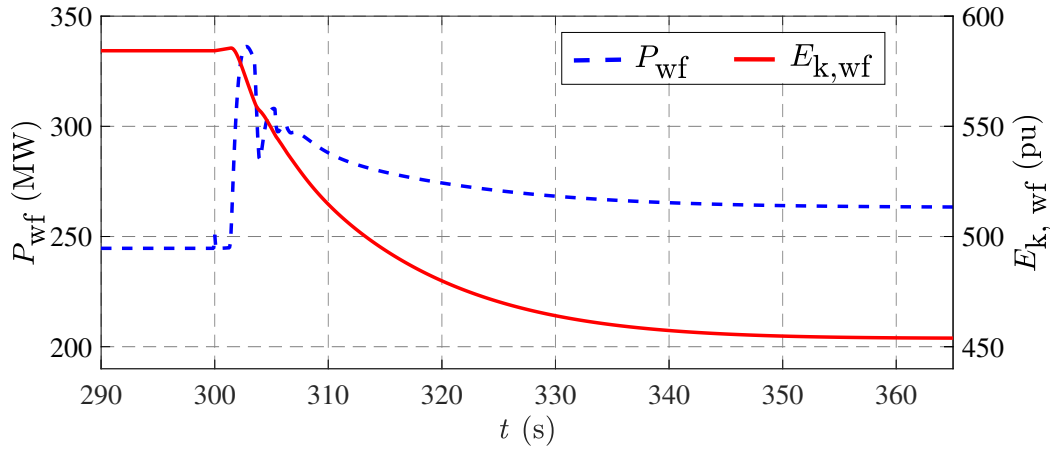


Fig. 5.10 Power and kinetic energy of the wind farm in Case MaxEk5.

5.4.3 The Performance of the Central Wind Farm Controller

The performance of the CWFC is evaluated with variable wind speed. Three cases are assessed: (A) MaxEk5, (B) MaxPwt and (C) changing the operation mode of the WF from MaxEk5 to MaxPwt at $t = 950$ s. Power and kinetic energy of the WF for all three cases are illustrated in Fig. 5.11. Observe that in cases A and B, WF's output power follows WF's reference power very closely, whereas in case C when WF's operation mode changes, the output power of the WF merges to the reference power of the WF with a slower rate. This is mainly because of the wake effect.

The effect of the wake on the output power of individual WTs is illustrated in Fig. 5.12. As shown, the changes in the operating condition of an up-WT is observed in the down-WTs with a time delay due to the wake effect. Consider the situation where the power set-points of an up-WT is increased; this consequently reduces the wind speed reaching the down-WTs.

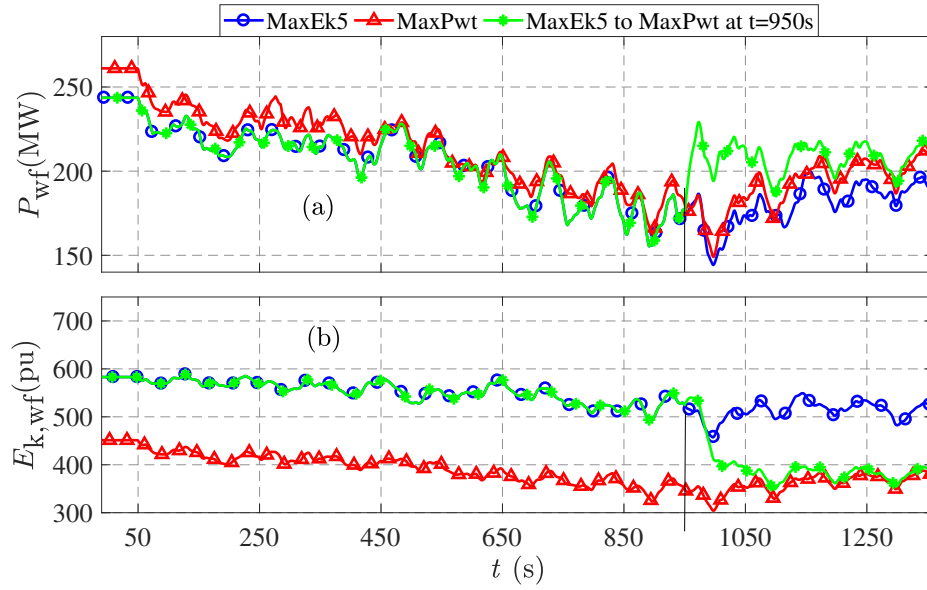


Fig. 5.11 Power and kinetic energy of the wind farm with variable wind speed.

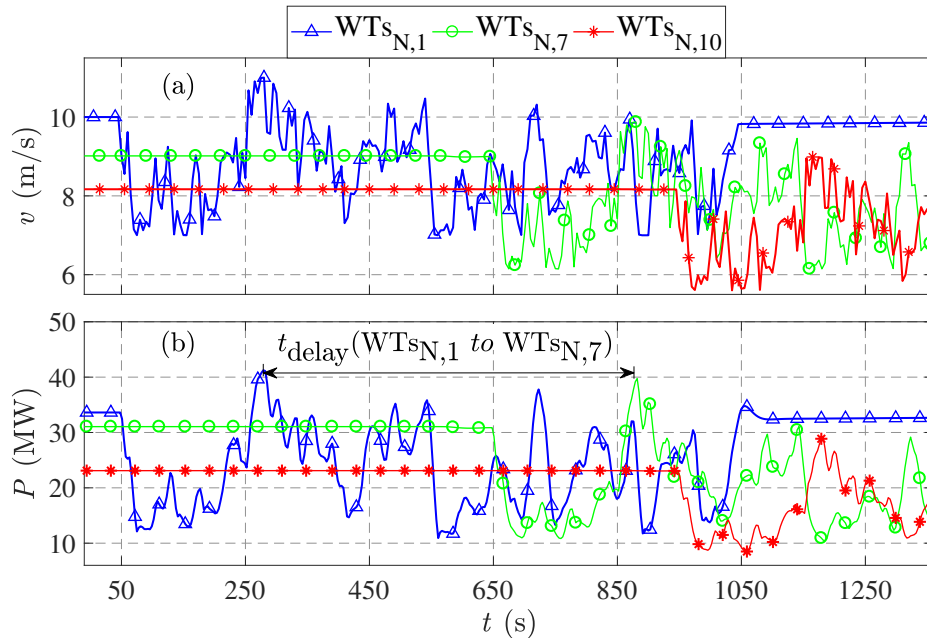


Fig. 5.12 The effect of wake on the wind speed and the output power of individual wind turbines within the wind farm for Case MaxEK5.

However, due to the wake effect, the down-WTs output power remains unchanged until they receive the reduced wind speed. As a result, the WF can provide extra power for a limited time until the reduced wind speed reaches the last WT in the WF. This characteristic becomes valuable when WFs participate in frequency control (see Subsection. 5.4.2).

5.5 Summary

The non-linear aerodynamic coupling between WT's in a WF due to wake interaction admits several operation strategies. In this chapter, we proposed three: maximisation of either kinetic energy or power capture and a de-loaded strategy whereby the amount of kinetic energy is maximised. The overall contribution of a WF to frequency control and its behaviour during a frequency event depend both on the strategy used before the frequency event and the transition to the new strategy after the event. For example, we have shown that in order to maximise the contribution of a WF in frequency response, the operator can switch between the proposed de-loaded strategy before the frequency event to a strategy where the total energy capture is maximised at the onset of the event. This strategy considerably increases the effective power reserve from the WF's.

In practice, the applicability of the proposed strategies will depend on the applicable grid code requirements, market structure and overall system condition, e.g. the amount of inertia available in the system. The proposed operation strategies are particularly well suited for off-shore wind farms with regular wind patterns and regular layouts with equal WT spacing.

Chapter 6

Conclusion

As discussed in Chapter 1, the increasing penetration of non-synchronous renewable energy sources (NS-RES) and demand side-technologies alter the dynamic characteristics, and consequently, the stability performance of a power system. With a high penetration level of NS-RES, power system frequency control becomes a challenging task and needs to be dealt with systematically. Thus, in this thesis, we assessed and quantified the impact of the above-mentioned changes on the system frequency performance, and identified the maximum NS-RES integration limits for the Australian future grid from the system frequency performance point of view. Furthermore, we quantified the contribution of some of the conventional and non-conventional technologies on system frequency response. To improve system frequency response, we proposed optimal operation and control strategies for participation of wind generation in frequency control.

First, in Chapter 2, we assessed the impact of high penetration levels of NS-RES and different penetration levels of prosumers on the performance and frequency stability of the Australian future grid. We quantified the connection between NS-RES penetration and frequency performance of the system and showed how the system frequency response can be affected with high penetration of NS-RES. Furthermore, it was shown that a low battery storage capacity of prosumers can worsen the frequency response of the system, whereas a higher battery storage capacity of prosumers can improve the frequency response of the system because of a flatter net demand profile and a more uniform operation of synchronous generators compared to lower battery storage capacity.

Second, in Chapter 3, we proposed a framework for assessing renewable integration limits concerning power system frequency performance using a time-series scenario-based approach. By considering a large number of future scenarios and their sensitivities with respect to different parameters- including inertia location, load model, network strength, and contingency size and location - we identified maximum non-synchronous instantaneous

penetration limits for a wide range of possible scenarios. Furthermore, we derived a dynamic inertia based frequency control security constraint and incorporated it into the market dispatch model to reduce the detrimental impacts of high NS-RES penetration on the frequency performance. The results using the Australian future grid as a test case show that such an explicit inertia based frequency control security constraint ensures power system frequency stability for all credible contingencies. To improve the frequency performance, we assessed and quantified the contribution of a wide range of technologies, including synchronous condensers, synthetic inertia from wind farms and a governor-like response from de-loaded wind farms. The results showed that the latter option is the most effective one.

Then, to enhance the frequency performance of the system with high penetration of NS-RES, we proposed optimised operation and control strategies for participation of wind farms in frequency control in Chapter 4. By explicitly modelling a wind farm and considering the wake interaction among the wind turbines within the wind farm, we maximised the rotational kinetic energy of the wind turbines, without compromising the overall efficiency of the wind farm. Furthermore, for optimal deployment of wind turbines' rotational kinetic energy into the system during a frequency event, we proposed an optimal control strategy. We showed that following a contingency, the proposed operation and control strategies can significantly improve the frequency response of the system.

Finally, in Chapter 5, we proposed a coordinated operation strategy for the wind farms that consists of an optimisation algorithm and a central wind farm control. In contrast to the conventional wind farm operation strategy where each wind turbine is optimised individually, we proposed different operation strategies for maximising the rotational kinetic energy or the output power of a wind farm. We showed that by operating the wind turbines within a wind farm in a coordinated way, the stored rotational kinetic energy or the output power of the wind farm can be increased significantly. The additional rotational kinetic energy can be used for frequency control services to add more flexibility to the system, while the additional power can be used to improve the financial viability of the wind farms by improving its overall efficiency.

The aim of this thesis is to assess and enhance the frequency performance of a power system with high penetration of NS-RES. To do this in a systematic way, we proposed an assessment framework and quantitatively showed the NS-RES limits from the system frequency performance point of view. Furthermore, we utilised some of the emerging generation technologies (e.g. wind farms) and optimised their contribution to the system frequency response. Considering these, the work of thesis can be extended into the following directions:

-
- The rapid advancement of technologies utilised in power systems (e.g. NS-RES, plug-in electric vehicles, rooftop-PV and battery storage, information and communication technologies) makes it difficult to predict the performance of future grids compared to conventional power systems. Therefore, studying and identifying fundamental issues related to performance and stability of future grids are becoming challenging tasks. Moreover, uncertainties associated with policies and regulations further increase the complexity of the problem. Considering these, we performed scenario-based sensitivity analysis, which is a pragmatic approach to understand future grids behaviour and unfold some of the fundamental issues. However, this approach is computationally very expensive; therefore, using some machine learning methods, such as feature selection techniques to extract the vulnerable operating points and assess the stability performance of the system on those points improves the computational efficiency of the above-mentioned method, while it can provide more information for system operators, as it is capable to analyse larger numbers of scenarios in a shorter period of time.
 - Power system inertia has recently attracted a lot of interest in the power systems literature due to the increasing penetration of NS-RES. It is well understood that replacement of synchronous machines by power electronic interfaced generation negatively impacts power system frequency performance. To address this issue, a more recent *system theoretic* approaches has focused on the problem of optimal placement of inertia. In these approaches, model reduction and simplification have been used extensively, which might result in some inaccurate outcomes. Therefore, it is very important to link the the two approaches (i.e. simulation based approach, discussed in this thesis, and the system theoretic approach), and quantitatively justify the simplification made in the system theoretic approach.
 - Once the system inertia requirement is determined through the simulation and theoretic approaches, the least-cost technical options have to be identified. In this thesis, we assessed and quantified the contribution of wind generation in frequency response. This approach can be extended for other technologies such as photovoltaic, battery energy storage systems, super-capacitors, etc. Then, a market or regulatory framework can be developed and implemented to manage the issues efficiently.
 - To increase the integration of NS-RES, either operational flexibility of the system should increase, or emerging technologies should provide similar services as the conventional synchronous generators, such as inertial contribution, primary frequency response, fault-ride through, etc. In this regard, a coordinated wind farm operation strategy was proposed in this thesis. This concept can be further developed to include

other technologies, such as distributed generations, battery energy storage systems, etc. Demand side technologies can also enhance flexibility of the system, as an example, in thesis, we showed how prosumers with a higher capacity of battery storage can improve the frequency performance of the system. With advancement in communication technologies, it might be even possible for the demand side technologies to provide ancillary services for the grid, such as inertial contribution, fast frequency response, primary frequency response, and so on.

References

- [1] P. Kundur, *Power system stability and control*. New York: McGraw-Hill Inc, 1994.
- [2] EirGrid and System Operator for Northern Ireland (SONI), “All Island Tso Facilitation of Renewables Studies,” EirGrid, Tech. Rep., 2010. [Online]. Available: <http://www.eirgrid.com/media/FacilitationRenewablesFinalStudyReport.pdf>
- [3] N. W. Miller, M. Shao, and S. Venkataraman, “California ISO (CAISO) Frequency Response Study,” CASIO, Tech. Rep., Nov 2011. [Online]. Available: <http://www.uwig.org/Report-FrequencyResponseStudy.pdf>
- [4] N. W. Miller, M. Shao, S. Pajić, and R. D. Aquila, “Western Wind and Solar Integration Study Phase 3 - Frequency Response and Transient Stability,” NREL, Tech. Rep. DRS8.3020, Dec 2014.
- [5] R. Doherty, A. Mullane, G. Nolan, D. Burke, A. Bryson, and M. O’Malley, “An Assessment of the Impact of Wind Generation on System Frequency Control,” *IEEE Transactions on Power Systems*, vol. 25, no. 1, pp. 452–460, Feb 2010.
- [6] Greenpeace Germany, “Power 2030: A European Grid for 3/4 Renewable Electricity by 2030,” Greenpeace, Tech. Rep., Mar 2014.
- [7] M. Wright and P. Hearps, “Australian Sustainable Energy: Zero Carbon Australia Stationary Energy Plan,” The University of Melbourne Energy Research Institute, Tech. Rep., July 2010.
- [8] AEMO, “100 Per Cent Renewables Study Modelling Outcomes,” AEMO, Tech. Rep., July 2013.
- [9] B. Elliston, I. MacGill, and M. Diesendorf, “Least cost 100% renewable electricity scenarios in the Australian National Electricity Market,” *Energy Policy*, vol. 59, pp. 270–282, 2013.
- [10] H. Marzooghi, D. J. Hill, and G. Verbič, “Performance and stability assessment of future grid scenarios for the Australian NEM,” in *2014 Australasian Universities Power Engineering Conference (AUPEC)*. IEEE, Sep 2014.
- [11] G. Masson and M. Brunisholz, “2015 Snapshot of global photovoltaic markets,” IEA, Paris, Tech. Rep., Jan 2016.

- [12] H. Marzoghi, S. Riaz, G. Verbič, A. C. Chapman, and D. J. Hill, "Generic Demand Modelling Considering the Impact of Prosumers for Future Grid Scenario Studies," *Submitted to IEEE Transaction on Smart Grid*, Feb 2017. [Online]. Available: <http://arxiv.org/abs/1605.05833>
- [13] Global Wind Energy Council, "Global Wind Report - Annual market update 2015," Global Wind Energy Council, Brussels, Tech. Rep., 2015.
- [14] IEA, "Special Report (World Energy Investment Outlook)," International Energy Agency, Paris, Tech. Rep., 2014.
- [15] E. Energy, "Wind Integration In Electricity Grids: International Practice And Experience," AEMO, Tech. Rep., Oct 2011. [Online]. Available: <http://www.aemo.com.au/Electricity/Planning/Related-Information/Wind-Integration-Investigation>
- [16] International Institute for Applied Systems Analysis, *Global Energy Assessment Toward a Sustainable Future*. Cambridge, UK: Cambridge University Press, 2012.
- [17] IEA, "Annual Energy Outlook 2013," International Energy Agency, Paris, Tech. Rep., 2012.
- [18] L. Holdsworth, J. B. Ekanayake, and N. Jenkins, "Power system frequency response from fixed speed and doubly fed induction generator-based wind turbines," *Wind Energy*, vol. 7, no. 1, pp. 21–35, Jan 2004.
- [19] G. Ramtharan, N. Jenkins, and J. Ekanayake, "Frequency support from doubly fed induction generator wind turbines," *IET Renewable Power Generation*, vol. 1, no. 1, p. 3, 2007.
- [20] A. Žertek, G. Verbič, and M. Pantoš, "A Novel Strategy for Variable-Speed Wind Turbines' Participation in Primary Frequency Control," *IEEE Transactions on Sustainable Energy*, vol. 3, no. 4, pp. 791–799, Oct 2012.
- [21] R. DeAlmeida, E. Castronuovo, and J. Pegas Lopes, "Optimum Generation Control in Wind Parks When Carrying Out System Operator Requests," *IEEE Transactions on Power Systems*, vol. 21, no. 2, pp. 718–725, May 2006.
- [22] P. Kundur, J. Paserba, V. Ajjarapu, G. Andersson, A. Bose, C. Canizares, N. Hatziargyriou, D. Hill, A. Stankovic, C. Taylor, T. Van Cutsem, and V. Vittal, "Definition and Classification of Power System Stability IEEE/CIGRE Joint Task Force on Stability Terms and Definitions," *IEEE Transactions on Power Systems*, vol. 19, no. 3, pp. 1387–1401, Aug 2004.
- [23] ERCOT, "ERCOT Concept Paper: Future Ancillary Services in ERCOT," ERCOT, Tech. Rep. Version 1.0, Sep 2013.
- [24] AEMO, "Future Power System Security Program," AEMO, Tech. Rep., Aug 2016.
- [25] EirGrid and SONI, "Annual Renewable Energy Constraint and Curtailment Report 2016," EirGrid, Tech. Rep., 2016. [Online]. Available: <http://www.eirgrid.ie/site-files/library/EirGrid/Annual-Renewable-Constraint-and-Curtailment-Report-2016-v1.0.pdf>

- [26] AEMO, “Guide to Ancillary Services in the National Electricity Market,” AEMO, Tech. Rep., Apr 2015.
- [27] —, “Black system South Australia 28 September 2016,” AEMO, Melbourne, Tech. Rep., Dec 2016.
- [28] DNV KEMA Energy & Sustainability, “RoCoF An independent analysis on the ability of Generators to ride through Rate of Change of Frequency values up to 2Hz /s .” DNV KEMA Energy, London, Tech. Rep. 4478894, 2013.
- [29] NERC, “Industry Advisory -Turbine Combustor Lean Blowout,” NERC, Tech. Rep., 2008.
- [30] J. O’Sullivan, A. Rogers, D. Flynn, S. Member, P. Smith, A. Mullane, and M. O’Malley, “Studying the Maximum Instantaneous Non-Synchronous Generation in an Island System - Frequency Stability Challenges in Ireland,” *IEEE Transactions on Power Systems*, vol. 29, no. 6, pp. 2943–2951, 2014.
- [31] H. Ahmadi and H. Ghasemi, “Maximum penetration level of wind generation considering power system security limits,” *IET Generation, Transmission & Distribution*, vol. 6, no. 11, pp. 1164–1170, Nov 2012.
- [32] NORDEL, “Nordic grid code (Nordic collection of rules),” NORDEL, Tech. Rep., 2007.
- [33] W. Hung, G. Ray, and G. Stein, “Frequency Changes during Large Disturbances WG,” National Grid, Tech. Rep., 2010.
- [34] AEMO, “Electricity System Operations Planning and Performance: Power System Frequency and Time Deviation Monitoring Report Reference Guide,” AEMO, Tech. Rep., July 2012.
- [35] AEMC, “National Electricity Rules Version 79,” AEMC, Tech. Rep., 2016.
- [36] Australia Energy Networks and CSIRO, “Electricity Network Transformation Roadmap: Key Concepts Report,” AEN, Tech. Rep., Dec 2016. [Online]. Available: <http://www.energynetworks.com.au/electricity-network-transformation-roadmap>
- [37] H. Marzooghi, G. Verbič, and D. J. Hill, “Aggregated demand response modelling for future grid scenarios,” *Sustainable Energy, Grids and Networks*, vol. 5, pp. 94–104, 2016.
- [38] M. Zugno, J. M. Morales, P. Pinson, and H. Madsen, “A Bilevel Model for Electricity Retailers’ Participation in a Demand Response Market Environment ,” *Energy Economics*, vol. 36, pp. 182 – 197, 2013.
- [39] W. Shi, N. Li, X. Xie, C. C. Chu, and R. Gadh, “Optimal Residential Demand Response in Distribution Networks,” *IEEE Journal on Selected Areas in Communications*, vol. 32, no. 7, pp. 1441–1450, July 2014.
- [40] S. Mathieu, Q. Louveaux, D. Ernst, and B. Cornelusse, “A quantitative analysis of the effect of flexible loads on reserve markets,” in *2014 Power Systems Computation Conference*. Wroclaw: IEEE, Aug 2014.

- [41] M. Gonzalez Vaya and G. Andersson, "Optimal Bidding Strategy of a Plug-In Electric Vehicle Aggregator in Day-Ahead Electricity Markets Under Uncertainty," *IEEE Transactions on Power Systems*, vol. 30, no. 5, pp. 2375–2385, Sep 2015.
- [42] P. A. Babu, N. Ramesh, "Wind Energy Conversion Systems - A Technical Review," *Journal of Engineering Science and Technology*, vol. 8, no. 4, pp. 493 – 507, 2013.
- [43] T. Ackermann, "Lessons Learned from International Wind Integration Studies," AEMO, Tech. Rep., 2011. [Online]. Available: <http://www.aemo.com.au/~media/Files/Other/planning/0400-0051pdf.pdf>
- [44] AEMO, "Integrating Renewable Energy - Wind Integration Studies Report," AEMO, Tech. Rep., 2012.
- [45] N. W. Miller and K. Clark, "Advanced controls enable wind plants to provide ancillary services," in *IEEE PES General Meeting*. IEEE, July 2010, pp. 1–6.
- [46] N. Troy and S. Twohig, "Wind as a price-maker and ancillary services provider in competitive electricity markets," in *IEEE PES General Meeting*. IEEE, July 2010, pp. 1–6.
- [47] Ping-Kwan Keung and H. Banakar, "Kinetic Energy of Wind-Turbine Generators for System Frequency Support," *IEEE Transactions on Power Systems*, vol. 24, no. 1, pp. 279–287, Feb 2009.
- [48] J. Ekanayake and N. Jenkins, "Comparison of the response of doubly fed and fixed speed induction generator wind turbines to changes in network frequency," *IEEE Transactions on Energy Conversion*, vol. 19, no. 4, pp. 800–802, Dec 2004.
- [49] M. Johan, P. J. de Haan, and S. W.H, "Inertial response of variable speed wind turbines," *Electric Power Systems Research*, vol. 76, pp. 980–987, 2006.
- [50] D. A. R.G and P. L. J.A, "Participation of Doubly Fed Induction Wind Generators in System Frequency Regulation," *IEEE Transactions on Power Systems*, vol. 22, no. 3, pp. 944–950, Aug 2007.
- [51] A. Žertek, G. Verbič, and M. Pantoš, "Optimised control approach for frequency-control contribution of variable speed wind turbines," *IET Renewable Power Generation*, vol. 6, no. 1, p. 17, 2012.
- [52] F. Diaz-Gonzalez, M. Hau, A. Sumper, and O. Gomis-Bellmunt, "Participation of wind power plants in system frequency control: Review of grid code requirements and control methods," *Renewable and Sustainable Energy Reviews*, vol. 34, pp. 551–564, June 2014.
- [53] G. C. Tarnowski, P. C. Kjar, P. E. Sorensen, and J. Ostergaard, "Variable speed wind turbines capability for temporary over-production," in *2009 IEEE Power & Energy Society General Meeting*. IEEE, July 2009, pp. 1–7.
- [54] I. A. Gowaid, A. El-Zawawi, and M. El-Gammal, "Improved inertia and frequency support from grid-connected DFIG wind farms," in *2011 IEEE/PES Power Systems Conference and Exposition*. IEEE, Mar 2011, pp. 1–9.

- [55] A. B. T. Attya and T. Hartkopf, "Control and quantification of kinetic energy released by wind farms during power system frequency drops," *IET Renewable Power Generation*, vol. 7, no. 3, pp. 210–224, May 2013.
- [56] S. Kuenzel, L. P. Kunjumuhammed, B. C. Pal, and I. Erlich, "Impact of Wakes on Wind Farm Inertial Response," *IEEE Transactions on Sustainable Energy*, vol. 5, no. 1, pp. 237–245, Jan 2014.
- [57] C. Pradhan and C. N. Bhende, "Adaptive deloading of stand-alone wind farm for primary frequency control," *Energy Systems*, vol. 6, no. 1, pp. 109–127, Aug 2014.
- [58] J. H. A. Crespo and S. Frandsen, "Survey of Modeling Methods for Wind Turbine Wakes and Wind Farms," *Wind Energy*, vol. 2, pp. 1–24, 1999.
- [59] A. D. Hansen, P. Sorensen, and et al, "Dynamic modelling of wind farm grid interaction," *Wind Energy*, vol. 26, no. 4, pp. 191–208, 2002.
- [60] M. Kayikci and J. Milanovic, "Dynamic Contribution of DFIG-Based Wind Plants to System Frequency Disturbances," *IEEE Transactions on Power Systems*, vol. 24, no. 2, pp. 859–867, May 2009.
- [61] G. Rousi, A. D. Hansen, and N. A. Cutululis, "Wind farm aggregation method for dynamic active power studies," in *13th International Workshop on Large-Scale Integration of Wind Power into Power Systems*, 2014. [Online]. Available: http://orbit.dtu.dk/fedora/objects/orbit:135307/datastreams/file_b1cc7fc2-8fa7-46ac-9d25-eca45a6da551/content
- [62] L. Y. Pao and K. E. Johnson, "A tutorial on the dynamics and control of wind turbines and wind farms," in *2009 American Control Conference*. IEEE, 2009, pp. 2076–2089. [Online]. Available: <http://ieeexplore.ieee.org/lpdocs/epic03/wrapper.htm?arnumber=5160195>
- [63] J. Rodríguez-Amenedo, S. Arnaltes, and M. Rodríguez, "Operation and coordinated control of fixed and variable speed wind farms," *Renewable Energy*, vol. 33, no. 3, pp. 406–414, Mar 2008. [Online]. Available: <http://www.sciencedirect.com/science/article/pii/S0960148107000730>
- [64] K. E. Johnson and N. Thomas, "Wind farm control: Addressing the aerodynamic interaction among wind turbines," in *2009 American Control Conference*. IEEE, 2009, pp. 2104–2109.
- [65] D. Madjidian and A. Rantzer, "A stationary Turbine Interaction Model for Control of Wind Farms," in *The 18th IFAC World Congress Milano*, 2011, pp. 4921–4926.
- [66] M. Adaramola and P.-A. Krogstad, "Experimental investigation of wake effects on wind turbine performance," *Renewable Energy*, vol. 36, no. 8, pp. 2078–2086, Aug 2011. [Online]. Available: <http://linkinghub.elsevier.com/retrieve/pii/S0960148111000462>
- [67] N. Jensen, "A note on wind generation interaction," Riso National Laboratory, Tech. Rep., 1983.

- [68] S. Frandsen, “Turbulence and Turbulence Generated Structural Loading in Wind Turbine Clusters,” Ph.D. dissertation, Riso, 2007.
- [69] M. Gibbard and D. Vowles, “Simplified 14-Generator Model of the SE Australian Power System,” The University of Adelaide, Tech. Rep., July 2010.
- [70] A. S. Ahmadyar, S. Riaz, G. Verbič, J. Riesz, and A. C. Chapman, “Assessment of Minimum Inertia Requirement for System Frequency Stability,” in *2016 IEEE International Conference on Power Systems Technology (POWERCON)*, Wollongong, 2016.
- [71] AEMO, “National Transmission Network Development Plan 2015,” AEMO, Tech. Rep., Nov 2015.
- [72] J. Riesz, B. Elliston, P. Vithayasrichareon, and I. MacGill, “100 % Renewables in Australia: A Research Summary,” UNSW, Tech. Rep., Mar 2016.
- [73] AEMO, “Emerging Technologies Information Paper, National Electricity Forecasting Report,” AEMO, Tech. Rep., June 2015.
- [74] —, “Power System Frequency and Time Deviation Monitoring Report Reference Guide,” AEMO, Tech. Rep., 2012.
- [75] H. Bevrani, *Robust power system frequency control*. New York, NY: Springer, 2009.
- [76] R. Doherty, G. Lalor, and M. O’Malley, “Frequency Control in Competitive Electricity Market Dispatch,” *IEEE Transactions on Power Systems*, vol. 20, no. 3, pp. 1588–1596, Aug 2005.
- [77] A. Ulbig, T. S. Borsche, and G. Andersson, “Impact of Low Rotational Inertia on Power System Stability and Operation,” in *IFAC*, Cape Town International Convention Centre, Cape Town, South Africa, Dec 2013.
- [78] E. Ørum, M. Laasonen, and E. al, “Future System Inertia,” ENTSOE, Brussels, Tech. Rep., 2015.
- [79] J. Riesz and B. Elliston, “Research priorities for renewable technologies - Quantifying the importance of various renewable technologies for low cost renewable electricity systems,” *Submitted to Energy Policy*, 2016.
- [80] J. Riesz and M. Milligan, “Designing electricity markets for a high penetration of variable renewables,” *Wiley Interdisciplinary Reviews: Energy and Environment*, vol. 4, no. 3, pp. 279–289, 2014.
- [81] E. Ela, V. Gevorgian, A. Tuohy, B. Kirby, M. Milligan, and M. O’Malley, “Market Designs for the Primary Frequency Response Ancillary Service Part I: Motivation and Design,” *IEEE Transactions on Power Systems*, vol. 29, no. 1, pp. 421–431, Jan 2014.
- [82] AEMO, “NEM Market Event Report High FCAS Price in South Australia,” AEMO, Melbourne, Tech. Rep., Nov 2015.

- [83] A. S. Ahmadyar and G. Verbič, “Coordinated operation strategy of wind farms for frequency control by exploring wake interaction,” *IEEE Transactions on Sustainable Energy*, vol. 8, no. 1, pp. 230–238, 2017.
- [84] T. S. Borsche, T. Liu, and D. J. Hill, “Effects of rotational inertia on power system damping and frequency transients,” in *2015 54th IEEE Conference on Decision and Control (CDC)*, Dec 2015, pp. 5940–5946.
- [85] T. Borsche and F. Dörfler, “On Placement of Synthetic Inertia with Explicit Time-Domain Constraints,” in *Arxiv*, May 2017. [Online]. Available: <https://arxiv.org/abs/1705.03244>
- [86] B. K. Poolla, S. Bolognani, and F. Dörfler, “Optimal Placement of Virtual Inertia in Power Grids,” *IEEE Transactions on Automatic Control*, vol. PP, no. 99, pp. 1–1, 2017.
- [87] M. Pirani, J. W. Simpson-Porco, and B. Fidan, “System-Theoretic Performance Metrics for Low-Inertia Stability of Power Networks,” in *Arxiv*, Mar 2017. [Online]. Available: <http://arxiv.org/abs/1703.02646>
- [88] A. Mešanović, U. Münz, and C. Heyde, “Comparison of H1, H2, and pole optimization for power system oscillation damping with remote renewable generation,” *IFAC-PapersOnLine*, vol. 49, no. 27, pp. 103–108, 2016.
- [89] S. S. Guggilam, C. Zhao, E. Dall’Anese, Y. C. Chen, and S. V. Dhople, “Engineering Inertial and Primary-frequency Response for Distributed Energy Resources,” in *Arxiv*, June 2017. [Online]. Available: <http://arxiv.org/abs/1706.03612>
- [90] C. D. Vournas and B. C. Papadias, “Power System Stabilization via Parameter Optimization Application to the Hellenic Interconnected System,” *IEEE Power Engineering Review*, vol. PER-7, no. 8, pp. 39–40, Aug 1987.
- [91] G. E. Boukarim, S. Wang, J. H. Chow, G. N. Taranto, and N. Martins, “A comparison of classical, robust, and decentralized control designs for multiple power system stabilizers,” *IEEE Transactions on Power Systems*, vol. 15, no. 4, pp. 1287–1292, Nov 2000.
- [92] EirGrid and SONI, “Annual Renewable Energy Constraint and Curtailment Report 2016,” EirGrid, Tech. Rep., 2016.
- [93] F. L. Alvarado, J. Meng, C. L. DeMarco, and W. S. Mota, “Stability analysis of interconnected power systems coupled with market dynamics,” *IEEE Transactions on Power Systems*, vol. 16, no. 4, pp. 695–701, Nov 2001.
- [94] S. Riaz, G. Verbič, and A. C. Chapman, “Computationally Efficient Market Simulation Tool for Future Grid Scenario Analysis,” *Submitted to IEEE Transaction on Sustainable Energy*, Apr 2017. [Online]. Available: <http://arxiv.org/abs/1701.07941>
- [95] A. Tasman, “Fuel resource, new entry and generation costs in the NEM,” ACIL Tasman Pty Ltd, Report, 2009.

- [96] IEEE Task Force on Load Representation for Dynamic Performance, "Load representation for dynamic performance analysis," *IEEE Transactions on Power Systems*, vol. 8, no. 2, pp. 472–482, 1993.
- [97] L. Pereira, S. Member, D. Kosterev, P. Mackin, S. Member, D. Davies, J. Undrill, and W. Zhu, "An Interim Dynamic Induction Motor Model for Stability Studies in the WSCC," *IEEE Transactions on Power Systems*, vol. 17, no. 4, pp. 1108–1115, 2002.
- [98] Cigre Working Group C4.605, "Modelling and Aggregation of Loads in Flexible Power Networks - Report 566," CIGRE, Tech. Rep. February, 2014.
- [99] L. Hiskens and J. V. Milanović, "Load modelling in studies of power system damping," *IEEE Transactions on Power Systems*, vol. 10, no. 4, pp. 1781–1788, 1995.
- [100] AEMO, "Frequency Control Fact Sheet," pp. 1–3, 2016.
- [101] P. Sorensen, A. D. Hansen, K. Thomsen, P. E. Morthorst, L. H. Nielsen, F. Iov, F. Blaabjerg, H. A. Nielsen, H. Madsen, and M. H. Donovan, "Operation and Control of Large Wind Turbines and Wind Farms - Final Report," RisøNational Laboratory, Roskilde, Tech. Rep., Sep 2005.
- [102] A. Zertek, G. Verbič, and M. Pantos, "A Novel Strategy for Variable-Speed Wind Turbines' Participation in Primary Frequency Control," *IEEE Transactions on Sustainable Energy*, vol. 3, no. 4, pp. 791–799, Oct 2012.
- [103] D. A. R. G. and J. A. Pecos Lopes, "Participation of Doubly Fed Induction Wind Generators in System Frequency Regulation," *IEEE Transactions on Power Systems*, vol. 22, no. 3, pp. 944–950, Aug. 2007.
- [104] L. H. Martin O, *Aerodynamics of Wind Turbines*, S. Edition, Ed. Earthscan, 2008.
- [105] J. Jonkman, S. Butterfield, W. Musial, and G. Scott, "Definition of a 5-MW Reference Wind Turbine for Offshore System Development," National Renewable Energy Laboratory (NREL), Colorado, Tech. Rep., 2009.
- [106] T. Ackermann, *Wind Power in Power Systems*. Wiley, 2005.
- [107] MATLAB, "Global Optimization Toolbox, Version 3.2.5 (R2014a)," The MathWorks Inc, Natick, Massachusetts, 2014.
- [108] IEEE-PES, "Dynamic Models for Turbine-Governors in Power System Studies," IEEE Power & Energy Society, Tech. Rep., 2013.
- [109] A. D. Hansen, P. Sorensen, F. Iov, and F. Blaabjerg, "Centralised power control of wind farm with doubly fed induction generators," *Renewable Energy*, vol. 31, no. 7, pp. 935–951, June 2006.
- [110] P. Sorensen, A. D. Hansen, F. Iov, and F. Blaabjerg, "Modeling of wind farm controllers," in *European Wind Energy Association (EWEA)*, 2006.
- [111] T. Ackermann, *Wind power in power systems*, 2d ed. Elsevier B.V, 2012.

-
- [112] C. Huang, F. Li, T. Ding, Z. Jin, and X. Ma, "Second-Order Cone Programming-Based Optimal Control Strategy for Wind Energy Conversion Systems Over Complete Operating Regions," *IEEE Transactions on Sustainable Energy*, vol. 6, no. 1, pp. 263–271, Jan 2015.
 - [113] M. Soliman, O. P. Malik, and D. T. Westwick, "Multiple Model Predictive Control for Wind Turbines With Doubly Fed Induction Generators," *IEEE Transactions on Sustainable Energy*, vol. 2, no. 3, pp. 215–225, July 2011.
 - [114] K. Clark, N. W. Miller, and J. J. Sanchez-Gasca, "Modeling of GE wind turbine generators for grid studies," GE, Schenectady, NY, Tech. Rep., 2010.

